ARO 27917.21-EL-S

CYCLIC FEATURE ANALYSIS, DESIGN, AND EXPLOITATION

FINAL REPORT

by

William A. Gardner and Chad M. Spooner

September 26, 1994

U. S. Army Research Office

Contract DAAL03-91-C-0018
Project P-27917-EL-S
1 Apr 91 - 31 Jul 94

Statistical Signal Processing, Inc.
6950 Yount Street
Yountville, CA 94599

MASTER COPY KEEP THIS COPY FOR REPRODUCTION PURPOSES

REPORT DOCUMENTATION PAGE

Form Approved
OMB No. 0704-0188

1. AGENCY USE ONLY (Leave blank)	2. REPORT DATE	3. REPORT TYPE AND DATES COVERED
	26 Sep 94	Final 1 Apr 91 - 31 Jul 94

4. TITLE AND SUBTITLE

Cyclic Feature Analysis, Design and Exploitation

5. FUNDING NUMBERS

DAAL03-91-C-0018

6. AUTHOR(S)

William A. Gardner and Chad M. Spooner

7. PERFORMING ORGANIZATION NAME(S) AND ADDRESS(ES)

Statistical Signal Processing, Inc.
6950 Yount Street
Yountville, CA 94599

8. PERFORMING ORGANIZATION REPORT NUMBER

9. SPONSORING/MONITORING AGENCY NAME(S) AND ADDRESS(ES)

U.S. Army Research Office
P.O. Box 12211
Research Triangle Park, NC 27709-2211

10. SPONSORING/MONITORING AGENCY REPORT NUMBER

ARO 27917.21-EL-S

11. SUPPLEMENTARY NOTES

The views, opinions and/or findings contained in this report are those of the author(s) and should not be construed as an official Department of the Army position, policy, or decision, unless so designated by other documentation.

12a. DISTRIBUTION/AVAILABILITY STATEMENT

Approved for public release; distribution unlimited.

12b. DISTRIBUTION CODE

13. ABSTRACT *(Maximum 200 words)*

In this research project, we characterized the n-th order cyclostationarity properties of general types of LPI signals and used the characterizations to investigate and develop methods for both secure communication and interception. For secure communication, this includes means for reduction of strength of, and elimination of, cyclic features that could be exploited by an interceptor. Signal design for LPI communication was considered from the viewpoints of both the communicator's reception task and the interceptor's reception task. For interception, the characterizations were used to propose feature sets and discrimination rules for signal classification and identification. The basic approach to characterizing n-th order cyclostationarity properties of signals was extended and generalized from the recently developed theory of 2nd-order cyclostationarity, in which spectral characterizations play a crucial role.

14. SUBJECT TERMS

Cyclostationary Signals
LPI Signal Design
Signal Interception
Cumulants

15. NUMBER OF PAGES

105

16. PRICE CODE

17. SECURITY CLASSIFICATION OF REPORT	18. SECURITY CLASSIFICATION OF THIS PAGE	19. SECURITY CLASSIFICATION OF ABSTRACT	20. LIMITATION OF ABSTRACT
UNCLASSIFIED	UNCLASSIFIED	UNCLASSIFIED	UL

CYCLIC FEATURE ANALYSIS, DESIGN, AND EXPLOITATION

FINAL REPORT

by

William A. Gardner and Chad M. Spooner

September 26, 1994

U. S. Army Research Office

Contract DAAL03-91-C-0018
Project P-27917-EL-S
1 Apr 91 - 31 Jul 94

Statistical Signal Processing, Inc.
6950 Yount Street
Yountville, CA 94599

THE VIEWS, OPINIONS, AND/OR FINDINGS CONTAINED IN THIS REPORT ARE THOSE OF THE AUTHOR(S) AND SHOULD NOT BE CONSTRUED AS AN OFFICIAL DEPARTMENT OF THE ARMY POSITION, POLICY, OR DECISION, UNLESS SO DESIGNATED BY OTHER DOCUMENTATION.

Table of Contents

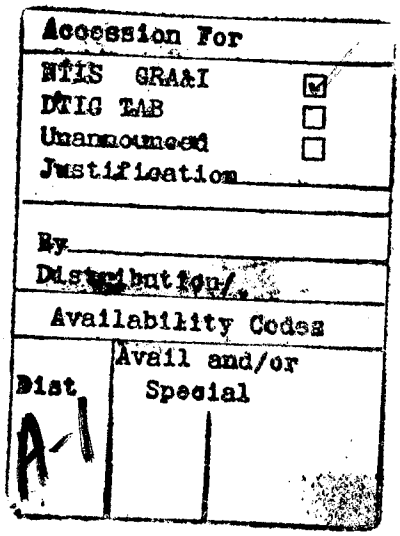

LIST OF APPENDICES

A. Problem Statement

The purpose of the proposed research was to characterize the n-th order cyclostationarity properties of general types of LPI signals and to use the characterizations to investigate and develop methods for both secure communication and interception. For secure communication, this includes means for reduction of strength of, and elimination of, cyclic features that could be exploited by an interceptor. Signal design for LPI communication was to be considered from the viewpoints of both the communicator's reception task and the interceptor's reception task. For interception, the characterizations were to be used to propose feature sets and discrimination rules for signal classification and identification. The basic approach to characterizing n-th order cyclostationarity properties of signals was to be extended and generalized from the recently developed theory of 2nd-order cyclostationarity, in which spectral characterizations play a crucial role.

B. Summary of Results

I. Fundamental Theory

In [1, 2, 3], the fundamental theory of higher-order cyclostationarity is presented, and some applications of the theory are discussed. The theory is an extension of the theory of second-order cyclostationarity, which analyzes the polyperiodic components of quadratic transformations of random time-series, to nth-order cyclostationarity, which analyzes the polyperiodic components of nth-order transformations of random time-series. The central parameters of the theory are nth-order moments and cumulants of both the time-series itself (time domain or temporal) and of finite-time Fourier transforms of the time-series (frequency-domain or spectral). Unlike all other work on cumulants, in which the cumulant is used because it has some well-known useful properties, we have shown that cumulants arise as the solution to a specific problem that is central to the study of higher-order cyclostationarity. That is, we have shown that each Fourier component of the nth-order temporal cumulant function (called a *cyclic cumulant*) for a random polycyclostationary time-series can be derived as the solution to the problem of calculating the part of a sine wave, which is generated by applying an nth-order homogeneous polynomial nonlinearity to the time-series, that excludes contributions that are due to the multiplication of sine waves that are generated by the lower-order factors in the homogeneous polynomial. In addition, Part I of the papers [2, 3] contains a detailed history of the cumulant from its inception in the late nineteenth century up to the present. The papers [2, 3] also contain results on the effect on the theory's central parameters of certain signal-processing operations that are performed on the time-series in question, including signal addition, signal multiplication, convolution, and periodic sampling. Methods for measurement of the central parameters are presented, analyzed mathematically, and evaluated by computer simulation. The book chapter [4] presents a tutorial treatment of much of the work presented in [1, 2, 3].

II. Theory and Method for Measurement of Cyclic Statistics

In the two conference papers [5] and [6], the measurement of the frequency-domain cumu-

lants, known as cyclic polyspectra, is considered. Much of the material in the first paper, [5], appears in the later publications [1, 2, 3], but the material in [6] has not been published in any other place. In [5], three methods of estimating the cyclic polyspectrum are presented and shown to converge to the correct theoretical functions when the data record length first increases without bound, and then the spectral resolution-width parameter is allowed to approach zero. The correctness of the methods for finite data-record lengths and spectral resolution-widths is verified by computer simulation. It is also shown that the three measurement methods reduce to well-known spectral estimation methods for order two and a cycle frequency of zero. In [6], a source of measurement error that is particular to the measurement of cyclic polyspectra, as opposed to polyspectra, which are the spectral cumulants for nth-order stationary time-series, is studied. This source of error is called *leakage from submanifolds*, and results from the presence of lower-order cyclic features. Leakage from submanifolds is the generalization to higher orders of the spectral leakage phenomenon that occurs in spectrum estimation when the data contains sine-wave components (when the ideal spectrum contains impulses). The leakage phenomenon is studied both analytically and by computer simulation (the latter only for $n = 4$).

III. Algorithms for TDOA Estimation

In [7, 8], the problem of estimating the time difference of arrival (TDOA) between the components of a signal that is received at two spatially separated sensors is studied for the case in which the signal does not exhibit sufficiently strong (exploitable) second-order cyclostationarity and is subject to cochannel interference and time-varying background noise. This can happen, for example, when the signal is a bandwidth-efficient communication signal or when it is a member of a class of low-probability-of-intercept signals. In [7, 8], work, a class of TDOA estimators is derived to solve the stated problem. This class of estimators is based on matching measurements of sets of nth-order cross cyclic cumulants in a least-squares sense. For $n = 2$, two of the estimators in the class reduce to known cyclostationarity-exploiting TDOA estimators (SPECCOA and CPD). The nth-order version of CPD has been implemented in software, but simulations aimed at characterizing its performance have not been completed.

IV. A Method for Waveform Extraction

In [9], the theory of higher-order cyclostationarity is applied to the problem of estimating a signal waveform in the presence of cochannel interference and noise from data obtained from a single sensor. In particular, the signal of interest can be completely spectrally and temporally overlapped by the interferers. If the signal exhibits strong second-order cyclostationarity, then linear frequency-shift filtering can be used to perform this waveform estimation. If the interferers also exhibit strong second-order cyclostationarity, then the quality of the waveform estimate can be improved by exploiting this cyclostationarity in addition to that of the signal of interest. However, for the case in which the signal and interferers do not exhibit sufficient second-order cyclostationarity, but do exhibit higher-order cyclostationarity, nonlinear frequency-shift filtering can be used to perform the waveform estimation.

In [9], a nonlinear frequency-shift filter consisting of a linear part and a cubic part is studied mathematically and by computer simulation. The mathematical analysis consists of deriving the minimum-mean-squared-error (MMSE) design equations for estimating a signal waveform contained in an arbitrary data record. The derived integral equations are complicated and have not yet been solved. The form of the equations can yield information that helps to specify the frequency shifts to be used in both the linear and cubic parts of the system. Such a system was implemented in software and simulations were performed to assess the potential of the method. In particular, it was desired to determine if there was enough potential for solving problems of practical interest to merit numerical evaluation of the MMSE design equations. The simulations performed to date show that, for a small number of frequency shifts and a small number of cubic transformations, the reduction in mean-squared error (with respect to linear time-invariant filtering) is about 50%. However, for the signal environments chosen, there is simply no known viable alternative for waveform estimation. Because the method appears to have some potential, it is recommended that further research be carried out on nonlinear frequency-shift filtering.

V. LPI Signal Design

In [10], the challenging problem of designing a low-probability-of-intercept (LPI) or, more accurately, a covert digital communication signal is tackled using the theory of higher-order cyclostationarity. The design philosophy is as follows. Signals are normally detected based on their observable characteristics, such as power level, center frequency, bandwidth, temporal

structure, etc. When these obvious *features* are hidden by a signal designer, as is the case with, for example, direct-sequence spread-spectrum signals, other features of the signal must be used to perform detection. A useful class of features are those periodic components that can be found in the outputs of nonlinear transformations of the signal. Examples of these are symbol rates, chip rates, and doubled carrier frequencies. The interceptor nonlinearly transforms the received signal and attempts to detect these periodic components in order to detect the presence of the hidden signal. Thus, the signal designer must take this interception strategy into account. He must design his covert signal such that no useful periodic components can be generated by a specified class of nonlinear transformations for a given data-record length. Our LPI signal design starts at this point.

We attempt to design a digital communication signal such that, ideally, no finite-strength additive sine-wave components (with nonzero frequency) can be generated using nonlinearities of order N or less. (The ability to generate sine-wave components with zero frequencies cannot be avoided, but this does not destroy the covertness of a signal either.) To minimize the detectability of these sine waves, the digital communication signal is chosen to be a spread-spectrum signal and is, therefore, hidden in the much stronger noise. The theory of second-order cyclostationary signals is sufficient to solve the remaining problem if N is less than or equal to three, but for larger N, the theory of higher-order cyclostationarity must be used. This latter theory completely characterizes all the finite-strength additive sine-wave components that can be generated by nonlinear transformation in terms of cyclic cumulants. We have found that the cyclic cumulants of digital QAM signals are equal to the product of the cumulant of the symbol variable with a nonlinear function of the complex envelope of the pulse.

To minimize the second-order cyclic cumulants of digital spread-spectrum QAM signals, the chip envelope cannot be the standard rectangular pulse. A zero-percent excess-bandwidth pulse, such as that used in partial-response signaling, can be used to eliminate all second-order features associated with the chip rate.

To minimize the second-order features associated with the carrier frequency, and all higher-order features, the signal constellation must be appropriately designed. This necessitates a departure from the standard ± 1 chip alphabet. These considerations result in a

cumulant-minimization problem that involves a set of nonlinear equality constraints on the chip alphabet and associated probabilities. Alternatively, the design problem can be cast in the form of a large system of nonlinear equations resulting from setting all the undesirable sine-wave strengths equal to zero, but further research is needed to determine if any exact solutions to these nonlinear equations exist.

In our work to date, we have developed numerical methods for solving the minimization problem described above. These numerical methods have been used to design covert/LPI signals with very small second-, third-, and fourth-order cyclic cumulants. Because of the relationships between moments and cumulants, the corresponding cyclic moments up to order four are also very small. As an example, a 16-QAM signal employing partial-response pulse-shaping has been designed for which the two largest sine-wave strengths for nonlinearities with orders four and less are 17.4 dB and 28.6 dB below the power level, although the strengths of most of the regeneratable sine waves are more than 30 dB below the power level. By comparison, for BPSK signals, the largest sine-wave strength is 6 dB above the power level, and for 16-QAM with the conventional square constellation and rectangular pulses, the two largest are 3.3 dB and 7.9 dB below the power level.

VI. Cochannel Signal Detection

In [11], the problem of determining the number of cyclostationary signals present (if any) in a given data record is addressed. The particular scenario of interest is that for which the signals are temporally and spectrally overlapping. Lack of prior knowledge, including the number of signals present, prohibits detection based on radiometry (detection of energy in certain spectral bands), and the possible presence of signals that do not exhibit strong second-order cyclostationarity rules out conventional cycle detectors. However, an algorithm for blindly estimating cyclic cumulants has been developed to solve this problem. This algorithm is called the *general search algorithm* (GSA), and its function is to produce estimates of the cyclic cumulants and their associated cycle frequencies of the given data for orders 1 through N, where N is specified by the user of the algorithm.

The output of the GSA consists of a set of estimates of cyclic cumulants and the associated cycle frequencies for each order of processing. However, this list of numbers is not enough to determine the number of signals that are present (which give rise to the cyclic cumulants).

To do this, the cyclic cumulant/cycle frequency pair estimates need to be grouped together such that each group corresponds to a single signal in the data. The *grouping algorithm* (GA) performs this task. The GA has been implemented for the case of signals of the digital QAM variety, but can be extended to include classes of signals for which formulas for the temporal cumulants are known. In [11], the GSA and GA are described and their performance is illustrated with simulations. This work, while in an early stage of research and development, is very promising and merits further research.

VII. Cochannel Modulation Identification

In [12], the GSA and GA algorithms are used to not only detect any cyclostationary signals present in a given data record, but to identify their modulation types as well. A catalog of feature vectors obtained by applying the GSA/GA tandem to a variety of noiseless simulated signals is obtained. This catalog reveals that signals with identical second-order cyclic features can have radically different higher-order cyclic features provided the order N is chosen large enough. For example, QPSK and 8PSK have identical second-order cyclic features, but have distinct fourth-order cyclic features (QPSK has features related to the carrier frequency for order four, whereas 8PSK does not). To distinguish between 8PSK and 16PSK requires $N = 8$. The features are useful because they can be estimated for each signal in the data (in principle) regardless of the amount of spectral overlap. An algorithm for identifying the modulation type of a signal given a measured feature has been devised but has not been thoroughly tested. This algorithm measures the distance between the measured feature and each feature in a set of candidate-signal features and chooses the modulation type that gives rise to the feature with minimum distance.

VIII. Nonlinear System Identification

In [13], the problem of identifying the kernels of a nonlinear Volterra system is studied. A new approach to obtaining sets of operators that are orthogonal to the Volterra operators for a class of input time-series is developed. It is shown how these orthogonal operators can be used in a crosscorrelation-based method to identify the Volterra kernels of nonlinear time-invariant systems. This class of inputs includes both Gaussian and finite-state (e.g., PSK) time-series, and simulations suggest that methods used with the finite-state inputs converge considerably more rapidly than the methods used with Gaussian inputs, which includes as

a special case the method of Wiener, Lee, and Schetzen.

For complex-valued inputs, the new methods are believed to be the only crosscorrelation-based methods known that identify arbitrary order Volterra kernels of an infinite-order system (with infinite memory). Such methods can be used to compute the Volterra kernels of nonlinear systems that can be simulated on a computer.

The computational efficiency of these new crosscorrelation-based methods can be increased by using an FFT algorithm to implement the frequency-domain counterparts developed in this project that are based on frequency-smoothed cross-spectra.

IX. Polyperiodic Nonlinear System Identification

In [14], the class of polyperiodic nonlinear (PPN) systems that admit a new double series representation, called the Fourier-Volterra series, is considered, and a class of cyclostationary random inputs that enables the analytical specification of sets of operators on the input that are orthonormal over all time to the Fourier-Volterra operators are defined. The reciprocal operators are used to obtain a crosscorrelation formula for identifying the Fourier-Volterra kernels of PPN systems. It is shown how the orthonormal operators for the finite-state phase-modulated and Gaussian amplitude-modulated inputs can be determined. The finite-state inputs are expected to result in computationally attractive identification relative to the computational load required for Gaussian inputs because of the substantially longer averaging times that are apparently required by the latter. Nevertheless, the computational load for the former can be very substantial not only because of the averaging time required, but also because of the number of terms required in the double series representation. Some reduction in the computational load of the crosscorrelation method can be achieved by using an FFT algorithm to implement its frequency-domain counterpart, which is based on frequency-smoothed cyclic cross-periodograms, and which was developed in this project.

References

[1] C. M. Spooner. "Theory and Application of Higher-Order Cyclostationarity," Ph.D. Dissertation, Department of Electrical and Computer Engineering, University of California, Davis CA, 1992.

[2] W. A. Gardner and C. M. Spooner. "The Cumulant Theory of Cyclostationary Time-Series, Part I: Foundation," *IEEE Transactions on Signal Processing*, Vol. 42, December

1994 (in press).

[3] C. M. Spooner and W. A. Gardner. "The Cumulant Theory of Cyclostationary Time-Series, Part II: Development and Applications," *IEEE Transactions on Signal Processing*, Vol. 42, December 1994 (in press).

[4] C. M. Spooner. "Higher-Order Statistics for Nonlinear Processing of Cyclostationary Signals," in *Cyclostationarity in Communications and Signal Processing,* (W. A. Gardner, ed.), IEEE Press, New York, 1994.

[5] C. M. Spooner and W. A. Gardner. "Estimation of Cyclic Polyspectra," (invited paper) *Proceedings of the Twenty-Fifth Annual Asilomar Conference on Signals, Systems and Computers,* Pacific Grove, CA, Nov. 4-6, 1991, pp. 370–376.

[6] C. M. Spooner and W. A. Gardner. "Performance Evaluation of Cyclic Polyspectrum Estimators," (invited paper) *Proceedings of the Twenty-Sixth Annual Asilomar Conference on Signals, Systems and Computers,* Pacific Grove, CA, pp. 477–483, October 26–28, 1992.

[7] C. M. Spooner and W. A. Gardner. "Exploitation of Higher-Order Cyclostationarity for Weak-Signal Detection and Time-Delay Estimation," *Proceedings of the Sixth Workshop on Statistical Signal & Array Processing*, Victoria, British Columbia, Canada, 1992.

[8] C. M. Spooner and W. A. Gardner. "Emitter Location Using Cyclic Cumulants," SSPI Report, 11 pages, 1994.

[9] C. M. Spooner and W. A. Gardner. "Nonlinear Frequency-Shift Filtering for Cochannel Interference Mitigation," SSPI Report, 6 pages, 1994.

[10] C. M. Spooner and W. A. Gardner. "Design of Low-Probability-of-Intercept Signals: Minimum-Cumulant Digital QAM Signals," SSPI Report, 22 pages, 1994 (included herewith in the appendix).

[11] C. M. Spooner and W. A. Gardner. "Signal Detection and Sorting Using Cyclic Cumulants in the General Search Algorithm," SSPI Report, 34 pages, 1994 (included herewith in the appendix).

[12] C. M. Spooner and W. A. Gardner. "Signal Classification Using the General Search Algorithm," SSPI Report, 32 pages, 1994 (included herewith in the appendix).

[13] W. A. Gardner and T. L. Archer. "Exploitation of Cyclostationarity for Identifying the Volterra Kernels of Nonlinear Systems," *IEEE Transactions on Information Theory* **39**, 1993.

[14] W. A. Gardner and G. Paura. "Identification of Polyperiodic Nonlinear Systems," SSPI Report, 11 pages, 1993.

C. List of Publications and Technical Reports*

a. Journal and Conference Papers

1. C. M. Spooner and W. A. Gardner. ESTIMATION OF CYCLIC POLYSPECTRA. Proceedings of the Twenty-fifth Annual Asilomar Conference on Signals, Systems, and Computers, pp. 370-376, (Invited paper), 1991.

2. C. M. Spooner and W. A. Gardner. PERFORMANCE EVALUATION OF CYCLIC POLYSPECTRUM ESTIMATORS. Proceedings of the Twenty-sixth Annual Asilomar Conference on Signals, Systems, and Computers, pp. 477-483, (Invited paper), 1992.

3. C. M. Spooner and W. A. Gardner. EXPLOITATION OF HIGHER-ORDER CYCLOSTATIONARITY FOR WEAK-SIGNAL DETECTION AND TIME-DELAY ESTIMATION. Proceedings of the IEEE Sixth SP Workshop on Statistical Signal and Array Processing, pp. 197-201, October 7-9, 1992.

4. W. A. Gardner and T. L. Archer. EXPLOITATION OF CYCLO-STATIONARITY FOR IDENTIFYING THE VOLTERRA KERNELS OF NONLINEAR SYSTEMS. IEEE Transactions on Information Theory, Vol. 39, pp. 535-542, 1993.

5. C. M. Spooner and W. A. Gardner. CUBIC FREQUENCY-SHIFT FILTERING FOR COCHANNEL INTERFERENCE REMOVAL. Proceedings of the 1993 International Symposium on Nonlinear Theory and Its Applications, 1993.

6. W. A. Gardner and C. M. Spooner. THE CUMULANT THEORY OF CYCLOSTATIONARY TIME-SERIES, PART I: FOUNDATION.

*submitted or published during the period of this ARO contract and under sponsorship from this ARO.

IEEE Transactions on Signal Processing, December 1994.

7. C. M. Spooner and W. A. Gardner. THE CUMULANT THEORY OF CYCLOSTATIONARY TIME-SERIES, PART II: DEVELOPMENT AND APPLICATIONS. Accepted for publication by the IEEE Transactions on Signal Processing, December, 1994.

8. C. M. Spooner. AN OVERVIEW OF RECENT DEVELOPMENTS IN CYCLOSTATIONARY SIGNAL PROCESSING. Proceedings of Second Workshop on Cyclostationary Signals, pp. 1-17, August 1-2, 1994.

9. C. M. Spooner and W. A. Gardner. CUMULANTS AND CYCLOSTATIONARY SIGNALS. IEEE Signal Processing Magazine, in preparation, 1994.

b. Books

10. W. A. Gardner. CYCLOSTATIONARITY IN COMMUNICATIONS AND SIGNAL PROCESSING. (Edited book with invited and reviewed contributions), Piscataway, NJ: IEEE Press, sponsored by IEEE Communications Society, 504 pages, 1994.

c. Book Chapters

11. W. A. Gardner. AN INTRODUCTION TO CYCLOSTATIONARY SIGNALS. Chapter 1 in Cyclostationarity in Communications and Signal Processing. Edited by W. A. Gardner, IEEE Press, pp. 1-90, 1994.

12. C. M. Spooner. HIGHER-ORDER STATISTICS FOR NONLINEAR PROCESSING OF CYCLOSTATIONARY SIGNALS, Chapter 2, in Cyclostationarity in Communications and Signal Processing.

13. W. A. Gardner and C. M. Spooner. CYCLOSTATIONARY-SIGNAL PROCESSING. Chapter in Control and Dynamic Systems, edited by C. T. Leondes, Academic Press, Vol. 65, pp. 1-92, 1994.

14. C. M. Spooner and W. A. Gardner. AN OVERVIEW OF THE THEORY OF HIGHER-ORDER CYCLOSTATIONARITY. Proceedings of the Workshop on Nonstationary Stochastic Processes and Their Applications, ed. by A. G. Miamee, Singapore: World Scientific, pp. 110-125, 1991.

d. Unpublished Reports

15. C. M. Spooner and W. A. Gardner. DESIGN OF LOW-PROBABILITY-OF-INTERCEPT SIGNALS: MINIMUM-CUMULANT DIGITAL QAM SIGNALS. 21 pages, July 8, 1994.

16. C. M. Spooner and W. A. Gardner. SIGNAL DETECTION AND SORTING USING CYCLIC CUMULANTS IN THE GENERAL SEARCH ALGORITHM. 33 pages, 1994.

17. C. M. Spooner and W. A. Gardner. SIGNAL CLASSIFICATION USING THE GENERAL SEARCH ALGORITHM. 31 pages, 1994.

18. C. M. Spooner and W. A. Gardner. EMITTER LOCATION USING CYCLIC CUMULANTS. 10 pages, 1994.

19. C. M. Spooner and W. A. Gardner. NONLINEAR FREQUENCY-SHIFT FILTERING FOR COCHANNEL INTERFERENCE MITIGATION. 6 pages, 1994.

20. W. A. Gardner and L. Paura. IDENTIFICATION OF POLYPERIODIC NONLINEAR SYSTEMS. 11 pages, 1993.

21. C. M. Spooner. THEORY AND APPLICATION OF HIGHER-ORDER CYCLOSTATIONARITY. Ph.D. Dissertation, Department of Electrical and Computer Engineering, University of California, Davis, 191 pages, June 1992.

22. C. M. Spooner and W. A. Gardner. A NOVEL DERIVATION OF THE CUMULANT AS THE SOLUTION TO A SINE-WAVE GENERATION PROBLEM. 12 pages, February 1993.

D. Participating Scientific Personnel

William A. Gardner, Ph.D., Principal Investigator

Chad M. Spooner, Ph.D., Senior Engineer, received Ph.D. degree in 1992

Stephan V. Schell, Ph.D., Senior Engineer

William A. Brown, Ph.D., Senior Engineer

Peter A. Murphy, MS, Engineer, received MS degree in 1993

E. Honors and Awards°

Chad M. Spooner received the campus-wide 1992-1993 Best Dissertation Award from the UC Davis Chapter of Sigma Xi, The Scientific Research Society, for his doctoral dissertation.

Stephan V. Schell and Chad M. Spooner received NSF sponsorship for the Second Workshop on Cyclostationary Signals held in August, 1994, which they co-organized and co-chaired.

William A. Gardner received IEEE Communications Society Sponsorship of his IEEE Press Book, *Cyclostationarity in Communications and Signal Processing* released in 1994.

William A. Gardner and Chad M. Spooner received invitations to be keynote speakers at the Second Workshop on Nonstationary Random Processes and their Applications to be held in May 1995. (Presentation in preparation.)

Chad M. Spooner and William A. Gardner were invited to submit a feature article on cumulants and cyclostationary signals for the *IEEE Signal Processing Magazine*, which is in preparation.

° During the period of this ARO contract and associated with the research conducted under this ARO contract.

William A. Gardner, Stephan V. Schell and Chad M. Spooner presented invited papers at the twenty-sixth and twenty-seventh Annual Asilomar Conference on Signals, Systems and Computers.

William A. Gardner gave an invited half-day tutorial research lecture at NSA in July 1994 on Cyclostationary Signal Processing.

William A. Gardner and Sumit Roy co-organized a session on cyclostationary signal processing at the twenty-eighth annual conference on Information Sciences and Systems, Princeton, in 1994.

William A. Gardner, Chad M. Spooner and Stephan A. Schell were invited to contribute two lead-off chapters on cyclostationary signal processing to C. T. Leondes' two volumes in the series, Control and Dynamic Systems, Academic press,1994.

F. Inventions

There are no inventions to report on.

H. Appendix

Copies of unpublished reports 10, 11, 12 cited in Section B

Design of Low-Probability-of-Intercept Signals: Minimum-Cumulant Digital QAM Signals

Chad M. Spooner and William A. Gardner

July 8, 1994

Abstract

Effective methods of signal interception for signals that are hidden in noise include those that are based on exploiting second-order cyclostationarity. The exploitability of second-order cyclostationarity for interception purposes can be measured by the peak strength of the sine-wave components that appear when the signal is subjected to certain quadratic nonlinearities. To counter such cyclostationarity-based interception, signals can be designed to yield quadratically regeneratable sine waves with small strengths. Thus, interceptors are forced to use other means to intercept such signals. One class of interception methods for these LPI signals is based on the exploitability of higher-order (order larger than two) cyclostationarity. For this interception to be effective, the peak strengths of the sine-wave components in the output of higher-order nonlinearities must be large enough to detect. The signal designers are then forced to minimize these strengths. In this work, digital QAM signals with minimum second-, third-, and fourth-order cyclostationarity are designed using a combination of pulse-shaping and amplitude/phase constellation design based on the newly developed theory of higher-order cyclostationarity.

1 Introduction

A substantial amount of recent research work on signal interception has focussed on exploiting the cyclostationary nature of digital communication signals, such as pulse-amplitude modulation (PAM), phase-shift keying (PSK), quadrature-amplitude modulation (QAM), direct-sequence spread-spectrum signals, and, to a lesser degree, frequency modulation, frequency-shift keying, and frequency-hopped spread-spectrum signals [5]–[9]. The key to such interception is the ability to generate a sine wave (or set of sine waves) by nonlinearly transforming the signal, and then detecting the presence of this regenerated sine wave. This interception can be accomplished even when the background noise and interference is very strong provided that enough data is available [1]. Thus, the degree of detectability of a cyclostationary signal can be measured in terms of the strength of its cyclostationarity, which can be defined in terms of the strengths of its regeneratable sine waves for a fixed signal-power level [6].

These interception considerations have necessarily had an impact on the design of low-probability-of-intercept (LPI) signals. In particular, it is desirable to limit the amount of

cyclostationarity that can be exploited by the interceptor, while simultaneously allowing the communicator to detect and demodulate the signal by using a receiver with reasonable complexity. Thus, it is desired to minimize the strengths of the regeneratable sine waves, but because regenerated sine waves are often used (explicitly or implicitly) by the intended receiver to synchronize to the signal, this is not just a simple minimization problem; there is a tradeoff between probability of intercept and difficulty of reception for the intended communicator. Nevertheless, in this report the focus is on the minimization problem without regard to the resulting complications for the intended communicator. The idea is to determine the limits on what can be done by using the proposed approach, and then to evaluate the difficulty of reception of the designed signals.

One way to minimize the strength of regeneratable sine waves that applies to the class of digital QAM signals is through pulse-shaping. That is, since digital QAM signals (at radio frequency) can be represented by complex-valued PAM signals (at baseband), then their spectral correlation functions are easily characterized in terms of the baseband pulse transform [1]. The support of this transform determines the number of regeneratable sine waves as well as their strengths. By bandlimiting the pulse transform to the Nyquist band (where the positive-frequency bandwidth of the pulse is equal to half the pulse rate), the second-order cyclostationarity of the signal that is associated with the pulse rate is annihilated [1]. The radio frequency signal can still exhibit cyclostationarity associated with the carrier if the symbol constellation (discrete support of the probability mass function of the complex-valued random symbols) does not meet certain symmetry requirements.

Pulse-shaping can be used to reduce the exploitable second-order cyclostationarity of a signal, but it is less effective at reducing the exploitable higher-order cyclostationarity of the signal. The positive-frequency bandwidth of the pulse transform would need to be reduced to $1/n$ times the pulse rate (or, more generally, the support of the pulse transform would have to be limited in some other way) in order to annihilate the nth-order regeneratable sine waves, which—for $n = 2$—would introduce an unacceptable amount of intersymbol interference to the transmitted signal, thus foiling the intended receiver. However, the symbol constellation itself can be designed to minimize the strength of the nth-order regeneratable sine waves. This is a result of the fact that the strengths of the *pure nth-order sine waves* [4] for a given digital QAM signal are directly proportional to the nth-order cumulant of the symbol constellation.

This report discusses the problem of minimizing the nth-order cumulants of discrete random variables by designing their probability mass functions for the purpose of designing signal constellations and associated probabilities for a digital QAM (DQAM) signaling scheme. The cumulant-minimization problem is also interesting from a mathematical viewpoint because it can be thought of as an attempt to find a small-alphabet discrete random variable that has a PDF that is, in some suitable sense, a good approximation to the continuous Gaussian probability density function (PDF). This follows because the higher-order cumulants for Gaussian random variables are all zero. In fact, this observation is the basis for one of the numerical methods described in this report.

In the following, the cumulants (and moments) of digital QAM signals are presented, and then the minimization problem is stated and explored analytically. Numerical approaches to this minimization problem are described, and some results are provided and discussed. The reader of this report is assumed to be familiar with higher-order statistics in general, and

with higher-order cyclostationarity in particular [4].

2 Moments and Cumulants of PAM Signals

The class of signals considered herein is specified by

$$s(t) = \Re\left\{ \sum_{m=-\infty}^{\infty} \left[\frac{e^{i\theta_c}}{2}(c_m - is_m) \right] p(t + mT_0 + t_0) e^{i2\pi f_c t} \right\}, \tag{1}$$

where $\Re\{\cdot\}$ is the real-part operator, f_c is the carrier frequency, θ_c is the carrier phase, T_0 is the pulse interval length, t_0 is the pulse timing constant, and c_m and s_m are real-valued independent symbol variables that take on values in some finite set. The analytic-signal representation of $s(t)$ is denoted by $s_a(t)$, and is given by

$$s_a(t) = \sum_{m=-\infty}^{\infty} \left[\frac{e^{i\theta_c}}{2}(c_m - is_m) \right] p(t + mT_0 + t_0) e^{i2\pi f_c t}, \tag{2}$$

and the complex envelope of the DQAM signal $s(t)$ is denoted by $s_c(t)$:

$$\begin{aligned} s_c(t) &= \sum_{m=-\infty}^{\infty} \left[\frac{e^{i\theta_c}}{2}(c_m - is_m) \right] p(t + mT_0 + t_0), \\ &= \sum_{m=-\infty}^{\infty} a_m p(t + mT_0 + t_0), \end{aligned} \tag{3}$$

which is a complex-valued PAM signal. This signal model includes PSK, Mary-QAM, and (more generally) amplitude-and-phase-shift-keying (APK) modulations.

The cumulants of a complex PAM signal $s_c(t)$ with independent and identically distributed symbols are given by [4]

$$\begin{aligned} C_{s_c}(t, \boldsymbol{\tau})_n &= \text{Cumulant } \{s_c^{(*)_j}(t + \tau_j)\}_{j=1}^n \\ &= C_{a,n} \sum_{m=-\infty}^{\infty} \left[\prod_{j=1}^{n} p^{(*)_j}(t + mT_0 + \tau_j + t_0) \right], \end{aligned} \tag{4}$$

where $(*)_j$ denotes optional conjugation of the jth element in the set $\{s_c^{(*)_j}(t + \tau_j)\}_{j=1}^n$, and $C_{a,n}$ is the nth-order cumulant of the symbol sequence $\{a_m\}$, and is given by

$$C_{a,n} \triangleq \sum_{P_n} \left[(-1)^{p-1}(p-1)! \prod_{j=1}^{p} R_{a,\nu_j} \right], \tag{5}$$

in which

$$R_{a,\nu_j} \triangleq \lim_{K\to\infty} \frac{1}{2K+1} \sum_{k=-K}^{K} \left[\prod_{q\in\nu_j} a_k^{(*)_q} \right], \tag{6}$$

and P_n is the set of all distinct partitions $\{\nu_1, \cdots, \nu_p\}$ of the set of indices $\{1, 2, \cdots, n\}$, and p is the size of the partition ($1 \leq p \leq n$) [2]. The reduced-dimension cyclic temporal cumulant function (RD-CTCF) and cyclic polyspectrum (CP) follow directly from (4):

$$\bar{C}_{s_c}^{\beta}(\boldsymbol{u})_n = \frac{C_{a,n}}{T_0} \int_{-\infty}^{\infty} p^{(*)_n}(t) \prod_{j=1}^{n-1} p^{(*)_j}(t+u_j) e^{-i2\pi\beta t}\, dt\, e^{i2\pi\beta t_0}, \quad \beta = k/T_0, \tag{7}$$

$$\bar{P}_{s_c}^{\beta}(\boldsymbol{f}')_n = \frac{C_{a,n}}{T_0} P^{(*)_n}((-)_n[\beta - \mathbf{1}^{\dagger}\boldsymbol{f}']) \prod_{j=1}^{n-1} P^{(*)_j}((-)_j f_j)\, e^{i2\pi\beta t_0}, \quad \beta = k/T_0, \tag{8}$$

where $P(f)$ is the Fourier transform of $p(t)$. Thus, the nth-order temporal and spectral cumulants of the PAM signal are directly proportional to the nth-order cumulant of the symbol variable.

The cyclic temporal moment functions (CTMFs) of the PAM signal $s_c(t)$ can be found by combining the cumulants of $s_c(t)$ in the following alternative ways [4]:

$$R_{s_c}^{\alpha}(\boldsymbol{\tau})_n = C_{s_c}^{\alpha}(\boldsymbol{\tau})_n + \sum_{\substack{P_n \\ p \neq 1}} \left[\sum_{\boldsymbol{\beta}^{\dagger}\mathbf{1}=\alpha} \prod_{j=1}^{p} C_{s_c}^{\beta_j}(\boldsymbol{\tau}_{\nu_j})_{n_j} \right]. \tag{9}$$

$$= C_{s_c}^{\alpha}(\boldsymbol{\tau})_n - \sum_{\substack{P_n \\ p \neq 1}} \left[(-1)^{p-1}(p-1)! \sum_{\boldsymbol{a}^{\dagger}\mathbf{1}=\alpha} \prod_{j=1}^{p} R_{s_c}^{\alpha_j}(\boldsymbol{\tau}_{\nu_j})_{n_j} \right], \tag{10}$$

where $\boldsymbol{a}$ and $\boldsymbol{\beta}$ are vectors of impure and pure cycle frequencies, respectively [4]. These expressions are complicated for $n > 3$, and no simplifications have been found. Clearly, the cyclic moment is not generally easy to compute, and it is obviously not proportional to the moment of the symbol variable $R_{a,n}$ in general. Nevertheless, for the case in which $p(\cdot)$ has width less than or equal to T_0, and $\tau_j = u$ for all j, the CTMF is given by

$$R_{s_c}^{\alpha}(\boldsymbol{u})_n = \frac{R_{a,n}}{T_0} \int_{-\infty}^{\infty} \prod_{j=1}^{n} p^{(*)_j}(t+u) e^{-i2\pi\alpha t}\, dt\, e^{i2\pi\alpha t_0},$$

for $\alpha = k/T_0$. Unfortunately, for rectangular pulses this particular CTMF is zero for $k \neq 0$ (but it is nonzero for other $\boldsymbol{\tau}$). In general, then, it is difficult to relate the CTMF, which is the strength of a sine-wave component of an nth-order lag product, to the probabilistic parameters of the signal constellation for arbitrary n and $\boldsymbol{\tau}$, whereas it is easy to relate the CTCF, which is the strength of a pure nth-order sine wave component in an nth-order lag product, to these parameters. However, if there is no lower-order cyclostationarity, then $R_{s_c}^{\alpha}(\boldsymbol{\tau})_n = C_{s_c}^{\alpha}(\boldsymbol{\tau})_n$, and the strength of the pure nth-order sine wave is equal to the strength of the impure nth-order sine wave. Thus, in this latter case, both strengths are directly proportional to $C_{a,n}$. The most common example of this is the case of $n = 4$ and 0% excess-bandwidth pulses (for example, partial response signals [3], of which duobinary signals are an example). For higher orders, it is much less likely that there will be no lower-order cyclostationarity and, therefore, the impure nth-order sine waves are more difficult to analyze. Nevertheless, we shall discover that designing a signal to exhibit minimum second-

and fourth-order cyclic cumulants results in a signal that has small second- and fourth-order cyclic moments as well.

In general, cyclic cumulants are signal selective and tolerant to Gaussian corruption, whereas cyclic moments are not [2, 4]. In addition, by inspection of the tables to be presented, the cumulants of the signal constellation get very large with increasing n whereas the moments do not (for a fixed constellation variance). Thus, an interceptor might be wise to compute cumulants instead of moments, and an LPI signal designer might be wise to focus on minimizing the exploitability of cumulants rather than moments. All these considerations lead us to focus on the cumulants of the signal constellation, rather than the moments.

3 Moments and Cumulants of Symbol Constellations

To better understand the nature of the cumulants and moments of the complex PAM signal $s_c(t)$, the values of $C_{a,n}$ and $R_{a,n}$ corresponding to some simple DQAM signals are presented in this section. The values of a_m (the signal constellation and associated probabilities) for $\theta_c = 0$ for BPSK, 4-level PAM, QPSK, 8PSK, 16PSK, 32PSK, 64PSK, 4QAM, 8QAM, 16QAM, and 64QAM signal types are tabulated in Table 1. The constellations are scaled so that their variance is equal to one.

For a few distributions of a_m (constellations), the nth-order cumulants can be computed analytically, but the resulting expressions always contain a number (a function of n) that can only be computed by means of a recursion or an infinite series. The values of moments and cumulants given in the tables herein were computed using a computer program written in C, and are shown in Tables 2, 3, and 4. This program can compute the nth-order moments and cumulants of any finite-alphabet random variable. The results for the analytically tractable cases match the corresponding results in the tables. Several analytical results concerning the cumulants of discrete random variables are given in Section 5. These moments and cumulants also indicate the relative strengths of the regeneratable sine waves for the various signal types that are listed. For example, the cumulants of BPSK grow most rapidly with the order n, indicating that this signal is the most detectable of those listed in the tables: in some sense the ± 1 binary random variable is the opposite of the Gaussian random variable. We have found no other random variable with larger cumulants. This observation is consistent with the fact that BPSK signal also exhibits the strongest second-order cyclostationarity of any known modulated signal.

4 Cycle Frequencies of Digital QAM Signals

From (7) and (8), the cycle frequencies of the complex-valued PAM signal (the complex envelope of the DQAM signal) are restricted to harmonics of the pulse rate $1/T_0$, and the width of the Fourier transform of the pulse function $p(t)$ determines the number of such harmonics that result in nonzero values of $C_{s_c}^{\beta}(\cdot)_n$. We'll not concern ourselves with the latter detail for now. We simply find the cycle frequencies for the analytic signal assuming that the complex envelope exhibits cyclostationarity at all harmonics of the pulse rate. This is the case, for example, when the function $p(t)$ is a rectangle with width T_0 because in this

case the Fourier transform $P(f)$ has infinite width. These results can be easily modified if the width (support) of $P(\cdot)$ is finite: there will be an upper limit to k in $|k|/T_0$ beyond which all cyclic cumulants are zero.

The cycle frequencies for the complex envelope for a particular modulation type can be determined by using the tables of values for the cumulants $C_{a,n}$. When $C_{a,n} = 0$, there are no cycle frequencies (because there are no features), and when $C_{a,n} \neq 0$, the cycle frequencies are simply the harmonics of the pulse rate.

Let A_n^m denote the cycle frequencies of the complex envelope $s_c(t)$ for order n with m factors conjugated. It can be shown by using results in [2] that the cycle frequency set B_n^m for the analytic signal is given by

$$B_n^m = \begin{cases} \{\alpha : \alpha = \gamma + (n-2m)f_c,\ \gamma \in A_n^m\}, & A_n^m \neq \emptyset, \\ \emptyset, & \text{otherwise.} \end{cases}$$

The cycle frequencies for the analytic-signal representations of some common digital communication signals are shown in Table 5.

5 Cumulants of Certain Discrete Random Variables

The cumulants of certain discrete random variables can be obtained by using the definition of the cumulant as the derivative of the logarithm of the characteristic function of the variable, say, A:

$$C_{A,n} = (i)^{-n} \frac{\partial^n}{\partial \omega^n} \ln \Phi(\omega) \bigg|_{\omega=0}.$$

Consider a binary symmetric real-valued random variable A with PDF

$$f_A(u) = \frac{1}{2}[\delta(u+a) + \delta(u-a)].$$

The characteristic function for A is

$$\Phi_A(\omega) = \cos(\omega a),$$

and the nth-order cumulant is given by

$$\begin{aligned} C_{A,n} &= (i)^{-n} \frac{\partial^n}{\partial \omega^n} \ln \Phi_A(\omega) \bigg|_{\omega=0} \\ &= (i)^{-n} \frac{\partial^{n-1}}{\partial \omega^{n-1}} \left[\frac{-a \sin(\omega a)}{cos(\omega a)} \right]_{\omega=0} \\ &= -a(i)^{-n} \frac{\partial^{n-1}}{\partial \omega^{n-1}} \tan(\omega a) \bigg|_{\omega=0}. \end{aligned}$$

Since

$$\tan(x) = \sum_{m=-\infty}^{\infty} \frac{(-1)^{m-1} 2^{2m} (2^{2m}-1) B_{2m}}{(2m)!} x^{2m-1},$$

where B_m is the mth Bernoulli number,

$$\frac{x}{e^x - 1} = \sum_{m=0}^{\infty} \frac{B_m x^m}{m!}, \tag{11}$$

the nth-order cumulant for A is zero for odd n, and for even n it simplifies to

$$C_{A,n} = \frac{a^n 2^n (2^n - 1) B_n}{n}. \tag{12}$$

Next, consider a quaternary symmetric variable with density function

$$f_A(u) = \frac{1}{4}[\delta(u+a) + \delta(u-a) + \delta(u+b) + \delta(u-b)].$$

The characteristic function for A is

$$\Phi_A(\omega) = \frac{1}{2}[\cos(\omega a) + \cos(\omega b)].$$

By using a trigonometric identity, the log-characteristic function can be expressed as

$$\ln \Phi_A(\omega) = \ln \cos(\omega[a+b]/2) + \ln \cos(\omega[a-b]/2).$$

It follows that the cumulant for A is given by

$$C_{A,n} = [(a+b)^n + (a-b)^n] \frac{B_n(2^n - 1)}{n}, \tag{13}$$

for even values of n, and is equal to zero for odd values of n. By looking up the values of the Bernoulli numbers, the values listed in Table 2 (for BPSK and 4-level PAM), which are obtained by numerical evaluation, can be confirmed[1].

6 Minimizing Cumulants

The cumulants of a binary symmetric random variable (12) are nonnegative and therefore their minima must correspond to the symbol values of $a = -a = 0$ (cf. (12)). Similarly, for the quaternary symmetric variable, the minimum cumulant (13) for each n corresponds to $a = b = 0$. However, if we incorporate the constraint that the variance of the variable must equal some constant, say 1, then it is not clear that there is no useful minimum. For example, for the symmetric quaternary random variable, if the variance is equal to 1, then the extrema of the fourth-order cumulant are given by the solutions to the following two equations

$$(a \pm \sqrt{2-a^2})^3 (1 \mp \frac{a}{\sqrt{2-a^2}}) + (a \mp \sqrt{2-a^2})^3 (1 \pm \frac{a}{\sqrt{2-a^2}}) = 0.$$

These equations are satisfied when $a = \pm 1$, and $a = 0$. The former two solutions result in the random variables $a_1 = 1$, $b_1 = -1$ with probabilities of 0.5, and the latter solution

[1] The first several Bernoulli numbers are given by $B_2 = 1/6, B_4 = -1/30, B_6 = 1/42, B_8 = -1/30$.

results in the random variable $a_1 = 0, b_1 = \sqrt{2}, b_2 = -\sqrt{2}$ with probabilities 0.5, 0.25, and 0.25, respectively. The fourth-order cumulant of the former random variable is given by (12) with $n = 4$ and $a = 1$ (which equals -2), and that for the latter random variable is given by

$$\frac{2\sqrt{2}^4 B_4(2^4 - 1)}{4} = -1.$$

These two random variables are not particularly useful because the associated DQAM signals still have relatively strong fourth-order cyclostationarity. It follows, then, that to obtain meaningful results from a minimization procedure, we must remove some of our constraints on the random variable distribution, that is, we must consider asymmetric random variables and/or those with unequal probabilities. In the case of the quaternary symmetric random variable, we might consider instead a quaternary equiprobable random variable with four arbitrary values, or we can allow the probabilities to deviate from 0.25, or both. In these cases, the resulting formulas for the cumulants are difficult to analyze, and we must resort to numerical methods.

In general, for a constellation with M real-valued symbols, the formula for $C_{a,n}$ is an nth-order polynomial in $2M$ variables (although one of the probability variables can be eliminated). Therefore, to minimize $|C_{a,n}|$ requires the simultaneous solution of $2M$ polynomial equations, with maximum order n. As seen from the example above, additional constraints (such as unit variance) must be incorporated for the results to be meaningful. Because of the large number of variables and the nonlinear nature of the equations, this problem appears to be generally too difficult to solve analytically, and so numerical methods must be used.

7 Constraints for Complex Symbols

In general, we consider the problem of finding a four-symbol signal constellation with minimum the fourth-order cumulant subject to the following constraints on the symbol variable:

1. Zero mean
2. Unit variance
3. No two symbols are the same (unique symbols)
4. No symbol has zero probability
5. Certain second-, third-, and fourth-order moments are zero.

The signal-design considerations that lead to these constraints are explained in detail next.

In order for the designed DQAM signal to be useful, the mean of the constellation must be zero for power efficiency. To compare the cumulants of the candidate constellations, it is necessary to normalize them somehow. The normalization chosen is unit variance. This constraint is important because the cumulants can be made very small (i.e., zero) by setting all the symbols to zero, and this trivial solution must be avoided. In order for the designed DQAM signal to be useful, the symbols must be unique, no symbol can have zero probability,

and the symbol magnitude cannot exceed some constant. If a symbol has zero probability, the constellation has fewer than the desired number of elements, that is, the bits can be coded with fewer than the specified number of symbols. The problem of finding a minimum cumulant for this smaller constellation size is deemed a distinct problem. If the symbols are not unique, then again we have a smaller-size constellation. Finally, the bound on the symbol magnitude is necessary to bound the dynamic range of the resultant DQAM signal.

Let $\{a_j\}_{j=1}^{M}$ denote the complex-valued symbols of the complex-envelope signal representation of the passband signal. Symbol a_j occurs with probability p_j. The foregoing constraints can be expressed mathematically as follows:

$$\sum_{j=1}^{M} a_j p_j = 0, \tag{14}$$

$$\sum_{j=1}^{M} |a_j|^2 p_j = 1, \tag{15}$$

$$0 \leq |a_j| < K, \quad 1 \leq j \leq M, \tag{16}$$

$$1 < p_j < \epsilon_2, \quad 1 \leq j \leq M. \tag{17}$$

The remaining constraints follow from forcing the carrier-related cyclic cumulant features for orders two, three, and four to zero, and then finding the constellation that minimizes the fourth-order symbol-rate features by minimizing the appropriate fourth-order cumulant.

The second-order cyclostationarity (SOCS) that is associated with the symbol-rate cycle frequencies vanishes because the pulse is assumed to have positive-frequency bandwidth less than or equal to half the pulse rate. The SOCS that is associated with the carrier frequency vanishes if the second-order cumulant of the symbol variable with no conjugations is zero, which leads to the fifth constraint:

$$C_{a,2}^{0} = \sum_{j=1}^{M} a_j^2 p_j = 0. \tag{18}$$

Equation (18) follows from (14); that is, the second-order cumulant is equal to the second-order moment if the mean is zero. Constraint (18) implies that the second-order cumulant with both factors conjugated ($C_{a,2}^{2}$) is also zero. Notice that the notation $C_{a,p}^{q}$ is used to denote the pth-order cumulant of a with q conjugated factors.

The third-order features are forced to zero in a similar manner. Because the third-order cumulants of the symbol variable are equal to the third-order moments with certain products of lower-order moments subtracted off (each of which contains at least one occurrence of the mean), the two constraints on the third-order cumulants reduce to the following:

$$C_{a,3}^{0} = (C_{a,3}^{3})^* = \sum_{j=1}^{M} a_j^3 p_j = 0, \tag{19}$$

$$C_{a,3}^{1} = (C_{a,3}^{2})^* = \sum_{j=1}^{M} a_j^2 a_j^* p_j = 0. \tag{20}$$

Similarly, the carrier-related fourth-order cyclic cumulant features, which occur for 0, 1, 3, and 4 conjugated factors are forced to zero by the following two constraints:

$$C_{a,4}^{0} = (C_{a,4}^{4})^{*} = \sum_{j=1}^{M} a_j^4 p_j = 0, \tag{21}$$

$$C_{a,4}^{1} = (C_{a,4}^{3})^{*} = \sum_{j=1}^{M} a_j^3 a_j^{*} p_j = 0. \tag{22}$$

If all these constraints are met, then the remaining cyclostationarity of order four or less can only occur for order four with two conjugated factors, which is cyclostationarity associated with the pulse rate. The goal of the numerical processing is to find the symbols and associated probabilities that meet the constraints (14)–(22) and minimize the fourth-order cumulant that is associated with the symbol-rate cyclic features:

$$C_{a,4}^{2} = \sum_{j=1}^{M} |a_j|^4 p_j - 2 \left[\sum_{j=1}^{M} |a_j|^2 p_j \right]^2 . \tag{23}$$

8 Constraints for Real Symbols

As with complex symbols, the constraints on real symbols can be determined by remembering that the symbols correspond to a PAM signal that multiplies a complex-valued carrier wave. It is desired to eliminate the cyclostationarity of the modulated signal. This can be done by minimizing the first-, third-, and fourth-order cumulants of the PAM signal by minimizing the cumulants of the symbol variable. Constraints (14)–(17) apply unchanged. The SOCS associated with the doubled-carrier frequency cannot be eliminated from the signal without forcing the power or bandwidth to zero. The third-order cyclostationarity is destroyed by constraint (19). The objective is to minimize the fourth-order cumulant of the symbol variable:

$$C_{a,4} = \sum_{j=1}^{M} a_j^4 p_j - 3 \left[\sum_{j=1}^{M} a_j^2 p_j \right]^2$$

subject to (14)–(17) and (19).

9 Digital QAM Signals From Real Random Variables

Although the real-valued distributions obtained by meeting the constraints described in the previous section cannot directly be used to construct a complex-valued digital QAM signal with small second-, third-, and fourth-order cyclic features, they can be used *indirectly* to do so, that is, the resulting signal has a complex-valued PAM representation that meets the constraints of Section 7, with the single exception of (21). Nevertheless, the cumulant $C_{a,4}^{0}$ is made as small as the cumulant that is minimized ($C_{a,2}^{2}$), as explained next.

Let b and c be independent and identically distributed real-valued random variables that meet the constraints of the previous section, and let these random variables have fourth-order

cumulant C. The results of Appendix A imply that the complex-valued random variable $a = (b + ic)/\sqrt{2}$ has the following cumulants:

$$\begin{aligned} C_{a,1}^0 &= 0 \\ C_{a,2}^0 &= 0 \\ C_{a,2}^1 &= 1 \\ C_{a,3}^0 &= 0 \\ C_{a,3}^1 &= 0 \\ C_{a,4}^0 &= C/2 \\ C_{a,4}^1 &= 0 \\ C_{a,4}^2 &= C/2. \end{aligned}$$

It follows that minimizing the fourth-order cumulant of b minimizes the fourth-order cumulants of a.

10 Numerical Methods of Minimization

The two numerical methods used to find random variables with minimum fourth-order cumulants are described in this section.

10.1 Exhaustive Search

This program searches for the real- or complex-valued symbol constellation that gives the smallest nth-order cumulant by exhaustive search. The range of symbol values and the fineness of the search grid are among the input parameters. An optional input parameter is an initial constellation, so that results from a coarse search can be refined. The symbol variable range and the probabilities are discretized and the constraints are checked for each possible combination of symbols and probabilities (with the additional constraint that the probabilities must sum to one). If the constraints are met, then the fourth-order cumulant is computed and compared to the minimum obtained thus far. This program is computationally expensive for random variables with large alphabet size, and can only be used to find small-alphabet distributions by using the currently available computing resources.

10.2 Gaussian Approximation

The real-valued discrete random variable with uniform spacing and with minimum nth-order cumulant obtained by approximating the Gaussian PDF is sought. By uniform spacing we mean that the difference between every two adjacent symbols (on the real line) is a constant. This approximation is specified by two parameters: *width* and *size*. The *width* parameter is the width of the Gaussian distribution that is split into *size* pieces, the centers of which are uniformly spaced. Thus, the first element in the constellation corresponds to the amount of area in the tail of the Gaussian, and subsequent elements have probability equal to the

area of the Gaussian centered at the element value, with width equal to *width/size*. The parameter *size* is equal to the size of the desired signal constellation.

This approximation method is an attempt to answer the question: Where does one place *size* impulses on the real line such that the higher-order cumulants for the resultant PDF are minimum?

11 Numerical Results

11.1 Real-Valued Constellations

In the case of real-valued variables, the exhaustive search method is used for the case of $M = 4$, and the Gaussian approximation method is used for $M = 4, 8$, and 16.

In the case of exhaustive search, the four symbols are constrained to have magnitude greater than or equal to 0.0, but less than or equal to $K = 3.0$. For a symbol grid with fineness δa and probability grid with fineness $\delta p = \epsilon_2$, the results of the computer searches using the exhaustive search method are shown in Table 6. For the case of equiprobable symbols, $\delta a = 0.05$, and the same bounds on the symbol magnitude, the resulting distribution is ± 1.4, ± 0.15, and the cumulant corresponding to this distribution has magnitude 1.03. Note that this distribution is close to that obtained by analysis in Section 6.

The Gaussian approximation technique yields the minimum cumulants and corresponding constellations shown in Table 7. For the case of $M = 4$, preliminary searches showed that the optimal width parameter was between 4.0 and 5.0, and for $M = 8$ and 16, it was between 5.0 and 6.0. For each of these cases, 1000 widths falling between the stated lower and upper bounds were used.

11.2 Complex-Valued Constellations

The exhaustive searches for complex-valued random variables were not as fruitful as those for real-valued random variables. In particular, the same alphabet size ($M = 4$) and bound on symbol magnitude ($K = 3$) parameters as used in the real-valued search were used in the search for complex-valued variables. The constraint (21) was omitted in light of the results of Appendix A, and the probabilities are constrained to be equal. The results are listed in Table 8. This random variable corresponds to a QPSK or 4QAM signal. The result is significant because it implies that the symbol alphabet size M is not large enough to allow the simultaneous satisfaction of the various constraints and small cumulant value. However, searching for larger-alphabet random variables is prohibitively computationally costly with available computing resources. As shown in the next section, there do indeed exist larger alphabet complex-valued random variables with small fourth-order cumulants.

11.3 Low-Probability-of-Intercept Signals

In this section, some of the distributions that were found by the aforementioned numerical techniques are used to design digital QAM signals. The strengths of the regenerated sine

waves (both pure and impure) for orders two, three, and four are measured and tabulated, and are compared to the strengths of BPSK, 16QAM, and duobinary signals.

The complex-valued random variables that are needed to create the complex-valued PAM signals are constructed from the minimum-cumulant real-valued random variables as described in Section 9. That is, let b and c be independent real-valued random variables with some minimum-cumulant distribution. The complex-valued random variable $a = (b+ic)/\sqrt{2}$ is used to create the PAM signal, which is the baseband representation of the radio-frequency digital QAM signal. The pulse function $p(t)$ is that for duobinary signaling [3]. This choice, as noted previously, eliminates the second-order cyclostationarity that is associated with the pulse rate. Two such signals, one corresponding to row three of Table 6 and the other corresponding to row one of Table 7, were simulated and their second-, third-, and fourth-order cyclic moments and cumulants for $\alpha = 0$ and $1/T_0$ were measured. The former signal is denoted by S_1 and the latter by S_2. The results are shown in Table 10. Similar measurements for three common digital communication signals are included for comparison. The signals were generated using independent bit sequences, and the total data length is 32768 samples, which corresponds to 4096 symbols. It can be seen from the table that the strengths of the cumulant sine waves for the signals S_1 and S_2 are very much smaller than those for the other three signals, indicating that the two signals have great potential to avoid detection by SOCS and cumulant-based interception techniques. Measurements of the cyclic moments were also made. The results are shown in Table 11. The results in the table indicate that the designed signals also have potential to avoid detection by moment-based interception techniques.

Finally, Table 9 provides one means for coding a bit stream into the symbols corresponding to S_1. The idea is to code each incoming pair of bits (which are equiprobable by assumption) into one of several symbols according to a particular probability rule. Thus, each dibit is not coded into a unique symbol (except for the dibit 00), but each received symbol can be decoded into only one dibit. In the table, the third column contains the probabilities that each symbol will be chosen as the transmitted symbol, given that the dibit in the first column is presented to the coder. It is evident that the price paid for low probability of intercept is an increased number of states in the modulation, which may in turn necessitate more power in the tranmitted signal for accurate demodulation.

12 Conclusions

This report documents a study of the possibility of designing low-probability-of-intercept signals by minimizing the cumulants of the complex-envelope representation of digital QAM signals. In particular, digital QAM signals at radio frequencies can be represented by complex-valued pulse-amplitude-modulated signals at baseband, and the cumulants of the discrete random variable used to modulate the pulses in this complex-envelope signal are studied for common modulation formats. These cumulants are directly proportional to the cumulants of the radio frequency signal. Discrete random variable distributions are sought that possess minimum cumulants and, therefore, that minimize the cumulants of the passband signal.

Several numerical methods are used to find such random variable distributions (for real-valued variables), complex-valued partial-response digital QAM signals are constructed from

these distributions, and their cumulants are measured. These cumulants are shown to be much less than those for ordinary digital QAM signals, and are less than those for commonly used partial-response signals. In addition, the moments of these signals are measured and are also seen to be small. Thus, these newly designed signals have potential as covert signals.

Searching directly for complex-valued random variable distributions was found to be too computationally costly for cases of interest. In particular, the size of the symbol constellation was limited to four. For this constellation size, the minimum fourth-order cumulant was found to be equal to -1, and the corresponding constellation is that for QPSK signaling. This is not a particularly small cumulant, since several constellations that were obtained by using real-valued random variables yielded fourth-order cumulants of about -0.01 and -0.001, but for a constellation size of sixteen. There is the possibility that better designs exist, but they cannot be found in a reasonable amount of time without substantially increased computing speed.

A numerical method based on approximating the continuous Gaussian probability density function with a discrete random variable was found to be computationally simple, but yields random variables whose cumulants that are larger than those found by exhaustive search. If distributions with larger alphabets than sixteen are desired, it is recommended that the exhaustive search method be used.

PDF	Size	Constellation Points (Values of a_m)
BPSK	2	± 1
4-level PAM	4	$(\pm 1, \pm 3) \times \sqrt{5}/5$
8-level PAM	8	$\pm 1, \pm 3, \pm 5, \pm 7 \times 1/\sqrt{21}$
QPSK	4	$\pm 1, \pm i$
8PSK	8	$\pm\sqrt{2}/2 \pm \sqrt{2}/2i, \pm 1 \pm i$
16PSK	16	$\exp(i2\pi q/16), q = 0, \cdots, 15$
32PSK	32	$\exp(i2\pi q/32), q = 0, \cdots, 31$
64PSK	64	$\exp(i2\pi q/64), q = 0, \cdots, 63$
4QAM	4	$\pm\sqrt{2}/2 \pm i\sqrt{2}/2$
8QAM	8	$(\pm 1, \pm i, \pm 1 \pm i) \times \sqrt{2/3}$
16QAM	16	$(\pm 1 \pm i, \pm 1 \pm i/3, \pm 1/3 \pm i/3, \pm 1/3 \pm i) \times 3/\sqrt{10}$
64QAM	64	$(\pm q/7 \pm ir/7) \times \sqrt{7/6}$, for $q, r = 1, 3, 5, 7$

Table 1: Numerical values of the points in the symbol constellations that correspond to some common digital communication signals.

References

[1] W. A. Gardner, *Statistical Spectral Analysis: A Nonprobabilistic Theory,* Prentice-Hall, Englewood Cliffs, New Jersey, 1987.

[2] C. M. Spooner. "Theory and Application of Higher-Order Cyclostationarity," Ph.D. Dissertation, Dept. of Electrical and Computer Engineering, University of California, Davis, CA, June 1992.

[3] A. Lender, "The Duobinary Technique for High-Speed Data Transmission," *IEEE Transactions on Communications and Electronics,* Vol. 82, No. 5, pp. 214–218, 1963.

[4] C. M. Spooner and W. A. Gardner. "The Cumulant Theory of Cyclostationary Time-Series, Part I: Foundation; Part II: Development and Applications," *IEEE Transactions on Signal Processing*, in press.

[5] W. A. Gardner, "Signal Interception: A Unifying Theoretical Framework for Feature Detection," *IEEE Transactions on Communications* **36**, pp. 897–906, 1988.

[6] W. A. Gardner and C. M. Spooner, "Signal Interception: Performance Advantages of Cyclic-Feature Detectors," *IEEE Transactions on Communications,* **40**, 1992.

[7] W. A. Gardner and C. M. Spooner, "Weak-Signal Detection and Source Location: Simplifications of the Maximum-Likelihood Receiver," *IEEE Transactions on Communications,* **41,** June 1993.

[8] W. A. Gardner and C. K. Chen, "Signal-Selective Time-Difference-of-Arrival Estimation for Passive Location of Man-made Signal Sources in Highly Corruptive Environments. Part I: Theory and Method," *IEEE Transactions on Signal Processing* **40**, pp. 1168–1184, 1992.

[9] C. K. Chen and W. A. Gardner, "Signal-Selective Time-Difference-of-Arrival Estimation for Passive Location of Man-made Signal Sources in Highly Corruptive Environments. Part II: Algorithms and Performance," *IEEE Transactions on Signal Processing* **40**, pp. 1185–1197, 1992.

A Cumulants of a Constructed Complex Variable

Suppose b and c are independent identically distributed real-valued random variables such that the following hold:

$$E[b] = E[c] = 0 \tag{24}$$
$$E[b^2] = E[c^2] = 1 \tag{25}$$
$$E[b^3] = E[c^3] = 0 \tag{26}$$
$$E[b^4] = E[c^4] = C + 3. \tag{27}$$

Find the cumulants of the random variable $a = b + ic$.

$$E[a] = C_{1,0} = C_{1,1}^* = E[b] + iE[c] = 0$$
$$E[|a|^2] = C_{2,1} = E[b^2 + c^2] = 1 + 1 = 2$$

$$
\begin{aligned}
E[a^2] &= C_{2,0} = C_{2,2}^* \\
&= E[b^2 - c^2 + 2ibc] = 1 - 1 + 0 = 0 \\
E[a^3] &= C_{3,0} = C_{3,3}^* = E[(b+ic)^3] \\
&= E[b^3 + 3ib^2c + 3b(ic)^2 + (ic)^3] = 0 \\
E[a^2a^*] &= C_{3,1} = C_{3,2}^* = E[(b+ic)^2(b-ic)] \\
&= E[b^3] + iE[c^3] + iE[b^2c] + E[bc^2] = 0 \\
E[a^4] &= C_{4,0} = C_{4,4}^* \\
&= E[(b+ic)^4] \\
&= E\left[\sum_{n=0}^{4} \binom{4}{n} b^n (ic)^{4-n}\right] \\
&= E[c^4 + b^4 - 6c^2b^2] = 2C \\
E[a^3a^*] &= C_{4,1} = C_{4,3}^* = E[(b+ic)^3(b-ic)] \\
&= E[b^4] - E[c^4] = 0 \\
E[|a|^4] &= C_{4,2} + 2E[|a|^2]^2 = C_{4,2} + 8 \\
&= E[b^4 + c^4 + 2b^2c^2] = 2E[c^4] + 2 \\
&\Rightarrow C_{4,2} = 2C.
\end{aligned}
$$

Constellation (PDF)	M/C	Order n				
		2	4	6	8	10
BPSK	M	1.0	1.0	1.0	1.0	1.0
4-level PAM	M	1.0	1.64	2.92	5.25	9.45
8-level PAM	M	1.0	1.76	3.62	7.92	17.9
BPSK	C	1.0	-2.0	16.0	-272.0	7936.0
4-level PAM	C	1.0	-1.36	8.32	-111.85	2603.14
8-level PAM	C	1.0	-1.24	7.19	-92.0	2039.5

Table 2: The moments (M) and cumulants (C) for the real-valued signal constellations shown in Table 1. The constellations are scaled so that their variance is one. Moments and cumulants for odd values of n are equal to zero.

PDF	Order of Moment (n)									
	4		6		8			10		
	Number of conjugated variables (m)									
	$0,4$	2	$1,5$	3	$0,8$	$2,6$	4	$1,9$	$3,7$	5
QPSK	1.0	1.0	1.0	1.0	1.0	1.0	1.0	1.0	1.0	1.0
8PSK	0.0	1.0	0.0	1.0	1.0	0.0	1.0	1.0	0.0	1.0
16PSK	0.0	1.0	0.0	1.0	0.0	0.0	1.0	0.0	0.0	1.0
32PSK	0.0	1.0	0.0	1.0	0.0	0.0	1.0	0.0	0.0	1.0
64PSK	0.0	1.0	0.0	1.0	0.0	0.0	1.0	0.0	0.0	1.0
4QAM	-1.0	1.0	-1.0	1.0	1.0	-1.0	1.0	1.0	-1.0	1.0
8QAM	-0.67	1.11	-1.04	1.33	1.68	-1.48	1.68	2.17	-2.04	2.17
16QAM	-0.68	1.32	-1.32	1.96	2.2	-2.48	3.12	4.3	-4.58	5.22
64QAM	-0.62	1.38	-1.3	2.23	1.91	-2.76	3.96	4.48	-5.94	7.58

Table 3: The moments for the complex-valued signal constellations shown in Table 1. All constellations have a mean of zero and second-order moment (variance) of 1. The moments for values of m not shown in the table are zero, as are moments for odd orders n.

PDF	Order of Cumulant (n)									
	4		6		8			10		
	Number of conjugated variables (m)									
	$0,4$	2	$1,5$	3	$0,8$	$2,6$	4	$1,9$	$3,7$	5
QPSK	1.0	-1.0	-4.0	4.0	-34.0	34.0	-34.0	496.0	-496.0	496.0
8PSK	0.0	-1.0	0.0	4.0	1.0	0.0	-33.0	-8.0	0.0	456.0
16PSK	0.0	-1.0	0.0	4.0	0.0	0.0	-33.0	0.0	0.0	456.0
32PSK	0.0	-1.0	0.0	4.0	0.0	0.0	-33.0	0.0	0.0	456.0
64PSK	0.0	-1.0	0.0	4.0	0.0	0.0	-33.0	0.0	0.0	456.0
4QAM	-1.0	-1.0	4.0	4.0	-34.0	-34.0	-34.0	496	496	496
8QAM	-0.67	-0.89	2.30	3.33	-13.9	-17.9	-26.3	178	245	352
16QAM	-0.68	-0.68	2.08	2.08	-14.0	-14.0	-14.0	162.7	162.7	162.7
64QAM	-0.62	-0.62	1.8	1.8	-11.5	-11.5	-11.5	127.5	127.5	127.5

Table 4: The cumulants for the complex-valued signal constellations shown in Table 1. All constellations have a mean of zero and second-order cumulant (variance) of 1. The cumulants for values of m not shown in the table are zero, as are the cumulants for odd orders n.

n	m	Modulation Type				
		BPSK	QPSK	8PSK	MPSK ($M \geq 16$)	APK
2	0,2	$k/T_0 \pm 2f_c$	$\emptyset$	$\emptyset$	$\emptyset$	$\emptyset$
2	1	k/T_0	k/T_0	k/T_0	k/T_0	k/T_0
4	0,4	$k/T_0 \pm 4f_c$	$k/T_0 \pm 4f_c$	$\emptyset$	$\emptyset$	$k/T_0 \pm 4f_c$
4	2	k/T_0	k/T_0	k/T_0	k/T_0	k/T_0
6	0,6	$k/T_0 \pm 6f_c$	$\emptyset$	$\emptyset$	$\emptyset$	$\emptyset$
6	1,5	$k/T_0 \pm 4f_c$	$k/T_0 \pm 4f_c$	$\emptyset$	$\emptyset$	$k/T_0 \pm 4f_c$
6	3	k/T_0	k/T_0	k/T_0	k/T_0	k/T_0
8	0,8	$k/T_0 \pm 8f_c$	$k/T_0 \pm 8f_c$	$k/T_0 \pm 8f_c$	$\emptyset$	$k/T_0 \pm 8f_c$
8	2,6	$k/T_0 \pm 4f_c$	$k/T_0 \pm 4f_c$	$\emptyset$	$\emptyset$	$k/T_0 \pm 4f_c$
8	4	k/T_0	k/T_0	k/T_0	k/T_0	k/T_0
10	0,10	$k/T_0 \pm 10f_c$	$\emptyset$	$\emptyset$	$\emptyset$	$\emptyset$
10	1,9	$k/T_0 \pm 8f_c$	$k/T_0 \pm 8f_c$	$k/T_0 \pm 8f_c$	$\emptyset$	$k/T_0 \pm 8f_c$
10	3,7	$k/T_0 \pm 4f_c$	$k/T_0 \pm 4f_c$	$\emptyset$	$\emptyset$	$k/T_0 \pm 4f_c$
10	5	k/T_0	k/T_0	k/T_0	k/T_0	k/T_0

Table 5: Potential cycle frequencies for the analytic signals corresponding to digital QAM signals. There are no cycle frequencies for the values of m that are not shown in the table, nor for odd values of n. The + sign is associated with the first value of m. The range of k for a given signal depends on the excess bandwidth.

$\delta a, \delta p$	Symbols and Probabilities								$C_{a,4}$
0.25, 0.1	2.0	0.1	-2.0	0.1	0.5	0.4	-0.5	0.4	0.25
0.1, 0.1	2.0	0.1	-2.0	0.1	0.5	0.4	-0.5	0.4	0.25
0.05, 0.1	-2.0	0.1	1.6	0.2	0.3	0.2	-0.35	0.5	-0.028
0.05, 0.05	2.45	0.05	-0.85	0.05	-1.45	0.25	0.45	0.65	-0.00175
Equiprobable constraint									
0.05, N/A	1.4	0.25	-1.4	0.25	0.15	0.25	-0.15	0.25	-1.03

Table 6: Results of a numerical search for real-valued distributions with minimum the fourth-order cumulant.

M	Symbols and Probabilities								$C_{a,4}$
4	-1.75	0.122	1.75	0.122	-0.582	0.378	0.582	0.378	-0.65
8	$\pm$2.29	0.025	$\pm$1.64	0.070	$\pm$0.98	0.161	$\pm$0.33	0.244	-0.32
16	$\pm$2.74	0.005	$\pm$2.37	0.009	$\pm$2.01	0.020	$\pm$1.64	0.038	-0.14
	$\pm$1.28	0.065	$\pm$0.91	0.096	$\pm$0.55	0.125	$\pm$0.18	0.143	

Table 7: Results of approximating the Gaussian distribution to obtain real-valued distributions with minimum the fourth-order cumulant.

δa	Symbols				$C_{a,4}$
0.5	-1.0 + i0.0	1.0 + i0.0	0.0 + i	0.0 - i	-1.0
0.25	-1.0 + i0.0	1.0 + i0.0	0.0 + i	0.0 - i	-1.0

Table 8: Results of a numerical search for complex-valued distributions with minimum the fourth-order cumulant. The symbols are constrained to have equal probabilities.

Bit Pair	Constellation Point	Coding Probability
00	(-0.35, -0.35)	1
01	(-2.0, -2.0)	0.04
	(1.6, 1.6)	0.16
	(1.6, -0.35)	0.40
	(0.3, -0.35)	0.40
10	(-2.0, 1.6)	0.08
	(1.6, 0.3)	0.16
	(0.3, 1.6)	0.16
	(-0.35, -2.0)	0.20
	(-0.35, 1.6)	0.40
11	(-2.0, 0.3)	0.08
	(-2.0, -0.35)	0.20
	(1.6, -2.0)	0.08
	(0.3, -2.0)	0.08
	(0.3, 0.3)	0.16
	(-0.35, 0.3)	0.40

Table 9: A possible coding of an independent, equiprobable bit stream into the symbols associated with signal S_1.

n	m	α	BPSK	Duobinary	16QAM	S_1	S_2
2	0	$2f_c$	0.0	0.0	−29.4	−35.8	−35.8
2	0	$2f_c \pm 1/T_0$	−9.7	−120.0	−37.4	−120.0	−120.0
2	1	0	0.0	0.0	0.0	0.0	0.0
2	1	$\pm 1/T_0$	−9.7	−120.0	−9.4	−120.0	−120.0
3	0	$3f_c$	−46.2	−37.1	−31.3	−32.1	−34.0
3	0	$3f_c \pm 1/T_0$	−56.6	−62.1	−39.2	−59.5	−55.2
3	1	f_c	−46.2	−37.1	−35.6	−40.9	−30.3
3	1	$f_c \pm 1/T_0$	−56.6	−62.1	−43.1	−51.5	−62.5
4	0	$4f_c$	6.0	1.6	−3.4	−30.6	−15.5
4	0	$4f_c \pm 1/T_0$	−4.0	−21.9	−13.6	−48.3	−33.4
4	1	$2f_c$	6.0	1.6	−27.4	−25.5	−33.5
4	1	$2f_c \pm 1/T_0$	−4.0	−21.9	−38.6	−43.4	−47.6
4	2	0	6.0	1.6	−3.3	−40.4	−14.4
4	2	$\pm 1/T_0$	−4.0	−21.9	−12.2	−46.8	−36.4

Table 10: Peak pure (cumulant) sine-wave strengths (in dB) for various complex-valued digital communication signals for orders n of 2, 3, and 4, and for various numbers of conjugated factors m. S_1 is the signal obtained by using a minimum-cumulant real-valued distribution, and S_2 is the signal obtained by using a minimum-cumulant real-valued distribution obtained by Gaussian approximation.

n	m	α	BPSK	Duobinary	16QAM	S_1	S_2
2	0	$2f_c$	0.0	0.0	−30.6	−28.6	−33.2
2	0	$2f_c \pm 1/T_0$	−9.2	−120.0	−37.6	−120.0	−120.0
2	1	0	0.0	0.0	0.0	0.0	0.0
2	1	$\pm 1/T_0$	−9.2	−120.0	−9.5	−120.0	−120.0
3	0	$3f_c$	−40.2	−31.5	−35.4	−31.0	−25.9
3	0	$3f_c \pm 1/T_0$	−49.8	−56.1	−40.0	−50.5	−53.6
3	1	f_c	−40.2	−31.5	−37.8	−32.2	−33.7
3	1	$f_c \pm 1/T_0$	−49.8	−56.1	−43.0	−53.8	−51.1
4	0	$4f_c$	0.0	5.3	−3.3	−32.3	−15.1
4	0	$4f_c \pm 1/T_0$	−10.1	−20.6	−13.5	−47.2	−32.6
4	1	$2f_c$	0.0	5.3	−36.4	−17.4	−26.1
4	1	$2f_c \pm 1/T_0$	−10.1	−20.6	−45.4	−43.6	−40.5
4	2	0	0.0	5.3	2.5	6.1	5.2
4	2	$\pm 1/T_0$	−10.1	−20.6	−7.9	−50.6	−38.6

Table 11: Peak impure (moment) sine-wave strengths (in dB) for various complex-valued digital communication signals for orders n of 2, 3, and 4, and for various numbers of conjugated factors m. S_1 is the signal obtained by using a minimum-cumulant real-valued distribution, and S_2 is the signal obtained by using a minimum-cumulant real-valued distribution obtained by Gaussian approximation.

Signal Detection and Sorting Using Cyclic Cumulants in the General Search Algorithm

by

Chad M. Spooner and William A. Gardner

Abstract

The problem of determining the number of cyclostationary signals that are present (if any) in a given data record is considered in this report. The signals can be completely spectrally and temporally overlapping. Nothing is assumed about the signals except that they exhibit cyclostationarity of some order. The detection algorithm, called the *general search algorithm*, can be interpreted as a blind order-recursive cyclic-cumulant estimator, and is tested on a variety of signal records containing one, two, and three cochannel signals. The results indicate that the algorithm works well and merits further study and refinement.

1 Introduction

When confronted with the problem of intercepting signals that do not originate from friendly transmitters, one of the first pieces of information required is whether or not a signal is present in the given data record. This signal detection problem becomes a bit more general—and more difficult—if one allows for the possibility of the presence of multiple signals in the data. In this report, the detection, enumeration, and characterization of multiple spectrally and temporally overlapping unknown signals is studied from the point of view of exploiting the structure of the statistics of communication signals. In particular, many (if not most) communication signals are more accurately modeled as cyclostationary signals rather than as stationary signals. It is possible to exploit the properties of the statistics of cyclostationary signals to successfully perform the tasks of detection, extraction, direction-finding, signal classification, and others even when the data contains multiple temporally and spectrally overlapping signals [1]–[21], [30, 31].

This report documents an initial inquiry into the possibility of using the higher-order moments and cumulants of a cyclostationary data record to determine the number of signals present in the record and to estimate some of their modulation parameters. The signals of interest herein are continuous-phase frequency-shift keying (CPFSK), phase-shift keying (PSK) and, more generally, digital quadrature-amplitude modulation (QAM), although the basic search algorithm will work for any cyclostationary signal. It is the processing of the output of the search algorithm that must be tailored to more specific signal classes.

A typical scenario of interest is described in the following. Suppose a given data record contains a binary PSK (BPSK) signal, a quaternary PSK (QPSK) signal, and an offset QPSK (OQPSK) signal as well as additive white Gaussian noise (WGN). This complex-valued data record is obtained by downconverting and sampling the original radio-frequency data. The carrier frequencies of the signals are sufficiently closely spaced so as to preclude linear time-invariant filtering to separate the signals. The processor does not know that these signals are present in the data record. The goal of the processing is to determine the number of signals that are present and to estimate their keying rates and, possibly, their carrier offsets (the differences between their carrier frequencies and the frequency used for downconversion).

The key to the method that is documented in this report is that the signals are statistically independent, which implies that the nth-order temporal cumulant function (TCF) for the data is asymptotically equal to the sum of the nth-order temporal cumulant functions for the individual signals. Each of these cumulant functions is a periodic or polyperiodic function of time, which can be expressed in a Fourier series. The frequencies of the Fourier components are related to the modulation parameters (the keying rate and carrier offset) of the signals. If the Fourier frequencies for each individual signal are distinct, then the Fourier components (sine waves) of each signal's nth-order temporal cumulant function can be estimated from the polyperiodic nth-order temporal cumulant function of the data. Thus, using the cumulant provides for a kind of signal selectivity in the processing. Alternatively, nth-order temporal moment functions can often be used to estimate the frequencies of the Fourier components of TCFs, but these parameters are not signal selective in general. That is, the amplitude and phase of the sine-wave components of the periodic or polyperiodic nth-order temporal moment function are functions of all signals that are present in the data, but only some of the frequencies are functions of all the signals. Thus, temporal moments can be analyzed for the purpose of detection, but are not useful for classification unless there is only one signal present (and no noise). A companion report presents some ideas for using cumulants to perform signal-selective modulation classification.

The remainder of the report is organized as follows. In Section 2 the problem of interest is stated and the reasons that it is difficult to solve are discussed. In Section 3 the proposed solution is described in detail, and some illustrative examples are provided in Section 4. Section 5 presents the results of several computer simulations for signals of practical interest, and conclusions are drawn in Section 6. The theory of the higher-order statistics of cyclostationary signals that forms the basis for the approach taken here is reviewed in Appendix A.

2 The General Search Problem

In this report, we are interested in solving the *general search problem.* The general search problem is defined as the problem of detecting the presence of all cyclostationary signals

present in a given finite-length data record. The problem is difficult in that there is little prior knowledge with which to devise an algorithmic solution. Classical decision theory is not tractable because no particular probabilistic models for the signals are assumed (except that they are cyclostationary), the signals are random with unknown power levels and modulation types, and the noise is arbitrary. If the signals occupy disjoint portions of the spectrum, then energy detection and filtering could be used to detect and sort the signals, but if the signals are spectrally overlapping, then both energy detection and filtering are ineffective. The kind of processing necessary is that for which the output of the processing can be effectively partitioned into subgroups, each of which can be associated with one and only one signal in the data. Since linear time-invariant processing is not effective (filtering cannot separate the signals) and second-order time-invariant statistical processing is also not effective (energy detection), both nonlinear and time-varying statistical signal processing are possibilities. As it turns out, cumulants of cyclostationary signals are polyperiodically time-varying parameters obtained by nonlinear operations.

The general approach is motivated by the two assumptions that are made: (i) the signals are cyclostationary and (ii) the signals are statistically independent. In words, and at the risk of oversimplifying, the approach consists of estimating the amplitude, frequency, and phase of all finite-strength additive sine-wave components that appear in the output of specific polynomial transformations of the data (TCFs). The sine-wave frequencies are then grouped by exploiting harmonic relationships.

The nth-order TCF can be analytically calculated for a large class of communication signals. This class is defined by its complex-envelope representation, which is a complex-valued pulse-amplitude-modulated signal with independent, identically distributed symbols and arbitrary pulse function. This class includes as special cases PSK, OOK, and Mary-QAM. For each order n and choice of the number of optional conjugations m, the nth-order TCF can be written as a Fourier series in which each sine-wave component has complex-valued amplitude given by the nth-order cyclic temporal cumulant function (CTCF). Thus, it is possible to list the amplitudes, frequencies, and phases for each order for signals of this class. A partial list of potential cycle frequencies is given in Table 1. As evidenced by the table, distinct modulation types give rise to distinct patterns (over n and m) of

cumulant sine-wave frequencies, even if the second-order sine-wave frequencies are identical. This observation can be used to devise classification methods based on estimates of TCFs and their constituent sine-wave components. For the purposes of detection and sorting, we need only focus on the case in which the number of conjugated factors m is half the order n. A consequence of this restriction is that only cumulant sine-waves with frequencies equal to harmonics of the symbol rates of the signals in the data are used, and these frequencies are enough to sort and detect provided that the symbol rates are distinct. If the symbol rates are not distinct, or if the modulation types need to be recognized, then other choices of numbers of conjugated factors must also be included. This restriction $n = 2m$ also substantially eases the computations necessary to perform the detection and sorting tasks when compared to performing these tasks based on the combined results of other choices of m.

The algorithm that estimates the TCFs (and, thereby, their Fourier components) is called the *general search algorithm* (GSA), and the algorithm that groups the output of the GSA is called the *grouping algorithm* (GA). These algorithms are described next.

3 The General Search and Grouping Algorithms

The approach taken to solving the general search problem consists of estimating the cycle frequencies of the data for nonlinear processing of various orders [5, 10, 8, 11]. In order to associate the resulting cycle frequency estimates with specific signals in the data, it is required to estimate cumulant sine-wave frequencies rather than moment cycle frequencies. This is because moment cycle frequencies can consist of sums and differences of the cycle frequencies for various distinct signals and are, therefore, not associated with any particular signal in the data, and because the strengths of the desired sine waves are functions of all signals in the data.

Let N be the maximum order of nonlinearity that is to be used for processing. The goal of the processing is to produce a list of cumulant cycle frequencies $\{\beta_n\}$ for each value of n from 1 to N. The list $\{\beta_n\}$ characterizes the detectable cyclostationarity of order n (and only n) that is associated with $x(t)$ because it is not contaminated by entries that are due to lower-order sine wave interactions. To accomplish this task, we estimate the temporal

cumulant function (TCF) for $x(t)$ for each order n. From this estimate, the cycle frequencies $\{\beta_n\}$, which are needed for the estimate of the TCF for order $n+1$, can be estimated.

This approach is justified by the well-known fact that the periodogram is the optimal estimator of the frequency of a sine wave in white Gaussian noise. Although we are not primarily interested in the case of white Gaussian noise, our algorithm essentially estimates the frequencies of a set of relatively strong sine waves in noise and, therefore, the periodogram is of interest. In addition, the algorithm implements an estimator of the pure-sine-waves function for each order n, which we have shown is the signal-selective function of interest in applications. More explicitly, the general search problem can be tackled using the following *general search algorithm* (GSA):

0 Let $n = 1$, fix $N > 1$, denote the data by $x(t), 0 \le t \le T$,
choose N delays $\tau_1, \cdots \tau_N$, and choose m optional conjugations.

1 Compute $\hat{C}'_x(t,\boldsymbol{\tau})_n = \left[\prod_{j=1}^{n} x^{(*)_j}(t+\tau_j)\right] - \sum_{\substack{P_n \\ p\neq 1}} \left[\prod_{j=1}^{p} \hat{C}_x(t,\boldsymbol{\tau}_{\nu_j})_{n_j}\right]$ for $\boldsymbol{\tau} = [\tau_1 \cdots \tau_n]$

2 Compute $Y(f) = \mathrm{FFT}_t \{\hat{C}'_x(t,\boldsymbol{\tau})_n\}$

3 Threshold detect the bins of Y to find $\{\beta_n\}$

4 Compute the CTCFs $\hat{C}_x^{\beta_n}(\boldsymbol{\tau})_n = \left\langle \hat{C}'_x(t,\boldsymbol{\tau})_n \, e^{-i2\pi\beta_n t} \right\rangle_T$

5 Compute the TCF $\hat{C}_x(t,\boldsymbol{\tau})_n = \sum_{\beta_n} \hat{C}_x^{\beta_n}(\boldsymbol{\tau})_n e^{i2\pi\beta_n t}$

6 $n \to n+1$; if $n \le N$ then go to 1, else stop.

The operation of the GSA and the notation that is introduced above are explained in detail next.

In Step 0, the maximum order of nonlinearity to be considered is fixed at $N > 1$, the N delays to be used are chosen, the m optional conjugations are chosen for each processing order $n < N$, and the processing order n is initialized to 1.

In Step 1, a pre-estimate of the nth-order TCF for order n is obtained by subtracting from the nth-order delay product $\prod_{j=1}^{n} x^{(*)_j}(t+\tau_j)$ the products of lower-order TCFs estimated in previous iterations of the algorithm. For $n = 1$, there are no previous iterations, so the

first-order pre-estimate of the TCF is set equal to the first-order lag product itself, which is just the data $x(t+\tau_1)$. For $n=2$, the product of the first-order TCF estimates for each of the selected lags τ_1 and τ_2 are subtracted from the second-order lag product. This removes from consideration any sine waves in the second-order lag product that result from products of first-order sine waves. For $n>2$, the sum of products of lower-order TCFs is determined by the set P_n, which is the set of distinct partitions of the set of indices $\{1,2,\cdots,n\}$. This set is described in Appendix A.

In Step 2, the pre-estimate of the TCF obtained in Step 1 is Fourier transformed in the t variable in order to determine its sine-wave components.

In Step 3, the values of this transformed TCF pre-estimate are compared to a threshold. The locations in f of the values of the transformed pre-estimate that exceed the threshold are declared to be cycle frequencies $\{\beta_n\}$.

In Step 4, the estimated cycle frequencies are used to compute estimates of the cyclic temporal cumulant functions (CTCFs), which are the Fourier coefficients of the TCF estimates. If the Fourier transform in Step 2 has length equal to the total amount of data available (T), then the CTCFs are already computed in Step 2, and do not need to be computed again. To handle the case in which the cycle frequencies do not lie on bin-center frequencies, interpolation techniques are used to estimate the frequency of the sine wave, and its magnitude and phase can then be estimated by direct computation of the discrete Fourier transform. If two adjacent bins are declared to correspond to sine-wave frequencies, then this interpolation is done. That is, if two adjacent bins have large magnitudes, then it is assumed that a single sine wave with frequency somewhere between the two bin frequencies is responsible for this energy.

In Step 5, the estimated cycle frequencies and CTCFs are combined to obtain an estimate of the TCF that replaces the pre-estimate obtained in Step 1.

Finally, in Step 6 the order of processing n is incremented and tested against its maximum allowed value N. If n is less than or equal to N then the algorithm returns to Step 1. Otherwise, processing is terminated.

Step 1 is the crucial step. Cycle frequencies could be estimated by Fourier transforming the lag product itself and thresholding its bins, but the resulting list of cycle frequencies would

contain entries due to interactions among the distinct signals in the data. By subtracting the particular sum of products of lower-order TCFs in step 1, these false cycle frequencies are removed from consideration.

The output of the GSA is a sequence of lists that are indexed by order. Each list entry contains two elements. The first is the cycle-frequency estimate, usually denoted by α or β, and the second is the amplitude of the sine wave with frequency α for the appropriate order (phase information is suppressed in the output of the GSA, but retained internally). Multiple delay sets and choices of conjugated factors can be accommodated by sequential runs of the algorithm. The software implementation of the GSA is described in the next section.

3.1 The GSA Program

The *GSA program* takes a data record as its input and produces cycle frequency and cumulant estimates for specified orders. The minimum order is 1 and the maximum order is denoted by N. Typically, the minimum order is set to 2, and—as explained below—only the even orders between 2 and N are used. The other inputs to the GSA program are a set of delay vectors of dimension N, and a set of conjugation flags of dimension N. The GSA program then estimates the Nth-order temporal cumulant function (TCF) for each delay vector for each conjugation set. For instance, the program could be used to compute the fourth-order cumulant of the input data for the two delay vectors

```
1 2 5 6
0 6 9 10
```

and the two conjugation-flag vectors

```
0 0 0 0
0 0 1 0
```

where 0 means do not conjugate and 1 means conjugate. This would result in four fourth-order temporal cumulant estimates. Two of these estimates are fourth-order estimates with 0 conjugations, and the remaining two are fourth-order estimates with the third variable

conjugated. The former are called (4, 0) estimates ($n = 4$ and $m = 0$), and the latter are (4, 1) estimates. Because the GSA algorithm is recursive, second-order cumulants are estimated in order to estimate the fourth-order cumulants (if desired, the first- and third-order estimates can be made as well, but this is often unnecessary because these cumulants are zero for almost all communication signals [except those with pilot tones]). Since TCFs are polyperiodic functions, an individual TCF estimate can be represented by a collection of ordered triplets where the first element is a sine-wave frequency, the second is a sine-wave amplitude, and the third is a sine-wave phase. For the purpose of detecting and sorting, the phase is not needed. Thus, the phase is retained while the program is running, but only the frequency and magnitude parameters are actually output. An individual datum in the output of the GSA program is the quadruple (n, m, α, C), where n is the order, m is the number of conjugations, α is the cycle frequency estimate, and C is the estimate of the magnitude of the (n, m) CTCF for frequency α. These quadruplets are indexed by the delay vectors $\boldsymbol{\tau}$.

The output of the GSA program contains data of two fundamental sorts: X_U, which is the set of *upper* data, and X_L, which is the set of *lower* data. These are defined as

$$n = 2m \Rightarrow x \in X_L,$$

$$n \neq 2m \Rightarrow x \in X_U.$$

Elements in X_L have cycle frequency estimates α that are not (typically) related to carrier frequencies, whereas elements in X_U have cycle frequency estimates that are related to carrier frequencies.

The goal of the *grouping algorithm*, and its implementation, the *grouping program*, is to group this multidimensional data into sets such that each set corresponds to one and only one signal in the original data record.

3.2 The Grouping Algorithm

The output of the GSA program is a set of lists that are indexed by the order of processing. Visual inspection of these lists is difficult and is not particularly revealing. Because the cycle frequencies of communication signals (especially digital QAM signals) are harmonically

related and appear at multiple orders of processing n, if there is a signal present in the data, then there will be a set of α estimates that are harmonically related. The main idea behind the *grouping algorithm* (GA) is to extract these cycle frequency estimates and group them together. The other cycle frequency-estimates in the output of the GSA program are discarded.

The word "cluster" in the following description of the GA refers to a standard unsupervised-learning partitioning algorithm [32]. This algorithm finds a collection of subsets of a given set such that a certain cost function related to the sample mean and variance of each subset is minimized. That is, at termination this cost would increase if any element of one of the sets is removed and then added to any of the other sets.

The grouping algorithm consists of the following steps:

1. Read GSA data: $x_j = (n, m, \alpha, \mathrm{C})_j$ for $j = 1, \cdots, M$, where $1 \leq n \leq N$ and $0 \leq m \leq N$ for each j.

2. Separate the data into two sets: X_U, which is the set of upper data ($n \neq 2m$), and X_L, which is the set of lower data ($n = 2m$).

3. Cluster the set X_L into three sets based on the value of C. That is, find a three-set partition of X_L such that the data with the largest C are in one set, those with the smallest C are in another called X_w (the w stands for "weak"), and the rest are in a third.

4. Find the union of the two sets with largest C; call this set X_s (the s stands for "strong").

5. Cluster X_s based on the value of α. This results in many sets, each of which contains only elements with α that are "close together."

6. Search the set X_w for any elements with α that are harmonically related (integer multiples or divisors) to the mean of any of the sets obtained in the previous step. If any are found, add them to an appropriate set. Discard the remaining elements of X_w.

7. Recluster X_s.

8. Group the sets obtained by the previous step. This results in a group of sets. Each of the groups is associated with a unique fundamental frequency. The members of the groups are sets that are assumed to contain cycle frequencies that correspond to the various harmonics of this fundamental. Compute the harmonic numbers for each of these sets.

9. Store the vector of fundamentals (one fundamental for each group) for later use.

10. Cluster the set X_U into three sets based on the value of C. That is, find a three-set partition of X_U such that the data with the largest C are in one set, those with the smallest C are in another called X_w, and the rest are in a third.

11. Find the union of the two sets with largest C; call this set X_s.

12. Cluster X_s based on the value of α.

13. Search the set X_w for any elements with α that are separated by a multiple of one of the stored fundamentals from the mean of any of the sets obtained in the previous step. This must be done only for data that have matching n and m values. If any such elements are found, add them to an appropriate set. Discard the remaining elements of X_w.

14. Recluster X_s.

15. Using the stored fundamentals, associate the sets obtained in the previous step with a group obtained in step 8. Thus, upper sets are associated with lower sets through a fundamental frequency.

16. Estimate the carrier offset for the upper elements in each group.

17. Compute the harmonic of each upper cluster in each group by using the fundamental and the estimated offset.

18. Splinter each set in the following way. Form a separate set for each of the distinct (n, m) pairs that appear in the set. At the end of this procedure, every set will correspond to a single (n, m) pair and to a single harmonic.

19. Output the matrix of detected harmonics for each group. The rows of these matrices correspond to the harmonic number, and the columns correspond to each (n, m) pair associated with that group. The value of an element of the matrix is the maximum value of the C parameters of all the data points x_j contained in the set that corresponds to the appropriate group and (n, m) pair. This matrix shall be called a *feature matrix.*

4 Illustration of the General Search Algorithm

In this section, some simple examples of the operation of the GSA are presented. These examples are meant to illustrate the properties of cumulants, estimates of which are used to solve the general search problem. More realistic examples are presented and discussed in Section 5, where the properties of the cumulant are more difficult to appreciate directly.

Since the nth-order temporal cumulant function is also the pure-sine-waves function [11], the nth-order TCF for any polyperiodic signal is equal to the signal itself for $n = 1$ and is identically zero for $n > 1$. This is because there can be no *pure nth-order sine waves* for $n > 1$ for such a signal—all sine-wave components in the higher-order delay products must result from products of first-order sine waves. A simple example of such a signal is a single sine wave. Other examples include the sum of a finite number of sine waves and any periodic function, such as a square wave (which is equal to a sum of an infinite number of sine waves).

Consider a sine wave with frequency 1/11 and amplitude 1.0. Estimates of the nth-order TCFs for orders one through four obtained by processing a sampled version of such a sine wave are shown in Figure 1. As is evident from the figure, the first-order TCF is equal to the sine-wave itself, and the other TCFs are zero. Next, consider the sum of two sine waves with frequencies 1/11 and 1/16 and amplitudes 1.0 and 2.0, respectively. Estimates of the nth-order TCFs for this signal are shown in Figure 2 for orders one through four. Again, only the first-order TCF is nonzero. A third sine wave with frequency 1/7 is added and the measurements repeated. The results are shown in Figure 3. Finally, a binary full-duty-cycle rectangular-pulse PAM signal with pulse rate 1/23 is added to a sine wave with frequency 1/11 and the measurement procedure is repeated. The results are shown in Figure 4. The second- and fourth-order TCF for the PAM signal for the chosen delay sets should be square

waves with 48% duty cycles. As can be seen in the figure, the sine wave does not affect the estimation of the two TCFs for the PAM signal, which do not appear as square waves with sharp corners due to truncation of the Fourier-series representation of the TCF.

These examples illustrate that nth-order cumulants do indeed compute pure nth-order sine waves. Thus, the GSA, which is based on TCFs, holds promise for computing the correct cycle frequencies and corresponding Fourier magnitudes for each signal in a given data set. The following section presents examples of the operation of the GSA for signals of interest.

5 Computer Simulations

The first example shows the capabilities of the GSA and GA program for the case of 16,384 samples of a binary rectangular-pulse PAM signal ($T_0 = 23$) in a small amount of WGN. The temporal cumulants of order 2, 4, 6, and 8 are estimated for six delay sets,

```
0 0 0 0 0 0 0 0
0 0 0 0 0 0 0 2
0 0 0 0 0 0 0 4
0 0 0 0 0 0 0 7
0 0 0 0 0 0 0 9
0 0 0 0 0 0 0 12
```

and 9 choices of conjugated factors (applied to each of the six delay sets),

```
0 0 0 0 0 0 0 0
0 0 0 0 0 0 0 1
0 0 0 0 0 0 1 1
0 0 0 0 0 1 1 1
0 0 0 0 1 1 1 1
0 0 0 1 1 1 1 1
0 0 1 1 1 1 1 1
0 1 1 1 1 1 1 1
1 1 1 1 1 1 1 1
```

Thirty cycle frequencies per cumulant are estimated and used in the computation of subsequent cumulants; only fifteen cycle frequencies per cumulant are actually output. This is done for the sake of constraining the amount of computation: the run time of the GA program is a function of the total number of cycle frequencies output by the GSA program. In this case, and all subsequent cases, the candidate symbol interval lengths are constrained to be greater than 2.0 and less than 25.0. The search grid has fineness 0.1. The remaining parameter to explain is the interval parameter, which specifies the number of intervals in which to segment the transform of each pre-estimate of the TCF. The maxima of each interval are found sequentially. The intervals parameter is set to thirty. The feature matrix (explained subsequently) for the output of the grouping program is shown in Figure 5.

The feature matrix consists of the detected harmonics versus the order/conjugation pairs, and the brightness of the squares indicates the strength of the detected harmonic. For all the feature matrices shown in this report, the first three columns corresponds to order two, the next five correspond to order four, the next seven to order six, and the remaining nine to order eight. For a single order, the columns start with $m = 0$ and end with $m = n$. In addition, only the positive harmonics are shown. If a negative harmonic is detected and the corresponding positive harmonic is not detected, then the positive harmonic is replaced by the negative. This effectively reduces the number of rows in the plot while representing the same information. Finally, the matrix entries that correspond to $\alpha = 0$ for each order are always set to zero (these are the matrix entries for $n = 2m$ and $k = 0$). The cyclic cumulants for these cycle frequencies are not signal selective—all signals in the data can contribute to these cyclic cumulants. Thus, they are not useful for defining a feature that depends only on a single signal.

In the second example, the measurement above is repeated for the case of a duobinary PAM signal, which exhibits no second-order cyclostationarity. The result is shown in Figure 6.

The next example shows the capabilities of the programs for the case of 16,384 samples of a complex-valued BPSK signal with symbol rate 1/23 and frequency offset 0.004. The same cumulants are measured with the same parameters as in the previous case. The feature matrix for this case is shown in Figure 7. The grouping program correctly estimates the

symbol rate and carrier offset. The same procedure is used to estimate and group the cycle frequencies for QPSK, 8PSK, and OQPSK signals. The results are shown in Figures 8, 9, and 10.

By examining Figures 5–10, and reviewing the relevant entries in Table 1, it can be seen that the observed patterns are correct, although there may be a few harmonics missing here and there. In particular, the feature matrix for BPSK should be "full," that is, all harmonics are exhibited by the signal for all even orders and, indeed, the feature matrix for BPSK does show harmonics for every order/conjugation pair that is output by the GSA program. For QPSK, only the (n, m) pairs such that $n - 2m$ is a nonzero multiple of 4 should exhibit carrier-related cyclostationarity (see Table 1), and for 8PSK, only the (8, 0) and (8, 8) pairs should exhibit carrier-related cyclostationarity. The case of offset (staggered) QPSK is particularly interesting because its higher-order statistics cannot be analyzed by using the previously derived cumulant formulas for complex PAM because its complex envelope is a PAM signal that does not have independent symbols. Nevertheless, the second-order cyclostationarity for this signal is known (see [15], page 447), and it matches with the first three columns of the Figure 10. This example shows that the GSA/GA programs can be used not only for detection and sorting, but also as research tools that facilitate a numerical evaluation of the cyclostationarity of a given data record.

The next set of examples shows the capability of the algorithms to sort two equipower signals. The same parameters are sued as in the previous cases. The first example shows the capability of the programs to detect and sort two real-valued rectangular-pulse PAM signals. One of the signals has a symbol rate of 1/15, and the other has a symbol rate of 1/23. The signals have equal power levels. The feature matrices are shown in Figures 11–12. Some harmonics are missing because the number of cycle frequency estimates output per delay set and conjugation set pair is not increased with respect to the measurements that were performed on single signals. Also, the bottom row of the feature matrix for 12 is missing because the two PAM signals have the same "carrier offset" of zero. Only one of the signals can claim these cycle frequency estimates, and in this case it is the first signal. The ability to correctly sort the cycle frequency estimates for the case of signals with shared cycle frequencies is to be added at a later date.

BPSK signals are considered next. One of the signals has carrier offset of -0.005 and a symbol rate of 1/15, and the other has offset 0.004 and a symbol rate of 1/23. The feature matrices are shown in Figures 13–14. This test is repeated for two QPSK, 8PSK, and OQPSK signals that have the same symbol rates and carrier frequencies as the two BPSK signals. The results are shown in Figures 15–16, 17–18, and 19–20, respectively.

The next set of examples shows the capability of the algorithms to sort three equipower signals. For these cases, only the lower cycle frequencies are used (those for $n = 2m$). This is done both to demonstrate that this is a viable approach, and to reduce the computational requirements of the experiments. The cases of rectangular-pulse PAM, BPSK, QPSK, 8PSK, and OQPSK are considered. The results are shown in Figures 21–33.

6 Conclusions

This report documents an initial inquiry into the possibility of using higher-order cyclostationarity, and in particular higher-order cyclic cumulants, to detect and sort an unknown number of cyclostationary signals in a given data record. The nth-order cyclic cumulants of complex-valued data record (analytic signal representation of a radio-frequency signal) for orders 2 through 8 are estimated and grouped such that the groups each correspond to one and only one signal in the data. The method was qualitatively tested for several signal environments consisting of one, two, and three cochannel signals and was seen to perform well.

7 Research and Development

The following list of tasks are suggested by the research that is documented in this report:

1. Detailed computer simulations for signal environments of interest,

2. Mathematical analysis of the higher-order cyclostationarity of communication signals that are not well modeled as complex-valued PAM signals at baseband, such as CPFSK, FSK, and analog FM,

3. Cataloging of the higher-order cyclic features of signals of interest,

4. Mathematical characterization of the quality of the GSA's cyclic cumulant estimates as a function of SNR, SIR, and collect time,

5. Development of generalizations of the GA to handle the case in which signals share certain cyclostationarity properties (e.g., two or more signals with the same symbol rate but distinct carrier frequencies),

6. Study alternate techniques for estimating sine-wave frequencies (rather than using the discrete Fourier transform).

7. Study alternate feature-extraction scheme that uses the cycle frequencies computed by the GSA and grouped by the GA to do precise cumulant measurements.

		Modulation Type				
n	m	BPSK	QPSK	8PSK	MPSK ($M \geq 16$)	APK
2	0,2	$k/T_0 \pm 2f_c$	$\emptyset$	$\emptyset$	$\emptyset$	$\emptyset$
2	1	k/T_0	k/T_0	k/T_0	k/T_0	k/T_0
4	0,4	$k/T_0 \pm 4f_c$	$k/T_0 \pm 4f_c$	$\emptyset$	$\emptyset$	$k/T_0 \pm 4f_c$
4	2	k/T_0	k/T_0	k/T_0	k/T_0	k/T_0
6	0,6	$k/T_0 \pm 6f_c$	$\emptyset$	$\emptyset$	$\emptyset$	$\emptyset$
6	1,5	$k/T_0 \pm 4f_c$	$k/T_0 \pm 4f_c$	$\emptyset$	$\emptyset$	$k/T_0 \pm 4f_c$
6	3	k/T_0	k/T_0	k/T_0	k/T_0	k/T_0
8	0,8	$k/T_0 \pm 8f_c$	$k/T_0 \pm 8f_c$	$k/T_0 \pm 8f_c$	$\emptyset$	$k/T_0 \pm 8f_c$
8	2,6	$k/T_0 \pm 4f_c$	$k/T_0 \pm 4f_c$	$\emptyset$	$\emptyset$	$k/T_0 \pm 4f_c$
8	4	k/T_0	k/T_0	k/T_0	k/T_0	k/T_0
10	0,10	$k/T_0 \pm 10f_c$	$\emptyset$	$\emptyset$	$\emptyset$	$\emptyset$
10	1,9	$k/T_0 \pm 8f_c$	$k/T_0 \pm 8f_c$	$k/T_0 \pm 8f_c$	$\emptyset$	$k/T_0 \pm 8f_c$
10	3,7	$k/T_0 \pm 4f_c$	$k/T_0 \pm 4f_c$	$\emptyset$	$\emptyset$	$k/T_0 \pm 4f_c$
10	5	k/T_0	k/T_0	k/T_0	k/T_0	k/T_0

Table 1: Cycle frequencies for the analytic signals corresponding to PSK and other digital QAM signals. APK signals include non-PSK digital QAM signals used in practice, such as 4QAM, 8QAM, etc. There are no cycle frequencies for the values of m that are not shown in the table, nor for odd values of n. The + sign is associated with the first value of m.

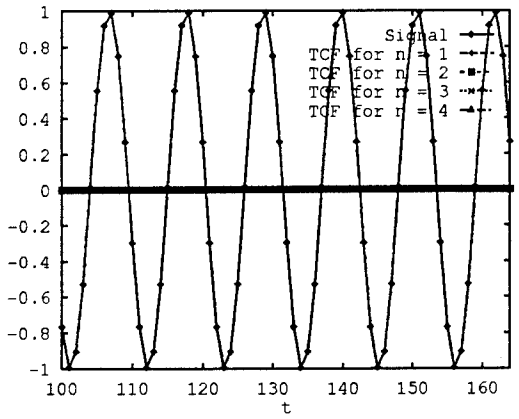

Figure 1: The temporal cumulant functions for a single sine wave. The delays are all zero for each order.

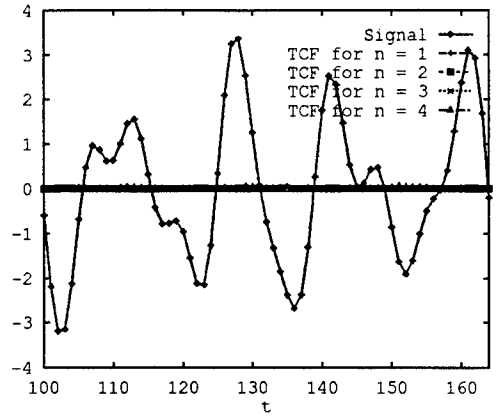

Figure 3: The temporal cumulant functions for the sum of three sine waves. The delays are all zero for each order.

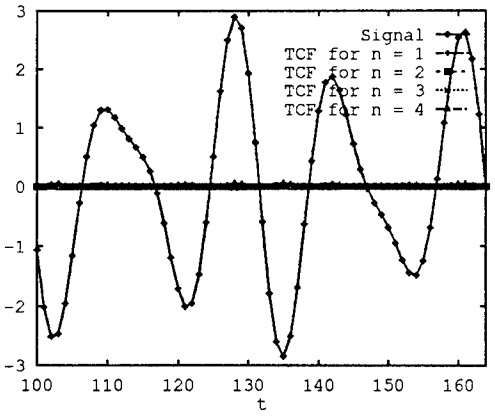

Figure 2: The temporal cumulant functions for the sum of two sine waves. The delays are all zero for each order.

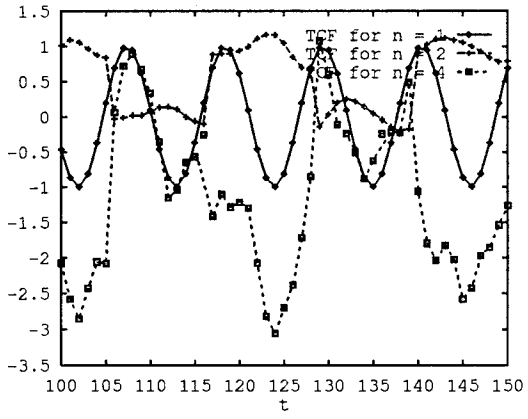

Figure 4: The temporal cumulant functions for the sum of a sine wave and a full-duty-cycle rectangular-pulse binary PAM signal. The delay sets are [0], [0 11], and [0 11 0 0], for orders one, two, and four, respectively.

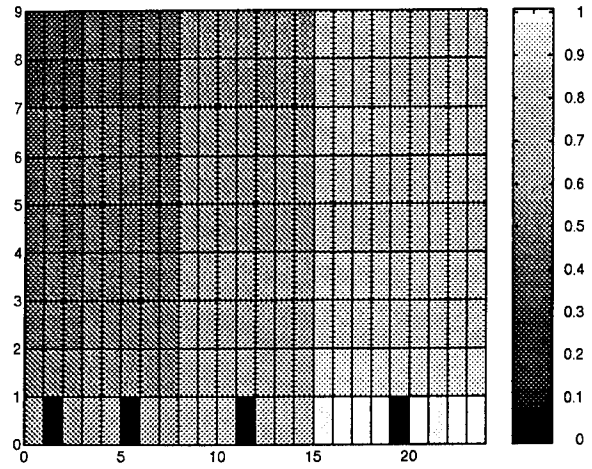

Figure 5: Measured feature matrix for rectangular-pulse PAM.

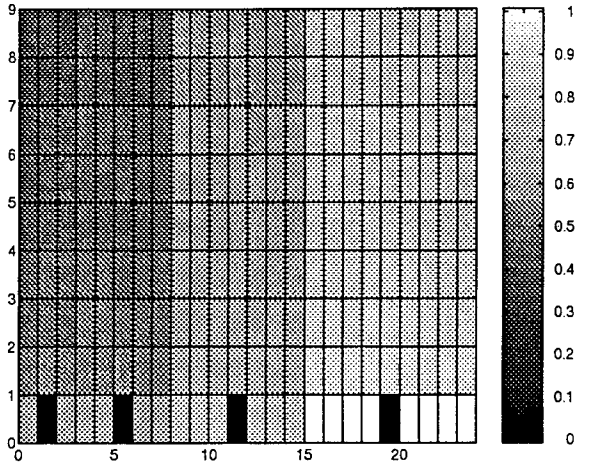

Figure 7: Measured feature matrix for complex-valued BPSK.

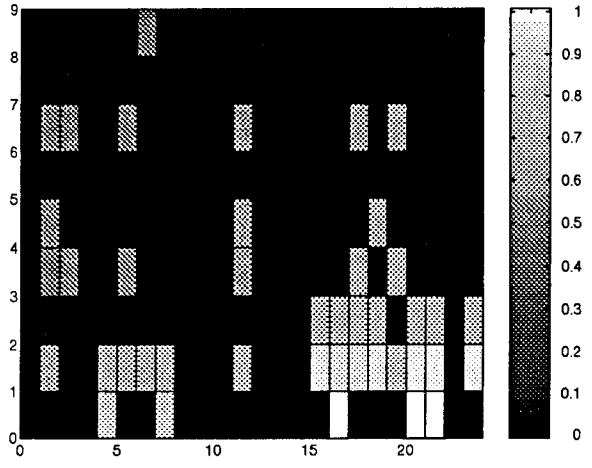

Figure 6: Measured feature matrix for duobinary (partial-response) PAM.

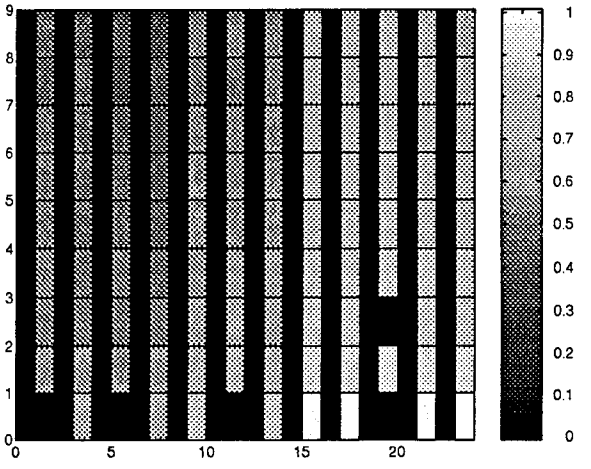

Figure 8: Measured feature matrix for complex-valued QPSK.

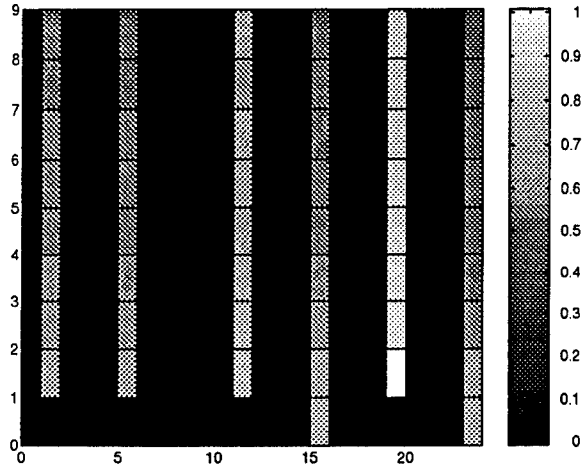

Figure 9: Measured feature matrix for complex-valued 8PSK.

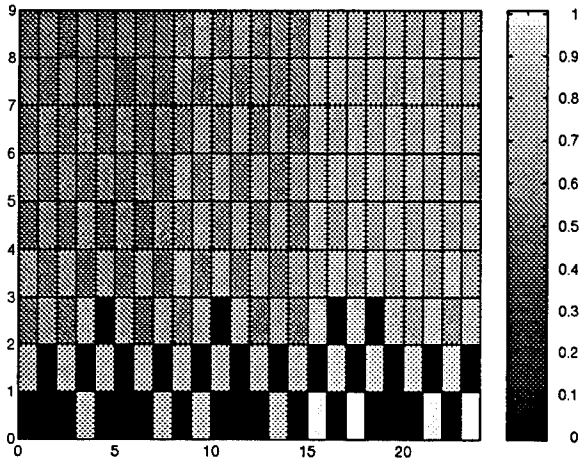

Figure 10: Measured feature matrix for complex-valued offset QPSK.

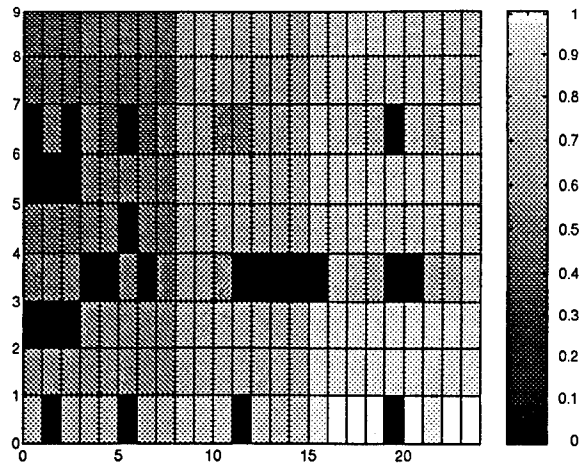

Figure 11: Measured feature matrix for one of the groups output by the GSA/GA programs. The input is the sum of two rectangular-pulse PAM signals. The program correctly identified the symbol rate as 1/23, and carrier offset as 0.004.

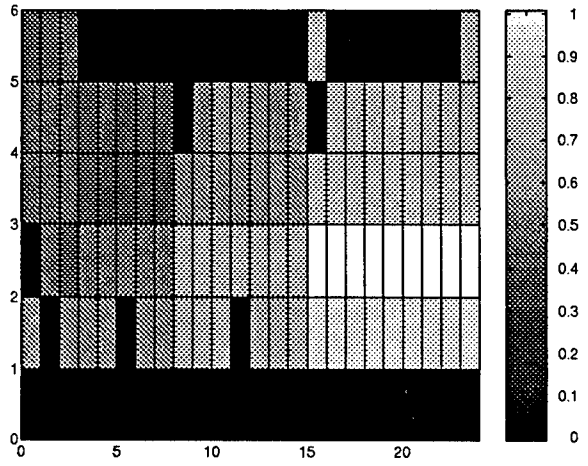

Figure 12: Measured feature matrix for one of the groups output by the GSA/GA programs. The input is the sum of two rectangular-puse PAM signals. The program correctly identified the symbol rate as 1/15, and carrier offset as -0.005.

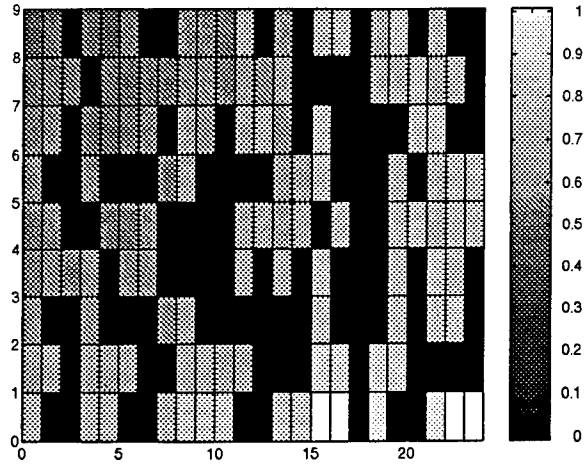

Figure 13: Measured feature matrix for one of the groups output by the GSA/GA programs. The input is the sum of two BPSK signals. The program correctly identified the symbol rate as 1/23, and carrier offset as 0.004.

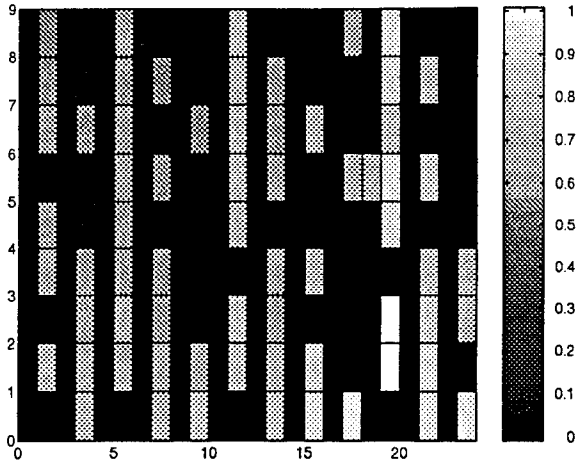

Figure 15: Measured feature matrix for one of the groups output by the GSA/GA programs. The input is the sum of two QPSK signals. The program correctly identified the symbol rate 1/23, and carrier offset as 0.004.

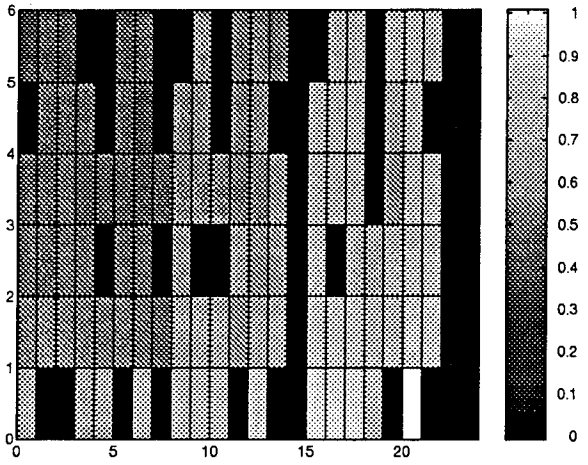

Figure 14: Measured feature matrix for one of the groups output by the GSA/GA programs. The input is the sum of two BPSK signals. The program correctly identified the symbol rate as 1/15, and carrier offset as -0.005.

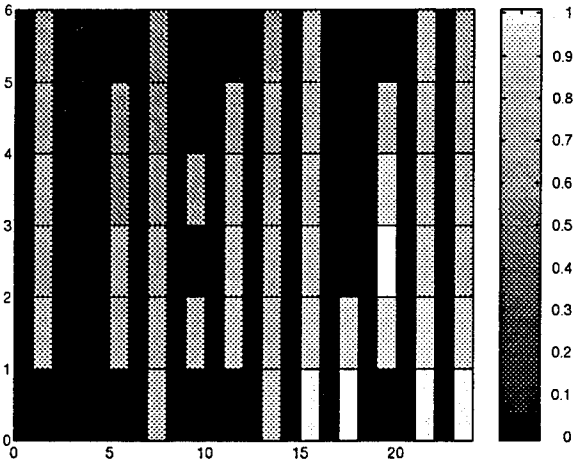

Figure 16: Measured feature matrix for one of the groups output by the GSA/GA programs. The input is the sum of two QPSK signals. The program correctly identified the symbol rate as 1/15, and carrier offset as -0.005.

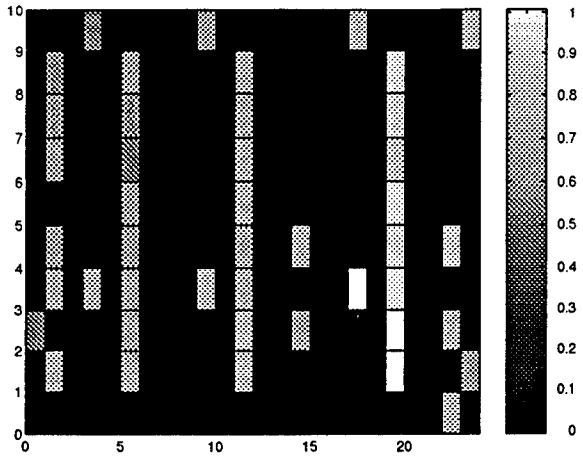

Figure 17: Measured feature matrix for one of the groups output by the GSA/GA programs. The input is the sum of two 8PSK signals. The program correctly identified the symbol rate as 1/23, but the carrier offset as 0.032.

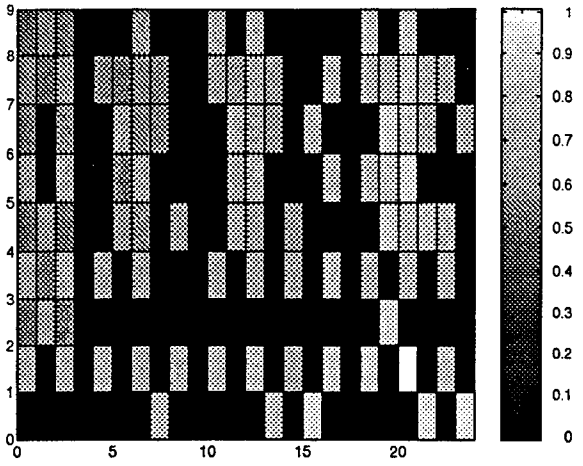

Figure 19: Measured feature matrix for one of the groups output by the GSA/GA programs. The input is the sum of two OQPSK signals. The program correctly identified the symbol rate as 1/23, and carrier offset as 0.004.

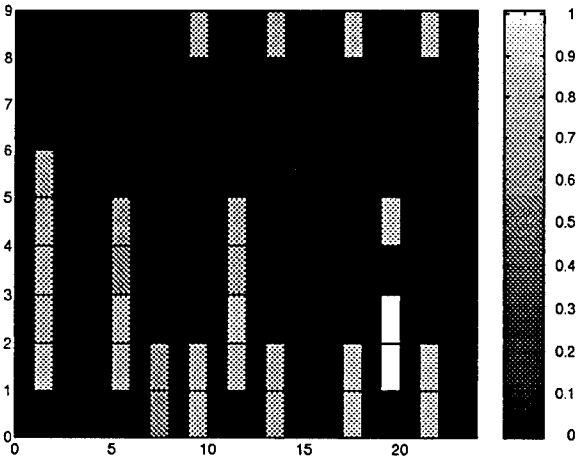

Figure 18: Measured feature matrix for one of the groups output by the GSA/GA programs. The input is the sum of two 8PSK signals. The program correctly identified the symbol rate as 1/15, but the carrier offset as 0.059.

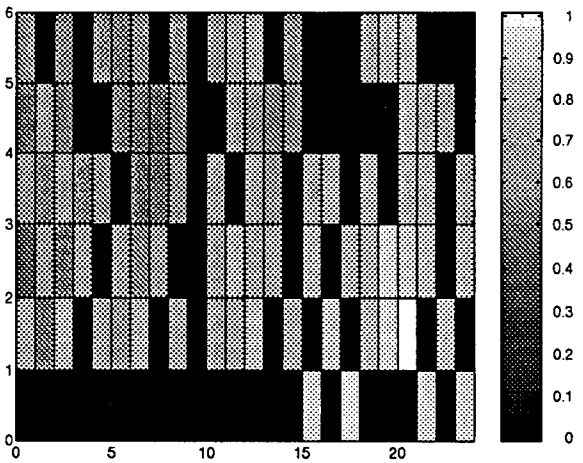

Figure 20: Measured feature matrix for one of the groups output by the GSA/GA programs. The input is the sum of two OQPSK signals. The program correctly identified the symbol rate as 1/15, and carrier offset as -0.005.

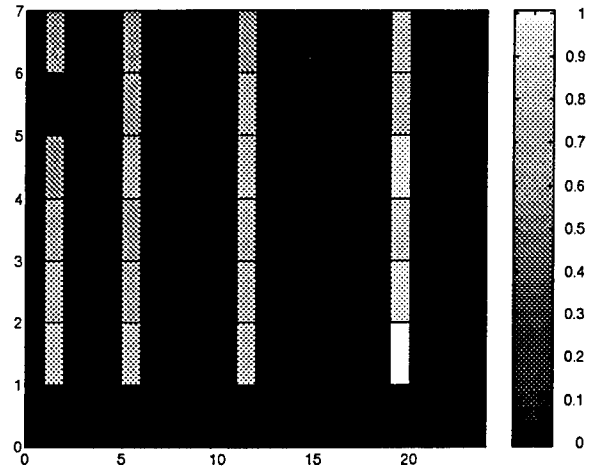

Figure 21: Measured feature matrix for one of the groups output by the GSA/GA programs. The input is the sum of three rectangular-pulse PAM signals. The program correctly identified the symbol rate as 1/19.

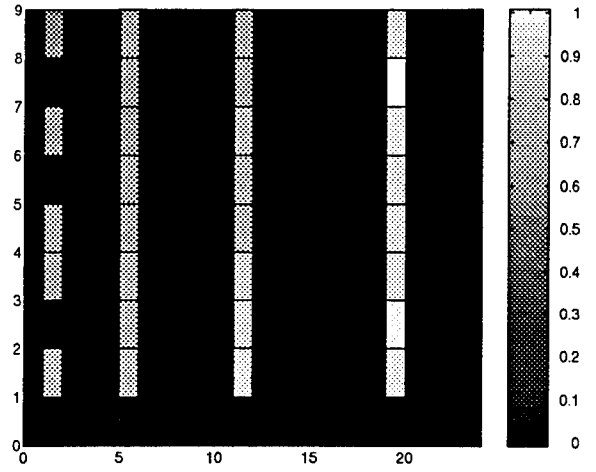

Figure 23: Measured feature matrix for one of the groups output by the GSA/GA programs. The input is the sum of three rectangular-puse PAM signals. The program correctly identified the symbol rate as 1/23.

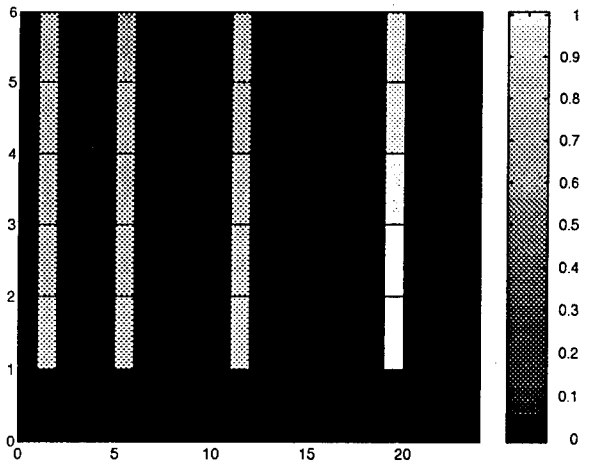

Figure 22: Measured feature matrix for one of the groups output by the GSA/GA programs. The input is the sum of three rectangular-puse PAM signals. The program correctly identified the symbol rate as 1/15.

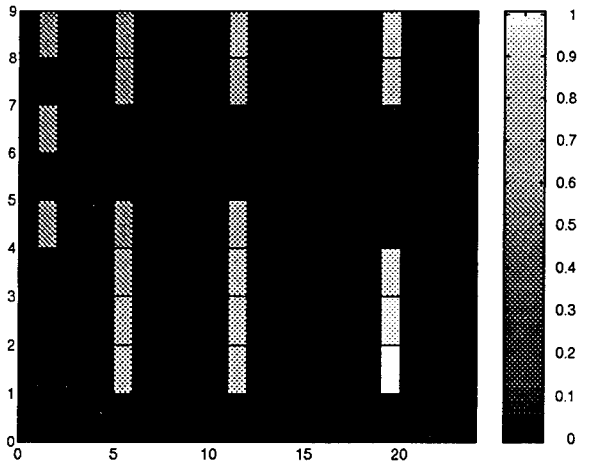

Figure 24: Measured feature matrix for one of the groups output by the GSA/GA programs. The input is the sum of three BPSK signals. The program correctly identified the symbol rate as 1/23.

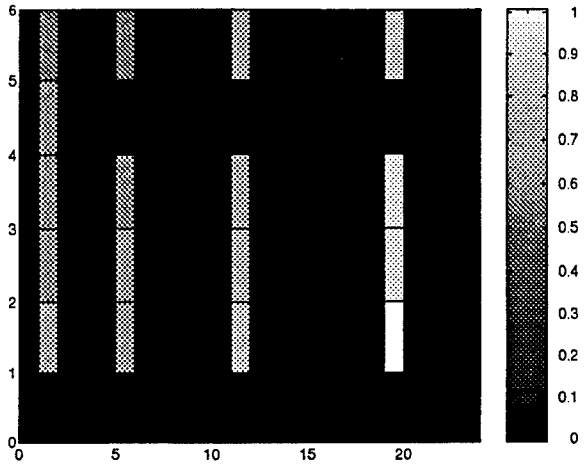

Figure 25: Measured feature matrix for one of the groups output by the GSA/GA programs. The input is the sum of three BPSK signals. The program correctly identified the symbol rate as 1/15.

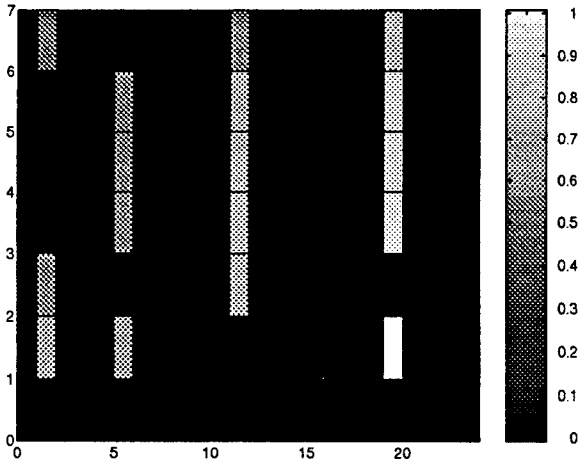

Figure 26: Measured feature matrix for one of the groups output by the GSA/GA programs. The input is the sum of three BPSK signals. The program correctly identified the symbol rate as 1/19.

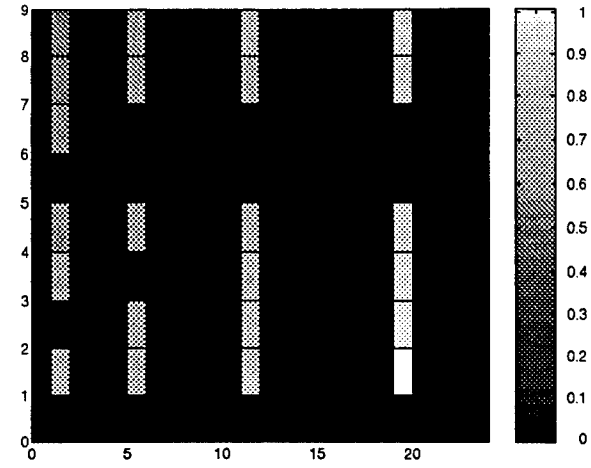

Figure 27: Measured feature matrix for one of the groups output by the GSA/GA programs. The input is the sum of three QPSK signals. The program correctly identified the symbol rate as 1/23.

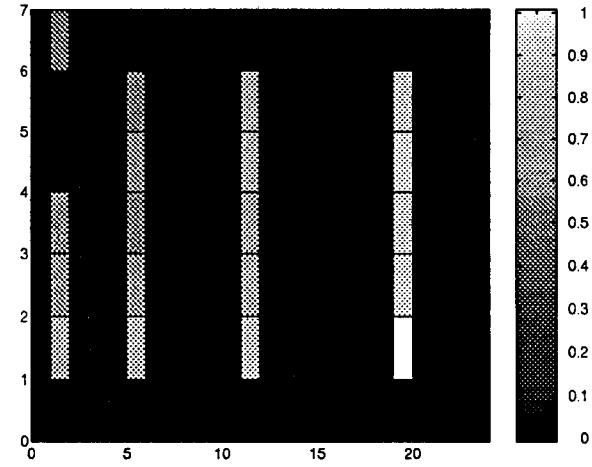

Figure 28: Measured feature matrix for one of the groups output by the GSA/GA programs. The input is the sum of three QPSK signals. The program correctly identified the symbol rate as 1/19.

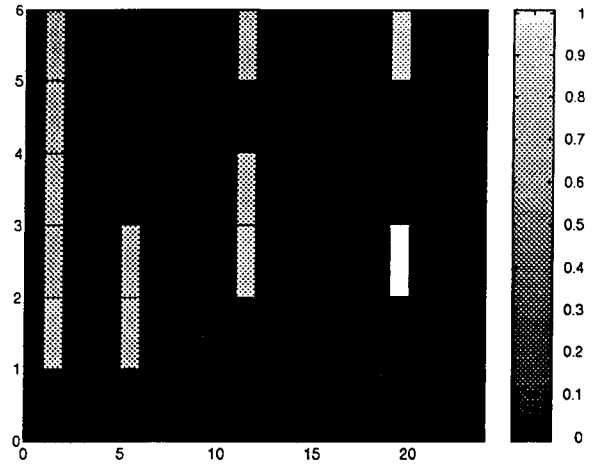

Figure 29: Measured feature matrix for one of the groups output by the GSA/GA programs. The input is the sum of three QPSK signals. The program correctly identified the symbol rate as 1/15.

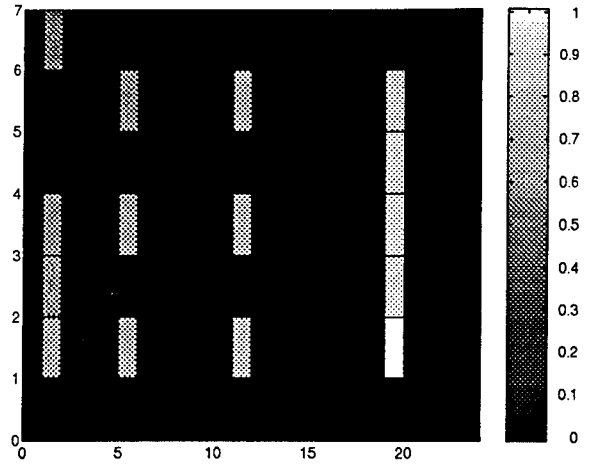

Figure 31: Measured feature matrix for one of the groups output by the GSA/GA programs. The input is the sum of three 8PSK signals. The program correctly identified the symbol rate as 1/19.

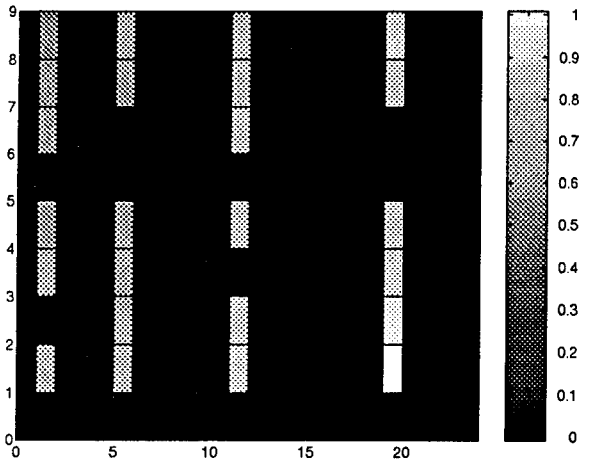

Figure 30: Measured feature matrix for one of the groups output by the GSA/GA programs. The input is the sum of three 8PSK signals. The program correctly identified the symbol rate as 1/23.

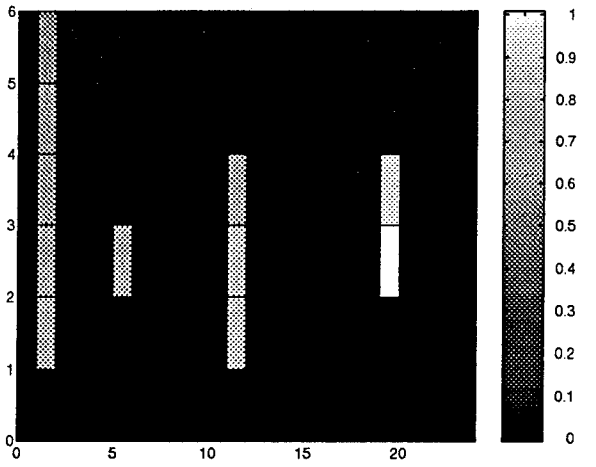

Figure 32: Measured feature matrix for one of the groups output by the GSA/GA programs. The input is the sum of three 8PSK signals. The program correctly identified the symbol rate as 1/15.

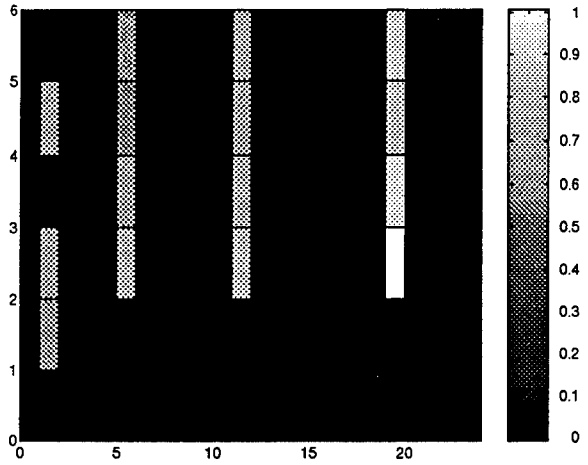

Figure 33: Measured feature matrix for one of the groups output by the GSA/GA programs. The input is the sum of three OQPSK signals. The program correctly identified the symbol rate as 1/15.

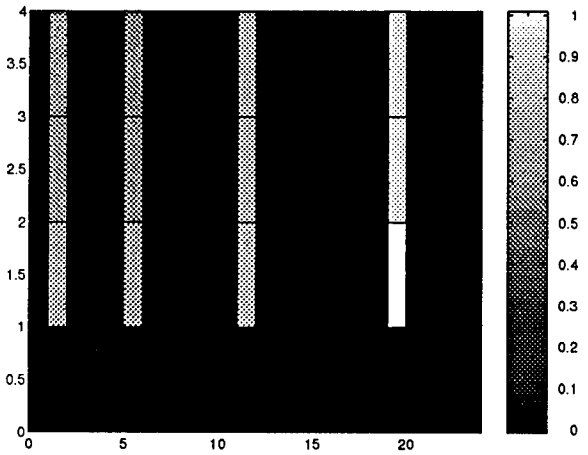

Figure 34: Measured feature matrix for one of the groups output by the GSA/GA programs. The input is the sum of three OQPSK signals. The program correctly identified the symbol rate as 1/9.5.

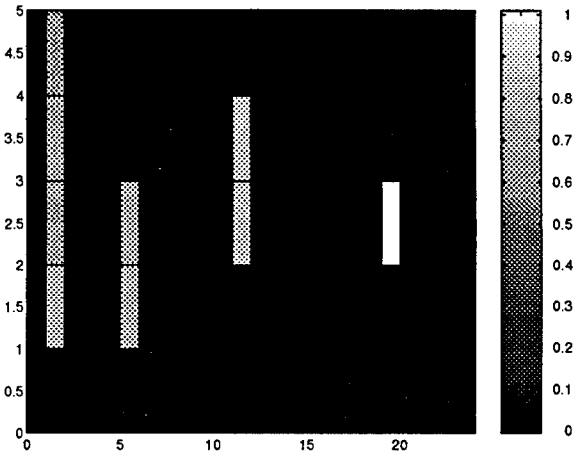

Figure 35: Measured feature matrix for one of the groups output by the GSA/GA programs. The input is the sum of three OQPSK signals. The program correctly identified the symbol rate as 1/11.5.

References

[1] W. A. Gardner, "Spectral Characterization of N-th Order Cyclostationarity," *Proceedings of the IEEE/ASSP Workshop on Spectrum Estimation,* Rochester New York, 1990.

[2] W. A. Gardner and C. M. Spooner, "Higher-Order Cyclostationarity, Cyclic Cumulants, and Cyclic Polyspectra," *Proceedings of the International Symposium on Information Theory and its Applications (ISITA),* Honolulu Hawaii, 1990.

[3] C. M. Spooner and W. A. Gardner, "An Overview of the Theory of Higher-Order Cyclostationarity," in *Proceedings of the Workshop on Nonstationary Stochastic Processes and Their Applications,* (A. G. Miamee, ed.), World Scientific, Singapore, 1992.

[4] C. M. Spooner, "Theory and Application of Higher-Order Cyclostationarity," Ph.D. Dissertation, Department of Electrical and Computer Engineering, University of California, Davis CA, 1992.

[5] C. M. Spooner, "Higher-Order Statistics for Nonlinear Processing of Cyclostationary Signals," in *Cyclostationarity in Communications and Signal Processing,* (W. A. Gardner, ed.), IEEE Press, New York, 1994.

[6] C. M. Spooner and W. A. Gardner, "Estimation of Cyclic Polyspectra," (invited paper) *Proceedings of the Twenty-Fifth Annual Asilomar Conference on Signals, Systems and Computers,* Pacific Grove, CA, Nov. 4-6, 1991, pp. 370–376.

[7] C. M. Spooner and W. A. Gardner, "Performance Evaluation of Cyclic Polyspectrum Estimators," (invited paper) *Proceedings of the Twenty-Sixth Annual Asilomar Conference on Signals, Systems and Computers,* Pacific Grove, CA, pp. 477–483, October 26–28, 1992.

[8] C. M. Spooner and W. A. Gardner, "Exploitation of Higher-Order Cyclostationarity for Weak-Signal Detection and Time-Delay Estimation," *Proceedings of the Sixth Workshop on Statistical Signal & Array Processing*, Victoria, British Columbia, Canada, 1992.

[9] C. M. Spooner and W. A. Gardner, "Cubic Frequency-Shift Filtering for Cochannel Interference Mitigation and Signal Equalization," in *Proceedings of the International Symposium on Nonlinear Theory and its Application,* Honolulu, Hawaii, December 1993.

[10] W. A. Gardner and C. M. Spooner. "Cyclostationary-Signal Processing," Chapter in *Digital Signal Processing Techniques and Applications,* C.T. Leondes, Editor, New York: Academic Press, 1993 (in press).

[11] C. M. Spooner and W. A. Gardner. "The Cumulant Theory of Cyclostationary Time-Series, Part I: Foundation; Part II: Development and Applications," *IEEE Transactions on Signal Processing*, accepted for publication.

[12] W. A. Gardner, "An Introduction to Cyclostationary Signals," Chapter in *Cyclostationarity in Communications and Signal Processing*, W. A. Gardner, Editor, New York: IEEE Press, 1994.

[13] W. A. Gardner and W. A. Brown. "Fraction-of-Time Probability for Time-Series that Exhibit Cyclostationarity," *Signal Processing,* Vol. 23, No. 3, pp. 273–292, June 1991.

[14] W. A. Gardner, *Introduction to Random Processes with Applications to Signals and Systems.* New York, New York: Macmillan, 1985 (second edition; New York: McGraw-Hill, 1990).

[15] W. A. Gardner, *Statistical Spectral Analysis: A Nonprobabilistic Theory,* Prentice-Hall, Englewood Cliffs, New Jersey, 1987.

[16] W. A. Gardner, "Signal Interception: A Unifying Theoretical Framework for Feature Detection," *IEEE Transactions on Communications* **36**, pp. 897–906, 1988.

[17] W. A. Gardner and C. M. Spooner, "Signal Interception: Performance Advantages of Cyclic-Feature Detectors," *IEEE Transactions on Communications,* **40**, 1992.

[18] W. A. Gardner and C. M. Spooner, "Weak-Signal Detection and Source Location: Simplifications of the Maximum-Likelihood Receiver," *IEEE Transactions on Communications,* **41,** June 1993.

[19] W. A. Gardner, "Cyclic Wiener Filtering: Theory and Method," *IEEE Transactions on Communications,* **41,** January, 1993.

[20] W. A. Gardner and C. K. Chen, "Signal-Selective Time-Difference-of-Arrival Estimation for Passive Location of Man-made Signal Sources in Highly Corruptive Environments. Part I: Theory and Method," *IEEE Transactions on Signal Processing* **40**, pp. 1168–1184, 1992.

[21] C. K. Chen and W. A. Gardner, "Signal-Selective Time-Difference-of-Arrival Estimation for Passive Location of Man-made Signal Sources in Highly Corruptive Environments. Part II: Algorithms and Performance," *IEEE Transactions on Signal Processing* **40**, pp. 1185–1197, 1992.

[22] A. N. Shiryaev, "Some Problems in the Spectral Theory of Higher-Order Moments – I," *Theory of Probability and Its Applications* **5**, pp. 265–284, 1960.

[23] D. R. Brillinger, "An Introduction to Polyspectra," *Annals of Mathematical Statistics* **36**, pp. 1351–1374, 1965.

[24] D. R. Brillinger and M. Rosenblatt, "Asymptotic Theory of Estimates of k-Th Order Spectra," in *Spectral Analysis of Time Series,* (B. Harris, ed.), Wiley, New York, 1967.

[25] D. R. Brillinger and M. Rosenblatt, "Computation and Interpretation of k-Th Order Spectra," in *Spectral Analysis of Time Series,* (B. Harris, ed.), Wiley, New York, 1967.

[26] M. Rosenblatt, *Stationary Sequences and Random Fields,* Birkhauser, Boston, 1985.

[27] V. P. Leonov and A. N. Shiryaev. "On a Method of Calculation of Semi-Invariants," *Theory of Probability and Its Applications,* Vol. 4, No. 3, pp. 319–328, 1959.

[28] R. D. Gitlin, J. F. Hayes, and S. B. Weinstein, *Data Communications Principles,* Plenum Press, New York, 1992.

[29] A. Lender, "The Duobinary Technique for High-Speed Data Transmission," *IEEE Transactions on Communications and Electronics,* Vol. 82, No. 5, pp. 214–218, 1963.

[30] W. A. Gardner and T. L. Archer, "Exploitation of Cyclostationarity for Identifying the Volterra Kernels of Nonlinear Systems," *IEEE Transactions on Information Theory* **39**, 1993.

[31] G. Fong, "Evaluation of Least-Squares Algorithms for Detection and Estimation of Cyclostationary Signals," MS Thesis, Department of Electrical and Computer Engineering, University of California, Davis, CA, 1993.

[32] R. O. Duda and P. E. Hart, *Pattern Classification and Scene Analysis,* Wiley, New York, 1973.

A The Theory of Higher-Order Cyclostationarity

In this appendix we define the temporal and spectral moment and cumulant functions that form the basis of the theory of HOCS. Then we give a brief tutorial explanation of how cumulants arise as the solution to the problem of generating pure nth-order sine waves. Finally, we explain the signal-selectivity property that is unique to the cyclic temporal cumulants and their Fourier transforms, the cyclic polyspectra, and we illustrate the parameters using the example of digital QAM signals.

For a time-series $x(t)$ for $-\infty < t < \infty$, we define the nth-order lag-product time-series by

$$L_x(t,\boldsymbol{\tau})_n \triangleq \prod_{j=1}^{n} x(t+\tau_j), \tag{1}$$

where $\boldsymbol{\tau} \triangleq [\tau_1 \cdots \tau_n]^\dagger$ and $[\cdot]^\dagger$ denotes matrix transposition. The *cyclic temporal moment function* (CTMF) of order n is defined by the limiting time average

$$R_x^\alpha(\boldsymbol{\tau})_n \triangleq \lim_{T\to\infty} \frac{1}{T} \int_{-T/2}^{T/2} L_x(t,\boldsymbol{\tau})_n \, e^{-i2\pi\alpha t} \, dt \equiv \left\langle L_x(t,\boldsymbol{\tau})_n e^{-i2\pi\alpha t} \right\rangle, \tag{2}$$

which is simply the Fourier coefficient associated with the component $e^{i2\pi\alpha t}$ in the time-series $L_x(t,\boldsymbol{\tau})_n$. It can be seen that the CTMF is a Fourier coefficient of a moment function because the nth-order fraction-of-time probabilistic moment (the *temporal moment function* [TMF]) associated with the lag product $L_x(t,\boldsymbol{\tau})_n$ is given by

$$R_x(t,\boldsymbol{\tau})_n \triangleq \hat{E}^{\{\alpha\}} \{L_x(t,\boldsymbol{\tau})_n\} \tag{3}$$

where $\hat{E}^{\{\alpha\}}\{\cdot\} = \sum_{\alpha\in\{\alpha\}} \langle (\cdot) e^{-i2\pi\alpha t} \rangle \, e^{i2\pi\alpha t}$, and can be expressed as [15, 13]

$$R_x(t,\boldsymbol{\tau})_n = \sum_{\alpha\in\{\alpha\}} R_x^\alpha(\boldsymbol{\tau})_n \, e^{i2\pi\alpha t}, \tag{4}$$

where the sum is over all real numbers α, called *nth-order cycle frequencies*, for which $R_x^\alpha(\boldsymbol{\tau})_n \not\equiv 0$. In (3), $\hat{E}^{\{\alpha\}}\{\cdot\}$ is the temporal expectation operation (or the sine-wave extraction operation). The functions (2) and (3) exist and are well-behaved for appropriate models of many time-series including amplitude modulated (AM), pulse-amplitude-modulated (PAM), phase-shift-keyed modulated (PSK), and digital quadrature AM (QAM) signals [10, 4], and others.

The *temporal cumulant function* (TCF) of order n for the set of time-series translates $\{x(t+\tau_j)\}_{j=1}^n$ is defined by

$$C_x(t,\boldsymbol{\tau})_n = \sum_{P=\{\nu_k\}_{k=1}^p} \left[k(p) \prod_{j=1}^p R_x(t,\boldsymbol{\tau}_{\nu_j})_{n_j} \right], \tag{5}$$

which is completely analogous to its stochastic-process counterpart in [22]. The sum in (5) is over all distinct partitions P_n of the set of indices $\{1,2,\cdots,n\}$, where each partition $\{\nu_k\}_{k=1}^p$ has p elements, $1 \le p \le n$, and $k(p) = (-1)^{p-1}(p-1)!$. The vector $\boldsymbol{\tau}_{\nu_j}$ is the vector of n_j lags with indices in the set ν_j.

The *cyclic temporal cumulant function* (CTCF) of order n is the Fourier coefficient of the TCF:

$$C_x^\beta(\boldsymbol{\tau})_n \triangleq \left\langle C_x(t,\boldsymbol{\tau})_n \, e^{-i2\pi\beta t} \right\rangle. \tag{6}$$

The set of real numbers $\{\beta\}$ for which $C_x^\beta(\boldsymbol{\tau})_n \not\equiv 0$ is called the set of *pure nth-order cycle frequencies*, for reasons that will become clear subsequently. Combining (3)–(6) reveals that the CTCF is given by the following explicit function of lower-order CTMFs:

$$C_x^\beta(\boldsymbol{\tau})_n = \sum_P \left[k(p) \sum_{\boldsymbol{\alpha}^\dagger \mathbf{1}=\beta} \left(\prod_{j=1}^p R_x^{\alpha_j}(\boldsymbol{\tau}_{\nu_j})_{n_j} \right) \right], \tag{7}$$

where $\mathbf{1} = [1 \cdots 1]^\dagger$, and $\boldsymbol{\alpha} = [\alpha_1 \cdots \alpha_p]^\dagger$. The CTCF was originally derived in [2] as the solution to the problem of removing from the Fourier coefficient $R_x^\beta(\boldsymbol{\tau})_n$ all contributions from Fourier coefficients $R_x^{\alpha_j}(\boldsymbol{\tau}_{\nu_j})_{n_j}$ of lower order. This is equivalent to removing from the finite-strength additive sine-wave component of frequency β in the lag product time-series $L_x(t,\boldsymbol{\tau})_n$ all contributions from products of sine-wave components in lag products $L_x(t,\boldsymbol{\tau}_{\nu_j})_{n_j}$ of lower order—whose frequencies sum to β—that can be obtained by factoring $L_x(t,\boldsymbol{\tau})_n$. By using the relationship between moments and cumulants[27], the CTMF can be expressed in terms of CTCFs of order n and lower:

$$R_x^\alpha(\boldsymbol{\tau})_n = \sum_P \left[\sum_{\boldsymbol{\beta}^\dagger \mathbf{1}=\alpha} \prod_{j=1}^p C_x^{\beta_j}(\boldsymbol{\tau}_{\nu_j})_{n_j} \right]. \tag{8}$$

The CTMF and the CTCF are not in general integrable due to the presence of sinusoidal components in $\boldsymbol{\tau}$. These components formally result in Dirac deltas in the n-dimensional Fourier transform of the CTCF. However, a reduced-dimension version of the CTCF is absolutely integrable for many time-series of interest and, therefore, it is strictly Fourier transformable [2]. The reduced-dimension CTCF (RD-CTCF) is simply the CTCF associated with the n variables $\{x(t+\tau_j)\}_{j=1}^n$ with $\tau_n = 0$. The RD-CTCF is denoted by

$$\bar{C}_x^\beta(\boldsymbol{u})_n \triangleq C_x^\beta(\boldsymbol{\tau})_n \quad \text{for } \tau_i = u_i \text{ and } \tau_n = 0, \tag{9}$$

where $\boldsymbol{u}$ is $(n-1)$-dimensional vector $[u_1 \cdots u_{n-1}]$. The $(n-1)$-dimensional Fourier transform of (9) is denoted by $\bar{P}_x^{\beta}(\boldsymbol{f}')_n$:

$$\bar{P}_x^{\beta}(\boldsymbol{f}')_n = \int_{-\infty}^{\infty} \cdots \int_{-\infty}^{\infty} \bar{C}_x^{\beta}(\boldsymbol{u})_n \, e^{-i2\pi \boldsymbol{u}^{\dagger} \boldsymbol{f}'} \, d\boldsymbol{u}, \tag{10}$$

where $\boldsymbol{f}' = [f_1 \cdots f_{n-1}]^{\dagger}$.

The *spectral moment, spectral cumulant,* and *cyclic polyspectrum* are defined as follows. Consider the n complex-demodulate time-series $X_T(t, f_j)$ for $j = 1, \cdots, n$, associated with narrow bandpass filtered versions of $x(t)$, where

$$X_T(t, f) = \int_{t-T/2}^{t+T/2} x(v) e^{-i2\pi f v} \, dv. \tag{11}$$

The limit as $T \to \infty$ of the limiting time-average of the product of these spectral components is called the *spectral moment function* (SMF) of order n

$$S_x(\boldsymbol{f})_n \triangleq \lim_{T \to \infty} \left\langle \prod_{j=1}^{n} X_T(t, f_j) \right\rangle, \tag{12}$$

and it can be shown that Dirac deltas can be factored out as follows:

$$S_x(\boldsymbol{f})_n = \sum_{\alpha} \bar{S}_x^{\alpha}(\boldsymbol{f}')_n \delta(\boldsymbol{f}^{\dagger}\mathbf{1} - \alpha), \tag{13}$$

where $\delta(\cdot)$ is the Dirac delta function. However, the factor $\bar{S}_x^{\alpha}(\boldsymbol{f}')_n$ contains additional Dirac deltas for many signals and $n > 2$ (e.g., BPSK and $n = 4$).

The *spectral cumulant function* (SCF) of order n is given by

$$P_x(\boldsymbol{f})_n = \sum_{P=\{\nu_k\}_{k=1}^{p}} \left[k(p) \prod_{j=1}^{n} S_x(\boldsymbol{f}_{\nu_j})_{n_j} \right], \tag{14}$$

where $\boldsymbol{f}_{\nu_j}$ is the vector of n_j frequencies with subscripts in the set ν_j, and it follows from (13) that Dirac deltas can again be factored out:

$$P_x(\boldsymbol{f})_n = \sum_{\beta} \bar{P}_x^{\beta}(\boldsymbol{f}')_n \delta(\boldsymbol{f}^{\dagger}\mathbf{1} - \beta). \tag{15}$$

Analogous to the definition of the cyclic spectrum (and power spectrum) in [15], the factor $\bar{P}_x^{\beta}(\boldsymbol{f}')_n$ is defined to be the *cyclic polyspectrum* (CP) and is given explicitly by

$$\bar{P}_x^{\beta}(\boldsymbol{f}')_n = \sum_{P=\{\nu_k\}_{k=1}^{p}} \left[k(p) \sum_{\boldsymbol{\alpha}^{\dagger}\mathbf{1}=\beta} \bar{S}_x^{\alpha_p}(\boldsymbol{f}'_{\nu_p})_{n_p} \prod_{j=1}^{p-1} \left\{ \bar{S}_x^{\alpha_j}(\boldsymbol{f}'_{\nu_j})_{n_j} \delta(\boldsymbol{f}_{\nu_j}^{\dagger}\mathbf{1} - \alpha_j) \right\} \right]. \tag{16}$$

As first shown in [2], the CP is the $(n-1)$-dimensional Fourier transform of the RD-CTCF $\bar{C}_x^{\beta}(\boldsymbol{u})_n$ (cf. (10)). This is a generalization of the Wiener relation between the power spectrum and autocorrelation from second-order stationary time-series (cf. [15]) to nth-order

cyclostationary time-series. Within the stochastic-process framework of generally nonstationary processes, it should be called the *cyclic Shiryaev-Kolmogorov* relation [22], which is the generalization of the Wiener-Khinchin relation (cf. [15]). Because the RD-CTCF can be absolutely integrable, the CP—unlike the SMF—contains no Dirac deltas. That is, all Dirac deltas present in the individual terms in (16) cancel.

Let us now see how the cumulant arises as the solution to the problem of generating pure nth-order sine waves. For low orders n, it is easy to mathematically characterize a pure nth-order sine wave in a way that matches our intuition. For notational simplicity, we choose the case of no conjugated factors in (1). For $n = 1$, the moment sine waves (the sine-wave components of the polyperiodic TMF) are, by definition, pure 1st-order sine waves. For $n = 2$, all products of 1st-order moment sine waves can be subtracted from the 2nd-order moment sine waves to obtain the pure 2nd-order sine waves, which are denoted by $\sigma_x(t, \tau_1, \tau_2)_2$,

$$\begin{aligned} \sigma_x(t, \tau_1, \tau_2)_2 &\triangleq \hat{E}^{\{\alpha\}} \{x(t+\tau_1)x(t+\tau_2)\} - \hat{E}^{\{\alpha\}} \{x(t+\tau_1)\} \hat{E}^{\{\alpha\}} \{x(t+\tau_2)\} \\ &= R_x(t, \boldsymbol{\tau})_2 - R_x(t, \tau_1)_1 R_x(t, \tau_2)_1. \end{aligned}$$

There are several interesting points to be made concerning pure 2nd-order sine waves: (i) since $R_x(t, \tau_i)_1, i = 1, 2$, and $R_x(t, \boldsymbol{\tau})_2$ are 1st- and 2nd-order moments respectively, then $\sigma_x(t, \tau_1, \tau_2)_2$ is a temporal covariance function; (ii) if $R_x(t, \tau)_1 \equiv 0$, then there are no lower-order sine waves, and the 2nd-order moment sine waves are equal to the pure 2nd-order sine waves; (iii) if the variables $x(t + \tau_1)$ and $x(t + \tau_2)$ are statistically independent (in the temporal sense [15, 13]), then $\hat{E}^{\{\alpha\}} \{x(t+\tau_1)x(t+\tau_2)\} = \hat{E}^{\{\alpha\}} \{x(t+\tau_1)\} \hat{E}^{\{\alpha\}} \{x(t+\tau_2)\}$ and therefore $\sigma_x(t, \tau_1, \tau_2)_2 = 0$, that is, there is no pure 2nd-order sine wave for this particular pair of delays τ_1 and τ_2. This latter point shows that the set of pure cycle frequencies $\{\beta\}$ can be considerably different from the set of impure (moment) cycle frequencies $\{\alpha\}$.

The pure 3rd-order sine waves are obtained next. From the 3rd-order moment sine waves, we want to subtract each possible product of lower-order sine waves, but only once each. Thus, we subtract products of *pure* 2nd-order and *pure* 1st-order sine waves from the 3rd-order moment sine waves, rather than subtracting products of 1st- and 2nd-order moment sine waves:

$$\begin{aligned} \sigma_x(t, \boldsymbol{\tau})_3 &= \hat{E}^{\{\alpha\}} \left\{ \prod_{j=1}^{3} x(t+\tau_j) \right\} - \sigma_x(t, \tau_1, \tau_2)_2 \, \sigma_x(t, \tau_3)_1 \; - \sigma_x(t, \tau_1, \tau_3)_2 \, \sigma_x(t, \tau_2)_1 \\ &\quad - \sigma_x(t, \tau_2, \tau_3)_2 \, \sigma_x(t, \tau_1)_1 \; - \sigma_x(t, \tau_1)_1 \, \sigma_x(t, \tau_2)_1 \, \sigma_x(t, \tau_3)_1 \; . \end{aligned}$$

Observe that there are no other possible products of *pure* lower-order sine waves. The terms in the sum of products that are subtracted can be enumerated by considering the distinct partitions of the index set $\{1, 2, 3\}$. A partition of a set G is a collection of p subsets of G, $\{\nu_j\}_{j=1}^{p}$, with the following properties: $G = \bigcup_{j=1}^{p} \nu_j$ and $\nu_j \bigcap \nu_k = \emptyset$ for $j \neq k$. The set P_3 of distinct partitions of $\{1, 2, 3\}$ is given by

$$\begin{array}{lllll} p = 1: & \{1,2,3\} & & & \\ p = 2: & \{1,2\}, \{3\} & \{1,3\}, \{2\} & \{2,3\}, \{1\} & \\ p = 3: & \{1\}, \{2\}, \{3\} \; . & & & \end{array}$$

Thus, we can express the pure 3rd-order sine wave $\sigma_x(t,\boldsymbol{\tau})_3$ as a sum over the elements of P_3:

$$\sigma_x(t,\boldsymbol{\tau})_3 = R_x(t,\boldsymbol{\tau})_3 - \sum_{\substack{P_3 \\ p\neq 1}} \left[\prod_{j=1}^{p} \sigma_x(t,\boldsymbol{\tau}_{\nu_j})_{n_j} \right], \tag{17}$$

where $\boldsymbol{\tau}_{\nu_j}$ is a subset of $\{\tau_j\}_{j=1}^3$ with elements having indices in ν_j, and n_j is the number of elements in ν_j. Notice that, as in the case of $n=2$, if the 1st-order moment sine waves are zero, then the 3rd-order moment sine waves are equal to the pure 3rd-order sine waves. In this case, there are no *products* of lower-order sine waves to subtract from the moment sine waves.

The formula for the pure nth-order sine waves is

$$\sigma_x(t,\boldsymbol{\tau})_n = R_x(t,\boldsymbol{\tau})_n - \sum_{\substack{P_n \\ p\neq 1}} \left[\prod_{j=1}^{p} \sigma_x(t,\boldsymbol{\tau}_{\nu_j})_{n_j} \right], \tag{18}$$

where P_n is the set of distinct partitions of the index set $\{1,2,\cdots,n\}$. The pure-sine-waves formula (18) gives all the pure nth-order sine waves associated with the delay set $\boldsymbol{\tau}$. A single pure nth-order sine wave with frequency β can be selected by computing the Fourier coefficient:

$$\sigma_x^{\beta}(\boldsymbol{\tau})_n\, e^{i2\pi\beta t} = \left\langle \sigma_x(u,\boldsymbol{\tau})_n \;\; e^{-i2\pi\beta(u-t)} \right\rangle, \tag{19}$$

and can be expressed in terms of pure lower-order sine waves by using the Fourier series for each $\sigma_x(t,\boldsymbol{\tau}_{\nu_j})_{n_j}$ in (18):

$$\sigma_x(t,\boldsymbol{w})_k = \sum_{\beta_k} \sigma_x^{\beta_k}(\boldsymbol{w})_k\, e^{i2\pi\beta_k t}, \qquad \boldsymbol{w} = [w_1 \cdots w_k]^{\dagger}, \tag{20}$$

where the sum is over all cycle frequencies β_k of order k. Thus, the strength of a single pure nth-order sine wave is given by

$$\sigma_x^{\beta}(\boldsymbol{\tau})_n = R_x^{\beta}(\boldsymbol{\tau})_n - \sum_{\substack{P_n \\ p\neq 1}} \left[\sum_{\mathbf{1}^{\dagger}\boldsymbol{\beta}=\beta} \prod_{j=1}^{p} \sigma_x^{\beta_j}(\boldsymbol{\tau}_{\nu_j})_{n_j} \right], \tag{21}$$

where $\boldsymbol{\beta}$ is the p-dimensional vector of pure cycle frequencies $[\beta_1 \;\cdots\; \beta_p]^{\dagger}$ and $\mathbf{1}$ is the p-dimensional vector of ones. Hence, the pure-sine-wave strength $\sigma_x^{\beta}(\boldsymbol{\tau})_n$ is given by the CTMF $R_x^{\beta}(\boldsymbol{\tau})_n$ with all products of pure lower-order sine-wave strengths, for sine waves whose frequencies sum to β, subtracted out. From (8), it is clear that the pure-sine-wave strength $\sigma_x^{\beta}(\boldsymbol{\tau})_n$ is identical to the CTCF $C_x^{\beta}(\boldsymbol{\tau})_n$.

Finally, let us see how the CTCF (and the CP) is signal selective. Let the signal $x(t)$ consist of the sum of M mutually independent signals $\{y_m(t)\}_{m=1}^M$,

$$x(t) = \sum_{m=1}^{M} y_m(t). \tag{22}$$

Then the addition rule for cumulants [4, 23] can be used to show that the nth-order TCF for $x(t)$ is the sum of TCFs for $\{y_m(t)\}$,

$$C_x(t,\boldsymbol{\tau})_n = \sum_{m=1}^{M} C_{y_m}(t,\boldsymbol{\tau})_n. \tag{23}$$

Thus, the pure nth-order sine waves in the delay products of each $y_m(t)$ add to form the pure nth-order sine wave in the delay product of $x(t)$:

$$C_x^{\beta}(\boldsymbol{\tau})_n = \sum_{m=1}^{M} C_{y_m}^{\beta}(\boldsymbol{\tau})_n. \tag{24}$$

The TMF does not in general obey this useful cumulative relation (24). That is, the nth-order TMF for $x(t)$ is not the sum of nth-order TMFs for each $y_m(t)$: $R_x(t,\boldsymbol{\tau})_n \neq \sum_{m=1}^{M} R_{y_m}(t,\boldsymbol{\tau})_n$. An exception is the case of zero-mean signals and $n \leq 3$, for which moments and cumulants are equal, which is a commonly encountered case in HOS.

To illustrate how (24) can be applied in practice, consider the situation in which $\{y_m(t)\}$ represent M interfering signals that overlap in time and frequency, but each $y_m(t)$ possesses some distinct nth-order cycle frequency, say β_m. Then it follows from (24) that

$$C_x^{\beta_m}(\boldsymbol{\tau})_n = C_{y_m}^{\beta_m}(\boldsymbol{\tau})_n, \quad m = 1, 2, \cdots, M. \tag{25}$$

This indicates that the presence or absence of each of the signals $y_m(t)$ can be detected by measuring (estimating) the CTCFs of $x(t)$ for the cycle frequencies $\{\beta_m\}$, and that parameters of each of the signals, on which these CTCFs depend, can be estimated. As illustrated in [15, 12, 14] for second order and in [4] for higher order, this signal-selectivity property can be exploited in numerous ways to accomplish noise-and-interference-tolerant signal detection and estimation.

As another application, let $M = 2$, $y_1(t)$ be non-Gaussian, and $y_2(t)$ be Gaussian. Then $C_{y_2}(t,\boldsymbol{\tau})_n \equiv 0$ for $n \geq 3$ and, from (23), we have $C_x(t,\boldsymbol{\tau})_n = C_{y_1}(t,\boldsymbol{\tau})_n, \quad n \geq 3$, which indicates the detectability of $y_1(t)$ with no knowledge about $y_2(t)$ except that it is Gaussian.

As an example of the cyclic polyspectrum, we consider the class of digital QAM signals described by their complex envelopes, which can be expressed as $x(t) = \sum_{m=-\infty}^{\infty} a_m p(t - mT_0 - t_0)$, where $p(t)$ is the complex pulse and $\{a_m\}$ is the complex digital data. Assuming that $\{a_m\}$ is an independent sequence, we have shown [10, 5, 11] that the CP for the set of variables $\{x^{(*)_j}(t+\tau_j)\}_{j=1}^{n}$ (with $\tau_n = 0$), where $(*)_j$ denotes an optional conjugation of the jth variable, is given by

$$\bar{P}_x^{\beta}(\boldsymbol{f}')_n = \frac{C_{a,n}}{T_0} P((-)_n[\beta - \mathbf{1}^{\dagger}\boldsymbol{f}'])^{(*)_n} \prod_{j=1}^{n-1} P((-)_j f_j)^{(*)_j} e^{i2\pi\beta t_0}, \quad \beta = k/T_0, \tag{26}$$

where $(-)_j$ is the optional minus sign corresponding to the optional conjugation $(*)_j$, $C_{a,n}$ is the cumulant of a_m, and

$$P(f) = \int_{-\infty}^{\infty} p(t) e^{-i2\pi f t}\, dt. \tag{27}$$

Thus, the CP is simply a scaled product of n pulse transforms.

Signal Classification Using the General Search Algorithm

by

Chad M. Spooner and William A. Gardner

Abstract

In this report the problem of determining the number and modulation types of cyclostationary signals that are present (if any) in a given data record is studied. The signals are assumed to be cochannel; that is, the signals are assumed to substantially overlap in time and frequency. The *general search algorithm* is used to blindly estimate, in an order-recursive procedure, higher-order cyclic cumulants, then the *grouping algorithm* is used to associate the cyclic cumulants with each other and, therefore, with signals in the data, and finally the *classification algorithm* is used to determine the modulation type for each signal based on the grouped cyclic cumulant estimates. The GSA/GA tandem is described in detail and applied to simulated data to produce a catalog of features for classification. These two algorithms are applied to data records that contain two cochannel signals to illustrate the fact that the measurements of the features are signal selective. Finally, the CA is described and it is shown that certain signal types cannot be uniquely classified (given the cochannel signal assumption) without using cyclic cumulants of order larger than two.

1 Introduction

There are several situations in which a signal reception system receives multiple signals with unknown modulation types. One example is the general nuisance of cochannel interference. In this situation, the signal of interest is received along with other signals that are not of interest, and about which nothing is known. Another example is when the radio spectrum is monitored for the purpose of regulating radio transmissions in a given geographical area. In the former situation, the task is to remove the effects of the interfering signals on the signal of interest, and in the latter situation, the task is to determine the types of signals that are received and, possibly, to demodulate the signals to determine their message content. A third example is that of signal search for interception, in which the goal is to determine as much information as possible about all the unknown signals that are present (including the modulation format, location and type of emitter, and, possibly, the message).

When a single signal is received in a small amount of noise, various techniques can be used to make a decision about the signal's modulation type [25]–[37]. For example, a phase histogram can be computed, the bandwidth and center frequency can be accurately estimated, the modulus can be measured, pilot tones can be detected, etc. Various automatic modulation classifiers can be constructed based upon these and other measurements. On the other hand, when multiple signals are received and these signals are substantially spectrally and temporally overlapping, or when the noise is strong with respect to the signal, these techniques tend to fail. The primary reason for this is that the above measurements are not signal selective; each signal (including noise) contributes to the measurements, thereby degrading them, and reducing the efficacy of the subsequent classification algorithm.

In this report, the possibility of using the cyclostationarity property of communication signals to perform modulation recognition is investigated. In particular, the second- and higher-order cyclostationarity [14, 11, 4, 5] of the signals is used to create signal-selective features for modulation classification and recognition. Because the relevant statistical parameters associated with cyclostationarity are asymptotically independent of stationary noise and interference, so are the derived feature vectors. In addition, if the modulation parameters of the received signals are distinct (e.g., distinct baud rates and carrier frequencies),

then the feature vector for a particular received signal will be asymptotically independent of all other received signals.

2 The Classification Problem

Let $x(t)$ denote the received data, which consists of the sum of M statistically independent signals $s_j(t)$ together with additive noise:

$$x(t) = \sum_{j=1}^{M} s_j(t) + w(t) \quad 0 \leq t \leq T. \tag{1}$$

M is assumed to be unknown and $w(t)$ is assumed to be stationary and Gaussian. The signal $x(t)$ is complex-valued, and it is assumed that it is obtained by in-phase and quadrature sampling of the downconverted radio-frequency signal. Thus, if the downconversion frequency is equal to the carrier frequency of the signal $s_k(t)$, then this signal has a carrier offset of zero. The carrier offsets of the M signals are assumed to be sufficiently closely spaced so as to preclude the use of filtering to separate the signals.

The classification problem considered herein is to determine the modulation type of each of the signals $s_j(t)$. The first part of this problem consists of determining the number of cyclostationary signals that are present in the data record. This is called the *general search problem.* Higher-order cyclostationarity is used to devise a solution to the general search problem. This solution provides estimates of a feature vector for each signal in the data. Classification can then be accomplished by using the measured feature for each signal.

The main idea behind the use of higher-order cyclostationarity to perform signal classification is that of sine-wave generation by nonlinear transformation. When a cyclostationary signal is subjected to a series of nonlinear transformations, a series of sets of finite-strength additive sine waves are produced. Distinct modulation formats produce distinct sets of sine waves if the series of nonlinear transformations is chosen correctly. When the series of transformations in applied to data that contains multiple signals with distinct modulation parameters, the resulting sine waves can be grouped into disjoint subsets such that each subset's strengths, frequencies, and phases depend (asymptotically) on only a single signal that is present in the data. The particular series of nonlinear transformations of the data

that is proposed here is the series of nth-order temporal cumulant functions.

The remainder of this report is organized as follows. In Section 3, an overview of the classification procedure is presented. In Section 4, the *general search algorithm* (GSA), which is used to compute the sequence of nth-order temporal cumulant functions, and the *grouping algorithm* (GA), which is used to associate (group) the detected sine-wave frequencies obtained by the GSA, are presented and explained. In Section 5, the feature vectors for classification are defined in terms of the output of the GA, and extensive computer simulation examples are presented. In Section 6, the proposed *classification algorithm* (CA) is presented. The fundamentals of the theory of the higher-order statistics of cyclostationary signals are provided in Appendix A.

3 Overview of Solution

A crude outline of the classification procedure is given in the following:

- Collect data.
- Fix maximum order N of nonlinearity for processing.
- Estimate temporal cumulant functions (TCFs) for orders 1 (or 2) through N using the *general search algorithm.*
- Extract from the estimated TCFs a set of TCFs for individual signals in the data using the *grouping algorithm.*
- Compare each extracted set of TCFs to known sets of TCFs for signals of interest. Classify the modulation type of the signal based on the similarity to the known TCFs using the *classification algorithm.*

4 The General Search and Grouping Algorithms

The approach taken to solving the general search problem consists of estimating the cycle frequencies of the data for nonlinear processing of various orders [5, 10, 8, 11]. In order

to associate the resulting cycle frequency estimates with specific signals in the data, it is required to estimate cumulant sine-wave frequencies rather than moment cycle frequencies. This is because moment cycle frequencies can consist of sums and differences of the cycle frequencies for various distinct signals and are, therefore, not associated with any particular signal in the data, and because the strengths of the desired sine waves are functions of all signals in the data.

Let N be the maximum order of nonlinearity that is to be used for processing. The goal of the processing is to produce a list of cumulant cycle frequencies $\{\beta_n\}$ for each value of n from 1 to N. The list $\{\beta_n\}$ characterizes the detectable cyclostationarity of order n (and only n) that is associated with $x(t)$ because it is not contaminated by entries that are due to lower-order sine wave interactions. To accomplish this task, we estimate the temporal cumulant function (TCF) for $x(t)$ for each order n. From this estimate, the cycle frequencies $\{\beta_n\}$, which are needed for the estimate of the TCF for order $n+1$, can be estimated.

This approach is justified by the well-known fact that the periodogram is the optimal estimator of the frequency of a sine wave in white Gaussian noise. Although we are not primarily interested in the case of white Gaussian noise, our algorithm essentially estimates the frequencies of a set of relatively strong sine waves in noise and, therefore, the periodogram is of interest. In addition, the algorithm implements an estimator of the pure-sine-waves function for each order n, which we have shown is the signal-selective function of interest in applications. More explicitly, the general search problem can be tackled using the following *general search algorithm* (GSA):

0 Let $n = 1$, fix $N > 1$, denote the data by $x(t), 0 \le t \le T$,
choose N delays $\tau_1, \cdots \tau_N$, and choose m optional conjugations.

1 Compute $\hat{C}'_x(t,\boldsymbol{\tau})_n = \left[\prod_{j=1}^{n} x^{(*)_j}(t+\tau_j)\right] - \sum_{\substack{P_n \\ p\neq 1}} \left[\prod_{j=1}^{p} \hat{C}_x(t,\boldsymbol{\tau}_{\nu_j})_{n_j}\right]$ for $\boldsymbol{\tau} = [\tau_1 \cdots \tau_n]$

2 Compute $Y(f) = \mathrm{FFT}_t \{\hat{C}'_x(t,\boldsymbol{\tau})_n\}$

3 Threshold detect the bins of Y to find $\{\beta_n\}$

4 Compute the CTCFs $\hat{C}_x^{\beta_n}(\boldsymbol{\tau})_n = \left\langle \hat{C}'_x(t,\boldsymbol{\tau})_n \, e^{-i2\pi\beta_n t} \right\rangle_T$

5 Compute the TCF $\hat{C}_x(t,\boldsymbol{\tau})_n = \sum_{\beta_n} \hat{C}_x^{\beta_n}(\boldsymbol{\tau})_n e^{i2\pi\beta_n t}$

6 $n \rightarrow n+1$; if $n \leq N$ then go to 1, else stop.

The operation of the GSA and the notation that is introduced above are explained in detail next.

In Step 0, the maximum order of nonlinearity to be considered is fixed at $N > 1$, the N delays to be used are chosen, the m optional conjugations are chosen for each processing order $n < N$, and the processing order n is initialized to 1.

In Step 1, a pre-estimate of the nth-order TCF for order n is obtained by subtracting from the nth-order delay product $\prod_{j=1}^{n} x^{(*)_j}(t+\tau_j)$ the products of lower-order TCFs estimated in previous iterations of the algorithm. For $n = 1$, there are no previous iterations, so the first-order pre-estimate of the TCF is set equal to the first-order lag product itself, which is just the data $x(t+\tau_1)$. For $n = 2$, the product of the first-order TCF estimates for each of the selected lags τ_1 and τ_2 are subtracted from the second-order lag product. This removes from consideration any sine waves in the second-order lag product that result from products of first-order sine waves. For $n > 2$, the sum of products of lower-order TCFs is determined by the set P_n, which is the set of distinct partitions of the set of indices $\{1, 2, \cdots, n\}$. This set is described in Appendix A.

In Step 2, the pre-estimate of the TCF obtained in Step 1 is Fourier transformed in the t variable in order to determine its sine-wave components.

In Step 3, the values of this transformed TCF pre-estimate are compared to a threshold. The locations in f of the values of the transformed pre-estimate that exceed the threshold are declared to be cycle frequencies $\{\beta_n\}$.

In Step 4, the estimated cycle frequencies are used to compute estimates of the cyclic temporal cumulant functions (CTCFs), which are the Fourier coefficients of the TCF estimates. If the Fourier transform in Step 2 has length equal to the total amount of data available (T), then the CTCFs are already computed in Step 2, and do not need to be computed again. To handle the case in which the cycle frequencies do not lie on bin-center frequencies, interpolation techniques are used to estimate the frequency of the sine wave, and its magnitude and phase can then be estimated by direct computation of the discrete

Fourier transform. If two adjacent bins are declared to correspond to sine-wave frequencies, then this interpolation is done. That is, if two adjacent bins have large magnitudes, then it is assumed that a single sine wave with frequency somewhere between the two bin frequencies is responsible for this energy.

In Step 5, the estimated cycle frequencies and CTCFs are combined to obtain an estimate of the TCF that replaces the pre-estimate obtained in Step 1.

Finally, in Step 6 the order of processing n is incremented and tested against its maximum allowed value N. If n is less than or equal to N then the algorithm returns to Step 1. Otherwise, processing is terminated.

Step 1 is the crucial step. Cycle frequencies could be estimated by Fourier transforming the lag product itself and thresholding its bins, but the resulting list of cycle frequencies would contain entries due to interactions among the distinct signals in the data. By subtracting the particular sum of products of lower-order TCFs in step 1, these false cycle frequencies are removed from consideration.

The output of the GSA is a sequence of lists that are indexed by order. Each list entry contains two elements. The first is the cycle-frequency estimate, usually denoted by α or β, and the second is the amplitude of the sine wave with frequency α for the appropriate order (phase information is suppressed in the output of the GSA, but retained internally). Multiple delay sets and choices of conjugated factors can be accommodated by sequential runs of the algorithm. The software implementation of the GSA is described in the next section.

4.1 The GSA Program

The *GSA program* takes a data record as its input and produces cycle frequency and cumulant estimates for specified orders. The minimum order is 1 and the maximum order is denoted by N. Typically, the minimum order is set to 2, and—as explained below—only the even orders between 2 and N are used. The other inputs to the GSA program are a set of delay vectors of dimension N, and a set of conjugation flags of dimension N. The GSA program then estimates the Nth-order temporal cumulant function (TCF) for each delay vector for each conjugation set. For instance, the program could be used to compute the fourth-order

cumulant of the input data for the two delay vectors

```
1 2 5 6
0 6 9 10
```

and the two conjugation-flag vectors

```
0 0 0 0
0 0 1 0
```

where 0 means do not conjugate and 1 means conjugate. This would result in four fourth-order temporal cumulant estimates. Two of these estimates are fourth-order estimates with 0 conjugations, and the remaining two are fourth-order estimates with the third variable conjugated. The former are called (4, 0) estimates ($n = 4$ and $m = 0$), and the latter are (4, 1) estimates. Because the GSA algorithm is recursive, second-order cumulants are estimated in order to estimate the fourth-order cumulants (if desired, the first- and third-order estimates can be made as well, but this is often unnecessary because these cumulants are zero for almost all communication signals [except those with pilot tones]). Since TCFs are polyperiodic functions, an individual TCF estimate can be represented by a collection of ordered triplets where the first element is a sine-wave frequency, the second is a sine-wave amplitude, and the third is a sine-wave phase. For the purpose of detecting and sorting, the phase is not needed. Thus, the phase is retained while the program is running, but only the frequency and magnitude parameters are actually output. An individual datum in the output of the GSA program is the quadruple (n, m, α, C), where n is the order, m is the number of conjugations, α is the cycle frequency estimate, and C is the estimate of the magnitude of the (n, m) CTCF for frequency α. These quadruplets are indexed by the delay vectors $\boldsymbol{\tau}$.

The output of the GSA program contains data of two fundamental sorts: X_U, which is the set of *upper* data, and X_L, which is the set of *lower* data. These are defined as

$$n = 2m \Rightarrow x \in X_L,$$

$$n \neq 2m \Rightarrow x \in X_U.$$

Elements in X_L have cycle frequency estimates α that are not (typically) related to carrier frequencies, whereas elements in X_U have cycle frequency estimates that are related to carrier frequencies.

The goal of the *grouping algorithm*, and its implementation, the *grouping program*, is to group this multidimensional data into sets such that each set corresponds to one and only one signal in the original data record.

4.2 The Grouping Algorithm

The output of the GSA program is a set of lists that are indexed by the order of processing. Visual inspection of these lists is difficult and is not particularly revealing. Because the cycle frequencies of communication signals (especially digital QAM signals) are harmonically related and appear at multiple orders of processing n, if there is a signal present in the data, then there will be a set of α estimates that are harmonically related. The main idea behind the *grouping algorithm* (GA) is to extract these cycle frequency estimates and group them together. The other cycle frequency-estimates in the output of the GSA program are discarded.

The word "cluster" in the following description of the GA refers to a standard unsupervised-learning partitioning algorithm [24]. This algorithm finds a collection of subsets of a given set such that a certain cost function related to the sample mean and variance of each subset is minimized. That is, at termination this cost would increase if any element of one of the sets is removed and then added to any of the other sets.

The grouping algorithm consists of the following steps:

1. Read GSA data: $x_j = (n, m, \alpha, \mathrm{C})_j$ for $j = 1, \cdots, M$, where $1 \leq n \leq N$ and $0 \leq m \leq N$ for each j.

2. Separate the data into two sets: X_U, which is the set of upper data ($n \neq 2m$), and X_L, which is the set of lower data ($n = 2m$).

3. Cluster the set X_L into three sets based on the value of C. That is, find a three-set partition of X_L such that the data with the largest C are in one set, those with the

smallest C are in another called X_w (the w stands for "weak"), and the rest are in a third.

4. Find the union of the two sets with largest C; call this set X_s (the s stands for "strong").

5. Cluster X_s based on the value of α. This results in many sets, each of which contains only elements with α that are "close together."

6. Search the set X_w for any elements with α that are harmonically related (integer multiples or divisors) to the mean of any of the sets obtained in the previous step. If any are found, add them to an appropriate set. Discard the remaining elements of X_w.

7. Recluster X_s.

8. Group the sets obtained by the previous step. This results in a group of sets. Each of the groups is associated with a unique fundamental frequency. The members of the groups are sets that are assumed to contain cycle frequencies that correspond to the various harmonics of this fundamental. Compute the harmonic numbers for each of these sets.

9. Store the vector of fundamentals (one fundamental for each group) for later use.

10. Cluster the set X_U into three sets based on the value of C. That is, find a three-set partition of X_U such that the data with the largest C are in one set, those with the smallest C are in another called X_w, and the rest are in a third.

11. Find the union of the two sets with largest C; call this set X_s.

12. Cluster X_s based on the value of α.

13. Search the set X_w for any elements with α that are separated by a multiple of one of the stored fundamentals from the mean of any of the sets obtained in the previous step. This must be done only for data that have matching n and m values. If any such elements are found, add them to an appropriate set. Discard the remaining elements of X_w.

14. Recluster X_s.

15. Using the stored fundamentals, associate the sets obtained in the previous step with a group obtained in step 8. Thus, upper sets are associated with lower sets through a fundamental frequency.

16. Estimate the carrier offset for the upper elements in each group.

17. Compute the harmonic of each upper cluster in each group by using the fundamental and the estimated offset.

18. Splinter each set in the following way. Form a separate set for each of the distinct (n, m) pairs that appear in the set. At the end of this procedure, every set will correspond to a single (n, m) pair and to a single harmonic.

19. Output the matrix of detected harmonics for each group. The rows of these matrices correspond to the harmonic number, and the columns correspond to each (n, m) pair associated with that group. The value of an element of the matrix is the maximum value of the C parameters of all the data points x_j contained in the set that corresponds to the appropriate group and (n, m) pair. This matrix shall be called a *feature matrix.*

5 Feature Vectors for Classification

The feature vector, which consists of a set of pairs of TCF Fourier component frequencies (cycle frequencies α) and magnitudes (cyclic cumulant magnitudes $|\mathrm{CTCF}_\alpha|$), can be viewed as a one-dimensional vector with complex-valued elements $(\alpha + i|\mathrm{CTCF}_\alpha|)$ indexed by (n, m), or as a two-dimensional vector (matrix) with real-valued elements indexed by $[\alpha, (n, m)]$. We will, therefore, use the terms feature vector and feature matrix interchangeably. The uniqueness of a particular signal's feature vector is most easily appreciated visually by using the matrix interpretation. The columns of the feature matrix correspond to the distinct order/number-of-conjugations pairs used (the (n, m) pairs), and the rows correspond to the harmonic number of the detected harmonic k, where $\alpha = k/T_0$ for which T_0^{-1} is the symbol rate of the signal that gives rise to the feature. The value of the matrix for a given row and

column is the maximum (over delay sets) absolute value of the amplitude of the sine wave with the harmonic specified by the row and corresponding to the (n, m) pair specified by the column. For example, the GSA might produce the cycle frequency α_0 for order 2 and number of conjugations 1 for several different delay pairs (τ_j, τ_k). The GA uses all of these instances of detection to properly group all the GSA-produced cycle frequencies, but it only outputs the largest amplitude. If the number and range of the delay vectors that are input to the GSA are large enough, then the GSA should produce among these instances of detection of this harmonic one that corresponds to its maximum theoretical value. Ideally, then, the feature matrix consists of the theoretical maximum of the amplitude of each harmonic that that signal actually exhibits for each input (n, m) pair. In practice, it consists of an estimate of this matrix. The definition of the feature matrix is shown graphically in Figure 1.

$\vdots$	$\vdots$	$\vdots$	$\vdots \ldots$
$k = 2$	$2f_c \pm 2/T_0$	$0f_c \pm 2/T_0$	$\ldots$
$k = 1$	$2f_c \pm 1/T_0$	$0f_c \pm 1/T_0$	$\ldots$
$k = 0$	$2f_c$	$0f_c$	$\ldots$
	$(n, m) = (2, 0)$	$(n, m) = (2, 1)$	$\ldots$

Figure 1: Definition of a feature matrix for detection and classification. An element of the feature matrix corresponds to the maximum of the magnitude of the cyclic cumulant for cycle frequency $\alpha = (n - 2m)f_c \pm k/T_0$, where k is uniquely specified by the row and the values of n and m are uniquely specified by the column.

Examples of measured feature vectors for a maximum order of eight (even orders only) are presented for a large number of modulated signals of interest in Figures 2–15. These examples include PSK, digital QAM, CPFSK, and partial-response signaling. These features were measured from data records of length 16384 (1024 symbols) samples of noise-free simulated signals. For all the feature matrices shown in this report, the first three columns corresponds to order two, the next five correspond to order four, the next seven to order six, and the remaining nine to order eight. For a single order, the columns start with $m = 0$ and end with $m = n$. It can be seen from these examples that the feature vectors are distinct for many kinds of modulations, but that a sufficiently large order of processing must be used to insure this distinction. For example, if the order of processing is restricted to six or less, then the feature matrices for 8PSK and 16PSK will be scaled versions of each other. But

for processing order of eight and greater, the feature matrices for these two modulations are distinct.

To perform classification of signals using these features, they must be made invariant to the signal power and to the specific carrier frequency and symbol rate. By design, the features are already invariant to the latter two parameters: the same feature occurs for any carrier and symbol rate because it is the existence and relative magnitudes of the symbol-rate harmonics that define the feature. However, two signals that are identical except for their power levels will not yield the same feature. Moreover, the two resulting features are not just multiples of each other. The effect of scaling a signal on the classification feature is explained in the next section. Following that, in Section 6, a classification algorithm is proposed, along with a method of normalizing the measured feature for the class of rectangular-pulse digital QAM signals. Further research is required to generalize the method to other signal classes.

5.1 Features of Scaled Signals

In this section, the effect of signal scaling on the classification features is investigated. This is an important topic because the power of the signals in the data is unknown. The effect of scaling a signal on the feature matrix is not linear. In particular, the scaling of the signal can be interpreted as a scaling of the symbol constellation and, therefore, the effect of scaling is reflected entirely in the cumulant of the symbol variable. Let a be a random variable with cumulants $C_{a,n}^m$, where n is the order of the cumulant and m specifies the number of times the variable is conjugated [11]. Then the random variable $x = Ba$, where B is a complex-valued constant, has cumulants $B^{n-m}(B^*)^m C_{b,n}^B$.

Let $s(t)$ represent a complex-valued PAM signal of interest with symbol sequence $\{a_j\}$. The magnitudes of the cyclic cumulants of the signal $x(t) = Bs(t)$, where B is a real number, are given by

$$|C_x^\beta(\boldsymbol{\tau})_n| = |B|^n \left| \frac{C_{a,n}^m}{T_0} \int_{-\infty}^{\infty} \prod_{k=1}^{n} p(t+\tau_k) e^{-i2\pi\beta t}\, dt \right| \tag{2}$$

where $1/T_0$ is the symbol rate, $p(t)$ is the pulse function, and β is the cycle frequency [11].

6 Classification Algorithms

6.1 Classification From the GSA/GA Output

The output of the GSA/GA combination can be used to classify the corresponding signal in the following way:

1. Input a measured feature matrix (one of the groups output by the GA).
2. Compute or retrieve theoretical feature matrices for all desired signal types for the same n, m values used to obtain the measured feature matrix.
3. Using a second- or fourth-order element of the measured feature matrix, determine the scaling factor (amplitude of the signal). (A method for doing this for rectangular-pulse digital QAM signals is explained in Section 6.2.) Scale the measured feature. Ideally, the candidate matrix for the true signal type and the input matrix will now have closely matching element values, whereas the other candidate matrices will have values that are significantly different.
4. Compute the difference between the normalized input feature and each theoretical candidate feature.
5. Declare the signal to be of the type that produced the matrix with the smallest difference between measured and theoretical features.

6.2 Rectangular-Pulse Signaling

In this section, the theoretical feature matrices for a subclass of the class of digital QAM signals are computed and the distance between them is evaluated. The subclass is that for which the pulse envelope is rectangular. The seven signals that are considered are BPSK, QPSK, 8PSK, MPSK, 8QAM, 16QAM, and 64QAM (for MPSK, $M > 8$). These signals contain subsets that have similar cyclostationarity properties for orders 1 through 8, as can be seen from the measurements presented in Section 5. The PSK signals have circular symbol constellations whereas the QAM signals do not.

The theoretical feature matrices can be computed for this subclass because the maximum of the cyclic temporal cumulant functions is relatively easy to compute for all orders and cycle frequencies. In particular, for any full-duty-cycle rectangular-pulse PAM signal with independent identically distributed symbols $\{a_m\}$, the maxima of the cyclic temporal cumulant functions are given by

$$\max_{\boldsymbol{\tau}} |C_x^{k/T_0}(\boldsymbol{\tau})_n| = \frac{|C_{a,n}^m|}{\pi |k|}, \qquad k \neq 0 \tag{3}$$

which occurs whenever the difference between the minimum and maximum values of the elements of the delay vector $\boldsymbol{\tau}$ equals $T_0 - (2j+1)T_0/(2|k|)$ for $j = 0, \cdots, |k|-1$. Note that the cumulant $C_{a,n}^m$ incorporates the optional conjugations employed in $C_x^{k/T_0}(\boldsymbol{\tau})_n$. For $k = 0$, the maxima are equal to $|C_{a,n}^m|$ which occur whenever the delay variables are equal to each other. A derivation of these results is contained in Appendix B. Since the complex envelope representations of digital QAM (including PSK) signals are exactly this type of PAM signal (when the pulse envelope is rectangular), these results are directly applicable.

The result (3) can be used to construct theoretical feature matrices for any order and number of harmonics. In this section, the theoretical features for the above-mentioned signals are computed and the differences between them measured for the purpose of evaluating the potential for classification. This is done for maximum processing orders N of two through eight. The results are displayed in terms of a type of confusion matrix. This confusion matrix is a plot of the distance between each of the feature matrices. If the features for the various signals are sufficiently distinct, then the confusion matrix will be zero along its main diagonal and large off this diagonal. If they are not sufficiently distinct, then small values appear off the main diagonal. The confusion matrices are shown in Figures 16–19. These figures show that the feature matrices become more and more distinct for these modulations as the order increases.

It is interesting to consider the possibility of performing signal classification based only on the symbol-rate cyclic features (for which the number of conjugated factors is equal to half the processing order). This classification possibility is well motivated because the most difficult and error-prone part of measuring the feature matrix involves the estimation of the carrier-related cyclic features (for which the number of conjugated factors is not equal to half

the processing order). The difficulty arises from the fact that there are typically many more cycle frequencies for $n \neq 2m$, and these are distinct for each such distinct n and m. There are many more false cycle frequencies that appear in this group because they must be associated with each other on the basis of their distances between each other. By coincidence, there can be many false cycle frequency pairs that have the required separation. The confusion matrices for the reduced-dimension classification features are shown in Figures 20–23. It can be seen that some degree of classification can be achieved using these features, but that it is less than that for the complete features.

6.3 Classification From Precise Cumulant Measurements

The GSA and GA perform the task of estimating and grouping the cycle frequencies corresponding to the signals in the data quite well, but the GSA is prone to estimating false cycle frequencies. These false cycle frequencies tend to degrade the quality of the estimates of higher-order temporal cumulant functions, which manifests itself in terms of errors in the estimate of the *strengths* of the cyclic cumulants, but not their frequencies. That is, the current implementation of the GSA and GA algorithms seems to be most well-suited to the cycle-frequency estimation problem, not the cyclic-cumulant estimation problem.

The classifier proposed herein depends on accurate measurements of not only the cycle frequencies, but also the cyclic cumulants. If another stage of processing is allowable, the cyclic cumulants can be measured using previously developed software (the relevant programs are called `ctcfn`, `partitions`, and `cross_cumulant`, which are written in C and were developed by the first author during his doctoral research [4]) written expressly for the purpose of estimating cyclic cumulants. This software requires knowledge of the lower-order cycle frequencies, which is exactly what is obtained by the GSA/GA tandem. In other words, the output of the GSA/GA tandem can be used by `ctcfn` and `cross_cumulant` to perform more precise estimates of the cyclic cumulants, which will result in more accurate estimates of the feature vectors and, therefore, better classification.

7 Research and Development

The following list of tasks are suggested by the research that is documented in this report:

1. Computer simulations for signal environments of interest,
2. Mathematical analysis of the higher-order cyclostationarity of communication signals that are not well modeled as complex-valued PAM signals at baseband, such as CPFSK, FSK, and analog FM,
3. Cataloging of the higher-order cyclic features of signals of interest,
4. Mathematical characterization of the quality of the GSA's cyclic cumulant estimates as a function of SNR, SIR, and collect time,
5. Study of the various metrics that can be used to measure the distance between feature vectors for classification,
6. Development of generalizations of the GA to handle the case in which signals share certain cyclostationarity properties (e.g., two or more signals with the same symbol rate but distinct carrier frequencies),
7. Design and development of fully automated and operator-assisted modes of operation,
8. Develop alternative hardware/software architectures for the two modes of operation,
9. Specify graphics for operator-assisted mode (and for demonstration),
10. Study feasibility of integrating into the GSA/GA system either or both of W. A. Brown's MLSC (maximum-likelihood spectral coherence) classifier and W. A. Gardner's ASCR (adaptive spectral correlation recognition) classifier, both of which utilize only second-order cyclostationarity,
11. Study alternate feature-extraction scheme that uses the cycle frequencies computed by the GSA and grouped by the GA to do precise cumulant measurements (see Section 6.3.

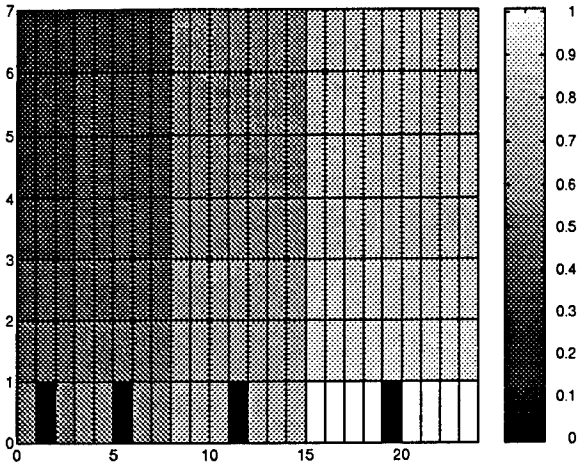

Figure 2: Measured feature matrix for a rectangular-pulse BPSK signal.

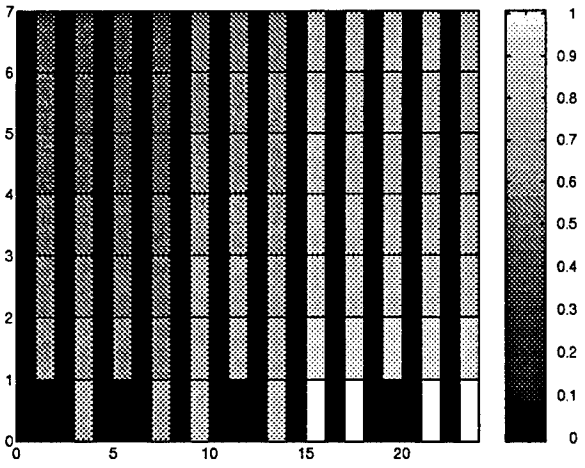

Figure 3: Measured feature matrix for a rectangular-pulse QPSK signal.

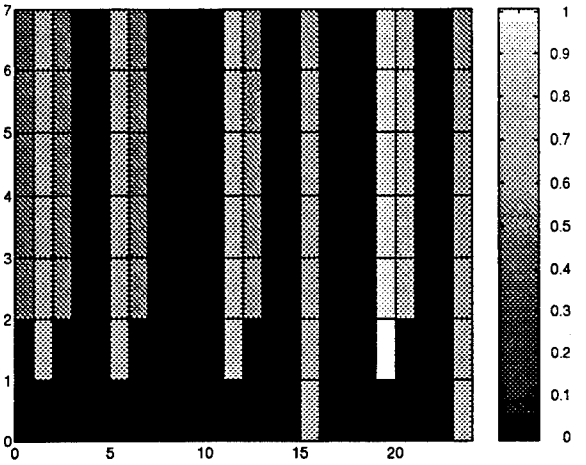

Figure 4: Measured feature matrix for a rectangular-pulse 8PSK signal. This feature contains some false cycle frequencies. In particular, the only upper cycle frequencies for this signal and $n \leq 8$ consist of those for 0 and 8 conjugations.

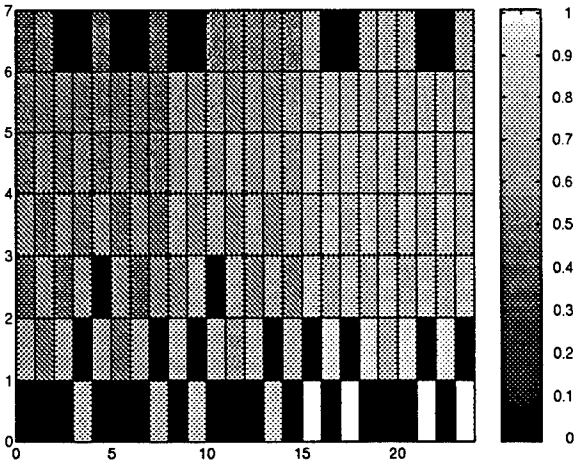

Figure 5: Measured feature matrix for a rectangular-pulse offset QPSK signal.

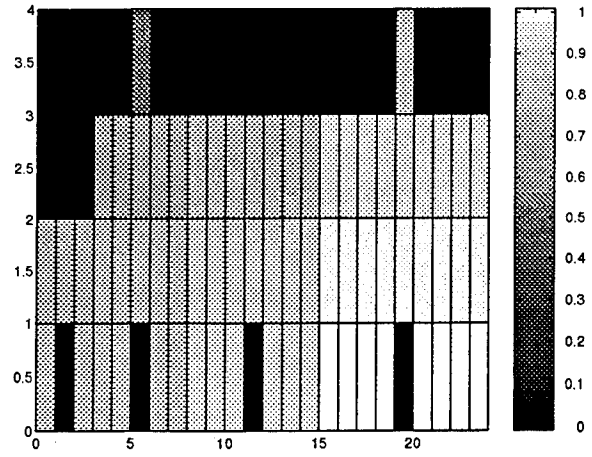

Figure 6: Measured feature matrix for a 100% excess-bandwidth BPSK signal.

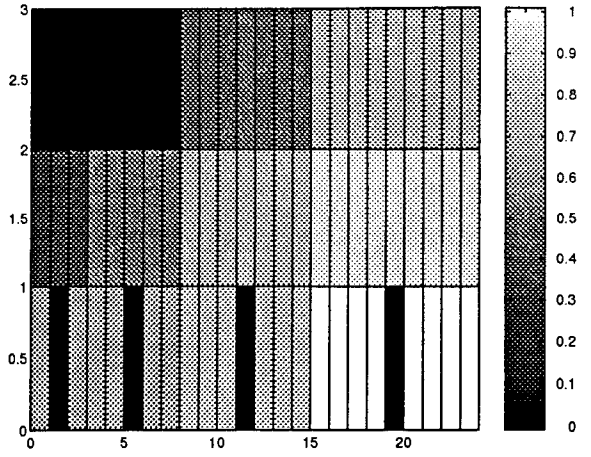

Figure 8: Measured feature matrix for a 25% excess-bandwidth BPSK signal. The gray cells for $n = 4$ and 6 and large k are false cycle frequencies.

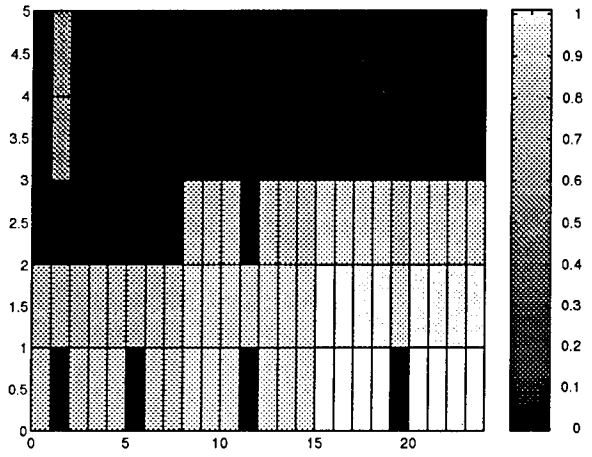

Figure 7: Measured feature matrix for a 50% excess-bandwidth BPSK signal. The gray cells for $n = 2$ and large k are false cycle frequencies.

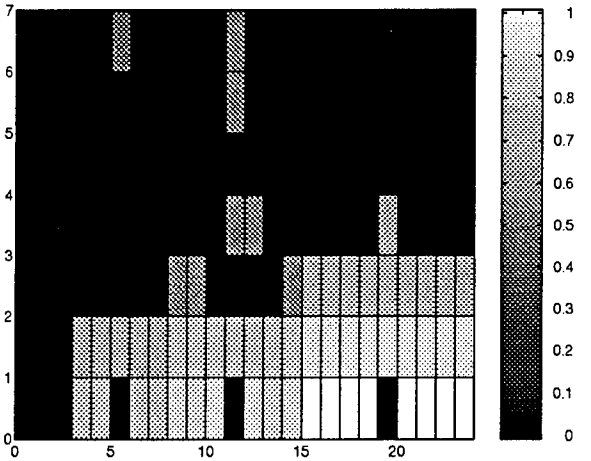

Figure 9: Measured feature matrix for a duobinary partial-response PAM signal.

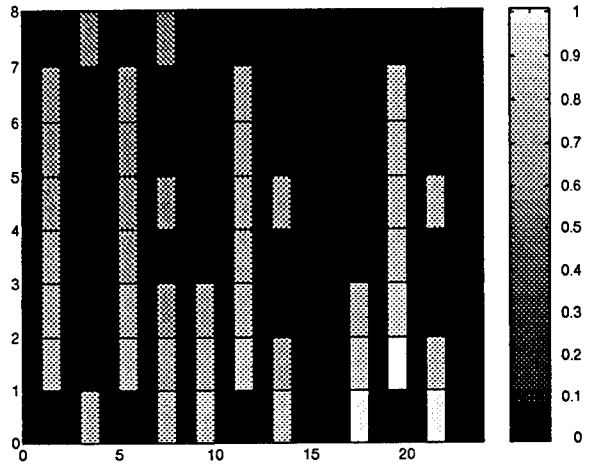

Figure 10: Measured feature matrix for a CPFSK signal with modulation index of 0.7. This signal does not fit the complex-valued PAM model that the GA is configured to recognize, and so the feature is not correct.

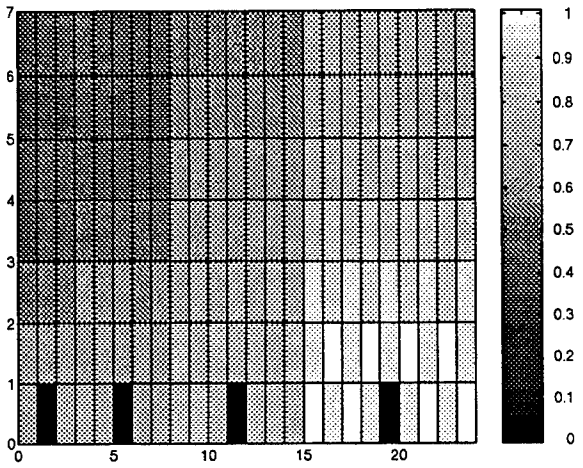

Figure 12: Measured feature matrix for a CPFSK signal with modulation index of 1.0.

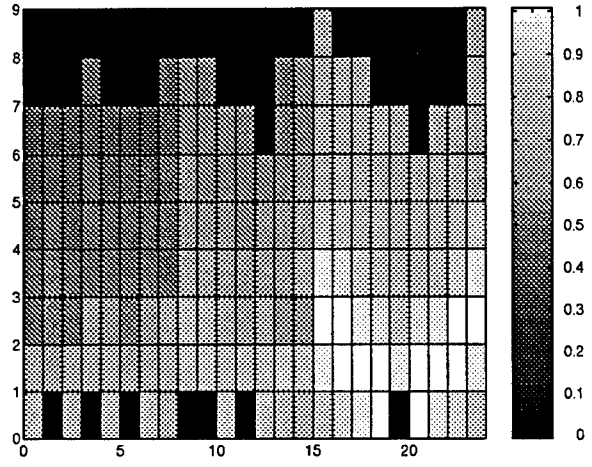

Figure 11: Measured feature matrix for a CPFSK signal with modulation index of 0.5.

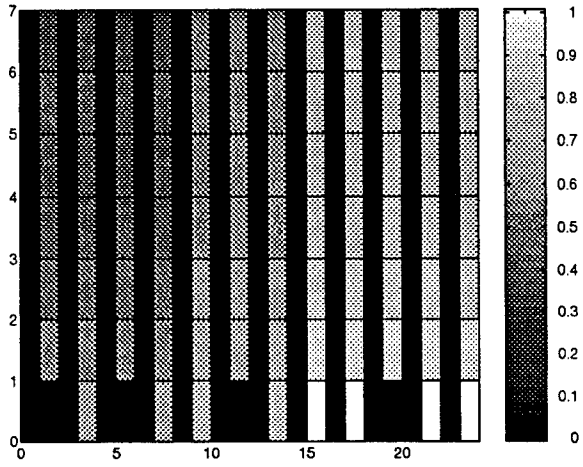

Figure 13: Measured feature matrix for a 4-QAM signal. Note similarity to the QPSK feature.

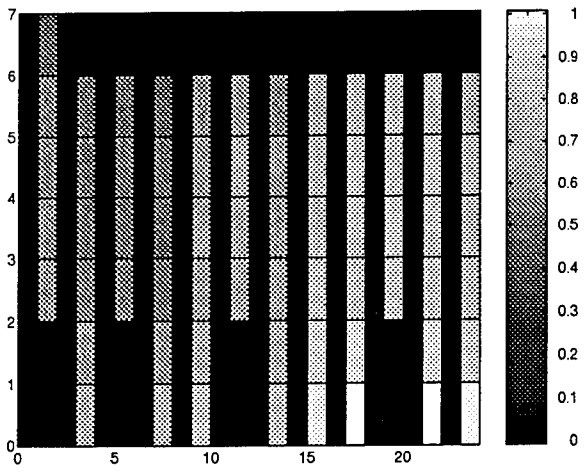

Figure 14: Measured feature matrix for a 8-QAM signal.

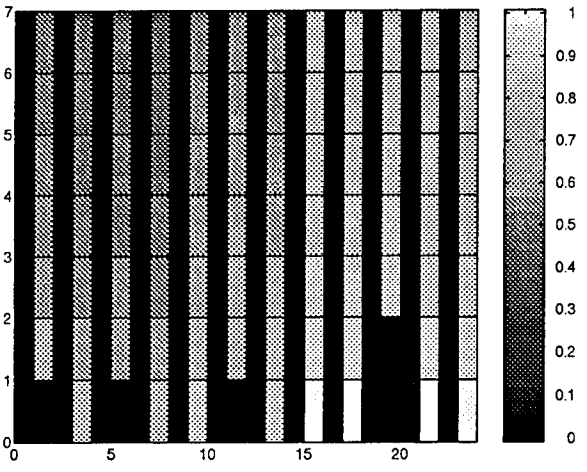

Figure 15: Measured feature matrix for a 16-QAM signal.

Figure 16: Theoretical-feature confusion matrix for seven full-duty-cycle rectangular-pulse digital QAM signals for maximum order $N = 2$ and $m = 0, 1, 2$. The signals are (from left to right and from lower to upper) BPSK, QPSK, 8PSK, MPSK, 4QAM, 8QAM, 16QAM, and 64QAM.

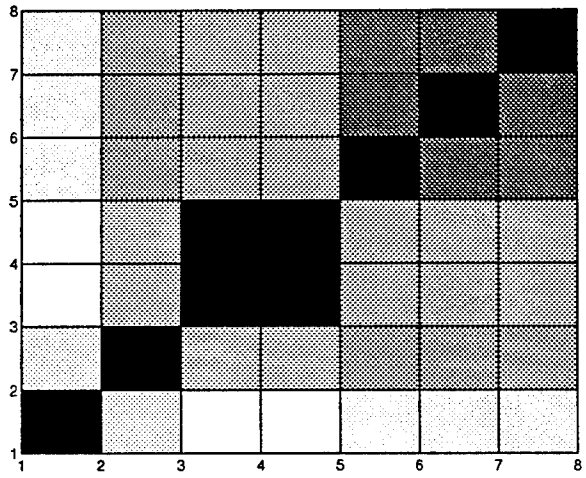

Figure 17: Theoretical-feature confusion matrix for seven full-duty-cycle rectangular-pulse digital QAM signals for maximum order $N = 4$ and $m = 0, \cdots, 4$. The signals are (from left to right and from lower to upper) BPSK, QPSK, 8PSK, MPSK, 4QAM, 8QAM, 16QAM, and 64QAM.

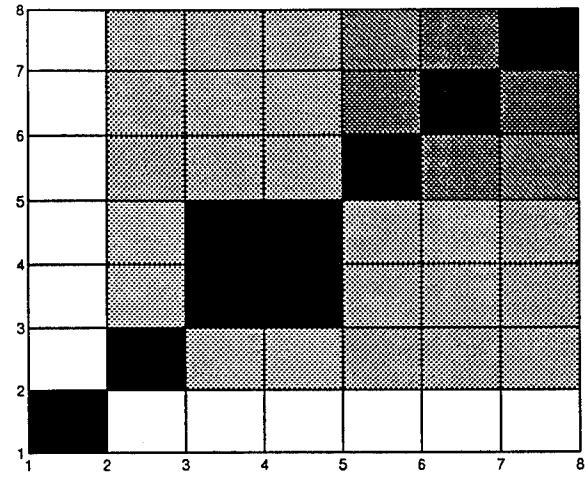

Figure 18: Theoretical-feature confusion matrix for seven full-duty-cycle rectangular-pulse digital QAM signals for maximum order $N = 6$ and $m = 0, \cdots, 6$. The signals are (from left to right and from lower to upper) BPSK, QPSK, 8PSK, MPSK, 4QAM, 8QAM, 16QAM, and 64QAM.

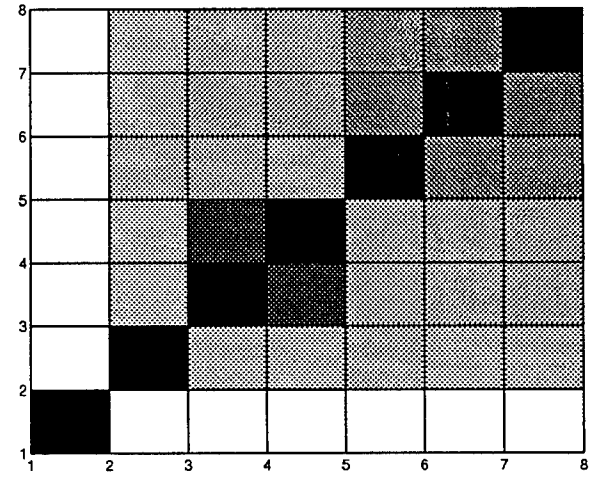

Figure 19: Theoretical-feature confusion matrix for seven full-duty-cycle rectangular-pulse digital QAM signals for maximum order $N = 8$ and $m = 0, \cdots, 8$. The signals are (from left to right and from lower to upper) BPSK, QPSK, 8PSK, MPSK, 4QAM, 8QAM, 16QAM, and 64QAM.

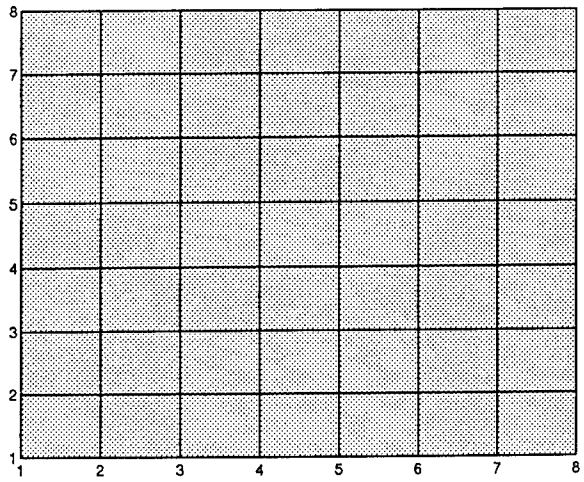

Figure 20: Theoretical-feature confusion matrix for seven full-duty-cycle rectangular-pulse digital QAM signals for maximum order $N = 2$ and $n = 2m$. (The features consist only of symbol-rate harmonics.) The signals are (from left to right and from lower to upper) BPSK, QPSK, 8PSK, MPSK, 8QAM, 16QAM, and 64QAM.

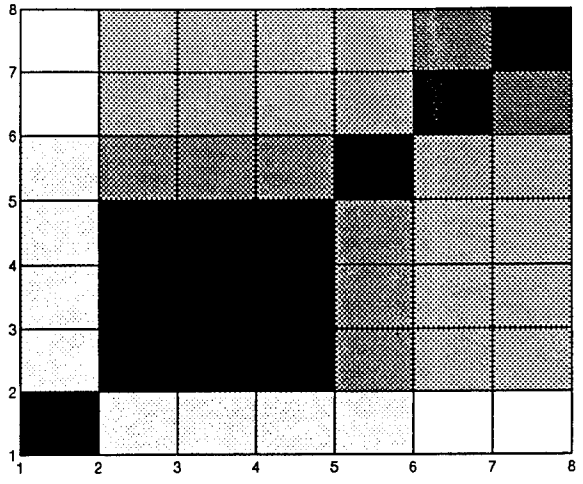

Figure 22: Theoretical-feature confusion matrix for seven full-duty-cycle rectangular-pulse digital QAM signals for maximum order $N = 6$ and $n = 2m$. (The features consist only of symbol-rate harmonics.) The signals are (from left to right and from lower to upper) BPSK, QPSK, 8PSK, MPSK, 8QAM, 16QAM, and 64QAM.

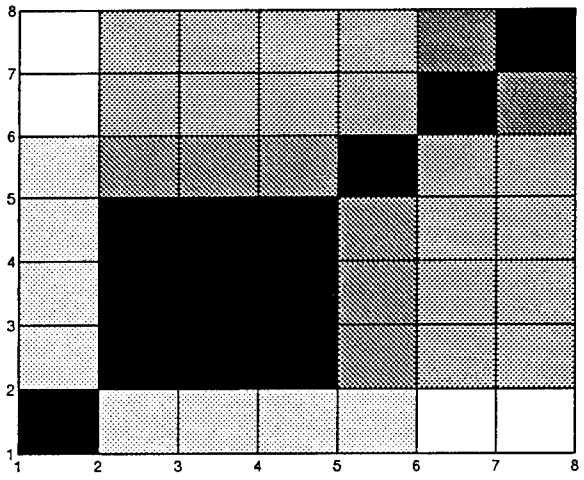

Figure 21: Theoretical-feature confusion matrix for seven full-duty-cycle rectangular-pulse digital QAM signals for maximum order $N = 4$ and $n = 2m$. (The features consist only of symbol-rate harmonics.) The signals are (from left to right and from lower to upper) BPSK, QPSK, 8PSK, MPSK, 8QAM, 16QAM, and 64QAM.

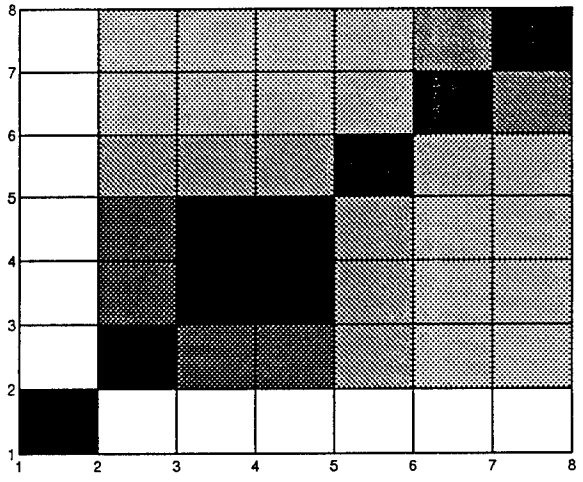

Figure 23: Theoretical-feature confusion matrix for seven full-duty-cycle rectangular-pulse digital QAM signals for maximum order $N = 8$ and $n = 2m$. (The features consist only of symbol-rate harmonics.) The signals are (from left to right and from lower to upper) BPSK, QPSK, 8PSK, MPSK, 8QAM, 16QAM, and 64QAM.

References

[1] W. A. Gardner, "Spectral Characterization of N-th Order Cyclostationarity," *Proceedings of the IEEE/ASSP Workshop on Spectrum Estimation,* Rochester New York, 1990.

[2] W. A. Gardner and C. M. Spooner, "Higher-Order Cyclostationarity, Cyclic Cumulants, and Cyclic Polyspectra," *Proceedings of the International Symposium on Information Theory and its Applications (ISITA),* Honolulu Hawaii, 1990.

[3] C. M. Spooner and W. A. Gardner, "An Overview of the Theory of Higher-Order Cyclostationarity," in *Proceedings of the Workshop on Nonstationary Stochastic Processes and Their Applications,* (A. G. Miamee, ed.), World Scientific, Singapore, 1992.

[4] C. M. Spooner, "Theory and Application of Higher-Order Cyclostationarity," Ph.D. Dissertation, Department of Electrical and Computer Engineering, University of California, Davis CA, 1992.

[5] C. M. Spooner, "Higher-Order Statistics for Nonlinear Processing of Cyclostationary Signals," in *Cyclostationarity in Communications and Signal Processing,* (W. A. Gardner, ed.), IEEE Press, New York, 1994.

[6] C. M. Spooner and W. A. Gardner, "Estimation of Cyclic Polyspectra," (invited paper) *Proceedings of the Twenty-Fifth Annual Asilomar Conference on Signals, Systems and Computers,* Pacific Grove, CA, Nov. 4-6, 1991, pp. 370–376.

[7] C. M. Spooner and W. A. Gardner, "Performance Evaluation of Cyclic Polyspectrum Estimators," (invited paper) *Proceedings of the Twenty-Sixth Annual Asilomar Conference on Signals, Systems and Computers,* Pacific Grove, CA, pp. 477–483, October 26–28, 1992.

[8] C. M. Spooner and W. A. Gardner, "Exploitation of Higher-Order Cyclostationarity for Weak-Signal Detection and Time-Delay Estimation," *Proceedings of the Sixth Workshop on Statistical Signal & Array Processing*, Victoria, British Columbia, Canada, 1992.

[9] C. M. Spooner and W. A. Gardner, "Cubic Frequency-Shift Filtering for Cochannel Interference Mitigation and Signal Equalization," in *Proceedings of the International Symposium on Nonlinear Theory and its Application,* Honolulu, Hawaii, December 1993.

[10] W. A. Gardner and C. M. Spooner. "Cyclostationary-Signal Processing," Chapter in *Digital Signal Processing Techniques and Applications,* C.T. Leondes, Editor, New York: Academic Press, 1993 (in press).

[11] C. M. Spooner and W. A. Gardner. "The Cumulant Theory of Cyclostationary Time-Series, Part I: Foundation; Part II: Development and Applications," *IEEE Transactions on Signal Processing*, in press.

[12] W. A. Gardner, "An Introduction to Cyclostationary Signals," Chapter in *Cyclostationarity in Communications and Signal Processing*, W. A. Gardner, Editor, New York: IEEE Press, 1994.

[13] W. A. Gardner, *Introduction to Random Processes with Applications to Signals and Systems.* New York, New York: Macmillan, 1985 (second edition; New York: McGraw-Hill, 1990).

[14] W. A. Gardner, *Statistical Spectral Analysis: A Nonprobabilistic Theory,* Prentice-Hall, Englewood Cliffs, New Jersey, 1987.

[15] W. A. Gardner and W. A. Brown. "Fraction-of-Time Probability for Time-Series that Exhibit Cyclostationarity," *Signal Processing,* Vol. 23, No. 3, pp. 273–292, June 1991.

[16] A. N. Shiryaev, "Some Problems in the Spectral Theory of Higher-Order Moments – I," *Theory of Probability and Its Applications* **5**, pp. 265–284, 1960.

[17] D. R. Brillinger, "An Introduction to Polyspectra," *Annals of Mathematical Statistics* **36**, pp. 1351–1374, 1965.

[18] D. R. Brillinger and M. Rosenblatt, "Asymptotic Theory of Estimates of k-Th Order Spectra," in *Spectral Analysis of Time Series,* (B. Harris, ed.), Wiley, New York, 1967.

[19] D. R. Brillinger and M. Rosenblatt, "Computation and Interpretation of k-Th Order Spectra," in *Spectral Analysis of Time Series,* (B. Harris, ed.), Wiley, New York, 1967.

[20] M. Rosenblatt, *Stationary Sequences and Random Fields,* Birkhauser, Boston, 1985.

[21] V. P. Leonov and A. N. Shiryaev. "On a Method of Calculation of Semi-Invariants," *Theory of Probability and Its Applications,* Vol. 4, No. 3, pp. 319–328, 1959.

[22] R. D. Gitlin, J. F. Hayes, and S. B. Weinstein, *Data Communications Principles,* Plenum Press, New York, 1992.

[23] A. Lender, "The Duobinary Technique for High-Speed Data Transmission," *IEEE Transactions on Communications and Electronics,* Vol. 82, No. 5, pp. 214–218, 1963.

[24] R. O. Duda and P. E. Hart, *Pattern Classification and Scene Analysis,* Wiley, New York, 1973.

[25] J. F. Moss and J. B. Beyer. "Universal Carrier Recovery for APK Signals," *Proceedings of the IEEE,* Vol. 71, No. 7, pp. 905–907, July 1983.

[26] F. F. Liedtke. "Computer Simulation of an Automatic Classification Procedure for Digitally Modulated Communication Signals with Unknown Parameters," *Signal Processing,* Vol. 6, No. 4, pp. 311–323, August 1984.

[27] T. G. Callaghan, J. L. Perry, and J. K. Tjho. "Sampling and Algorithms Aid Modulation Recognition," *Microwaves RF,* pp. 117–121, Sept. 1985.

[28] F. Jondral. "Automatic Classification of High Frequency Signals," *Signal Processing,* Vol. 9, No. 3, pp. 177–190, 1985.

[29] J. E. Hipp. "Modulation Classification Based on Statistical Moments," *IEEE MILCOM 1986 Proceedings*, pp. 20.2.1–20.2.6, 1986.

[30] R. J. Mammone, R. J. Rothaker, C. I. Podilchuk, S. Davidovici, and D. L. Schilling. "Estimation of Carrier Frequency, Modulation Type and Bit Rate of an Unknown Modulated Signal," *Proceedings of the International Communications Conference (ICC)*, pp. 28.4.1–28.4.7, 1987.

[31] J. Aisbett. "Automatic Modulation Recognition Using Time Domain Parameters," *Signal Processing*, Vol. 13, No. 3, pp. 323–328, October 1987.

[32] D. Nicholson. "Issues in Signal Design to Lower Probability of Classification and Identification," *IEEE MILCOM 1987 Proceedings*, pp. 32.4.1–32.4.3, 1987.

[33] K. Kim and A. Polydoros. "Digital Modulation Classification: The BPSK versus QPSK Case," *IEEE MILCOM 1988 Proceedings*, pp. 24.4.1–24.4.6, 1988.

[34] D. Chu. "Phase Digitizing Sharpens Timing Measurements," *IEEE Spectrum*, pp. 28–32, July 1988.

[35] S-Z Hsue and S. S. Soliman. "Automatic Modulation Recognition of Digitally Modulated Signals," *IEEE MILCOM 1989 Proceedings*, pp. 37.4.1–37.4.5, 1989.

[36] Y. T. Chan and L. G. Gadbois. "Identification of the Modulation Type of a Signal," *Signal Processing*, Vol. 16, No. 2, pp. 149–154, February 1989.

[37] Y. K. Kim and C. L. Weber. "Generalized Single Cycle Classifier with Applications to SQPSK v.s. 2^kPSK," *IEEE MILCOM 1989 Proceedings*, pp. 46.1.1–46.1.5, 1989.

A The Theory of Higher-Order Cyclostationarity

In this appendix we define the temporal and spectral moment and cumulant functions that form the basis of the theory of HOCS. Then we give a brief tutorial explanation of how cumulants arise as the solution to the problem of generating pure nth-order sine waves. Finally, we explain the signal-selectivity property that is unique to the cyclic temporal cumulants and their Fourier transforms, the cyclic polyspectra, and we illustrate the parameters using the example of digital QAM signals.

For a time-series $x(t)$ for $-\infty < t < \infty$, we define the nth-order lag-product time-series by

$$L_x(t,\boldsymbol{\tau})_n \triangleq \prod_{j=1}^{n} x(t+\tau_j), \tag{4}$$

where $\boldsymbol{\tau} \triangleq [\tau_1 \cdots \tau_n]^\dagger$ and $[\cdot]^\dagger$ denotes matrix transposition. The *cyclic temporal moment function* (CTMF) of order n is defined by the limiting time average

$$R_x^\alpha(\boldsymbol{\tau})_n \triangleq \lim_{T\to\infty} \frac{1}{T} \int_{-T/2}^{T/2} L_x(t,\boldsymbol{\tau})_n \, e^{-i2\pi\alpha t} \, dt \equiv \left\langle L_x(t,\boldsymbol{\tau})_n e^{-i2\pi\alpha t} \right\rangle, \tag{5}$$

which is simply the Fourier coefficient associated with the component $e^{i2\pi\alpha t}$ in the time-series $L_x(t,\boldsymbol{\tau})_n$. It can be seen that the CTMF is a Fourier coefficient of a moment function because the nth-order fraction-of-time probabilistic moment (the *temporal moment function* [TMF]) associated with the lag product $L_x(t,\boldsymbol{\tau})_n$ is given by

$$R_x(t,\boldsymbol{\tau})_n \triangleq \hat{E}^{\{\alpha\}}\{L_x(t,\boldsymbol{\tau})_n\} \tag{6}$$

where $\hat{E}^{\{\alpha\}}\{\cdot\} = \sum_{\alpha\in\{\alpha\}} \langle (\cdot)e^{-i2\pi\alpha t}\rangle e^{i2\pi\alpha t}$, and can be expressed as [14, 15]

$$R_x(t,\boldsymbol{\tau})_n = \sum_{\alpha\in\{\alpha\}} R_x^{\alpha}(\boldsymbol{\tau})_n\, e^{i2\pi\alpha t}, \tag{7}$$

where the sum is over all real numbers α, called *nth-order cycle frequencies*, for which $R_x^{\alpha}(\boldsymbol{\tau})_n \not\equiv 0$. In (6), $\hat{E}^{\{\alpha\}}\{\cdot\}$ is the temporal expectation operation (or the sine-wave extraction operation). The functions (5) and (6) exist and are well-behaved for appropriate models of many time-series including amplitude modulated (AM), pulse-amplitude-modulated (PAM), phase-shift-keyed modulated (PSK), and digital quadrature AM (QAM) signals [10, 4], and others.

The *temporal cumulant function* (TCF) of order n for the set of time-series translates $\{x(t+\tau_j)\}_{j=1}^n$ is defined by

$$C_x(t,\boldsymbol{\tau})_n = \sum_{P=\{\nu_k\}_{k=1}^p} \left[k(p) \prod_{j=1}^{p} R_x(t,\boldsymbol{\tau}_{\nu_j})_{n_j} \right], \tag{8}$$

which is completely analogous to its stochastic-process counterpart in [16]. The sum in (8) is over all distinct partitions P_n of the set of indices $\{1,2,\cdots,n\}$, where each partition $\{\nu_k\}_{k=1}^p$ has p elements, $1 \le p \le n$, and $k(p) = (-1)^{p-1}(p-1)!$. The vector $\boldsymbol{\tau}_{\nu_j}$ is the vector of n_j lags with indices in the set ν_j.

The *cyclic temporal cumulant function* (CTCF) of order n is the Fourier coefficient of the TCF:

$$C_x^{\beta}(\boldsymbol{\tau})_n \triangleq \left\langle C_x(t,\boldsymbol{\tau})_n\, e^{-i2\pi\beta t}\right\rangle. \tag{9}$$

The set of real numbers $\{\beta\}$ for which $C_x^{\beta}(\boldsymbol{\tau})_n \not\equiv 0$ is called the set of *pure nth-order cycle frequencies*, for reasons that will become clear subsequently. Combining (6)–(9) reveals that the CTCF is given by the following explicit function of lower-order CTMFs:

$$C_x^{\beta}(\boldsymbol{\tau})_n = \sum_{P} \left[k(p) \sum_{\boldsymbol{\alpha}^{\dagger}\mathbf{1}=\beta} \left(\prod_{j=1}^{p} R_x^{\alpha_j}(\boldsymbol{\tau}_{\nu_j})_{n_j} \right) \right], \tag{10}$$

where $\mathbf{1} = [1\cdots 1]^{\dagger}$, and $\boldsymbol{\alpha} = [\alpha_1\cdots\alpha_p]^{\dagger}$. The CTCF was originally derived in [2] as the solution to the problem of removing from the Fourier coefficient $R_x^{\beta}(\boldsymbol{\tau})_n$ all contributions from Fourier coefficients $R_x^{\alpha_j}(\boldsymbol{\tau}_{\nu_j})_{n_j}$ of lower order. This is equivalent to removing from the finite-strength additive sine-wave component of frequency β in the lag product time-series $L_x(t,\boldsymbol{\tau})_n$ all contributions from products of sine-wave components in lag products $L_x(t,\boldsymbol{\tau}_{\nu_j})_{n_j}$ of lower order—whose frequencies sum to β—that can be obtained by factoring $L_x(t,\boldsymbol{\tau})_n$.

By using the relationship between moments and cumulants[21], the CTMF can be expressed in terms of CTCFs of order n and lower:

$$R_x^{\alpha}(\boldsymbol{\tau})_n = \sum_P \left[\sum_{\boldsymbol{\beta}^\dagger \mathbf{1} = \alpha} \prod_{j=1}^{p} C_x^{\beta_j}(\boldsymbol{\tau}_{\nu_j})_{n_j} \right]. \tag{11}$$

The CTMF and the CTCF are not in general integrable due to the presence of sinusoidal components in $\boldsymbol{\tau}$. These components formally result in Dirac deltas in the n-dimensional Fourier transform of the CTCF. However, a reduced-dimension version of the CTCF is absolutely integrable for many time-series of interest and, therefore, it is strictly Fourier transformable [2]. The reduced-dimension CTCF (RD-CTCF) is simply the CTCF associated with the n variables $\{x(t+\tau_j)\}_{j=1}^n$ with $\tau_n = 0$. The RD-CTCF is denoted by

$$\bar{C}_x^{\beta}(\boldsymbol{u})_n \triangleq C_x^{\beta}(\boldsymbol{\tau})_n \quad \text{for } \tau_i = u_i \text{ and } \tau_n = 0, \tag{12}$$

where $\boldsymbol{u}$ is $(n-1)$-dimensional vector $[u_1 \cdots u_{n-1}]$. The $(n-1)$-dimensional Fourier transform of (12) is denoted by $\bar{P}_x^{\beta}(\boldsymbol{f}')_n$:

$$\bar{P}_x^{\beta}(\boldsymbol{f}')_n = \int_{-\infty}^{\infty} \cdots \int_{-\infty}^{\infty} \bar{C}_x^{\beta}(\boldsymbol{u})_n \, e^{-i2\pi \boldsymbol{u}^\dagger \boldsymbol{f}'} \, d\boldsymbol{u}, \tag{13}$$

where $\boldsymbol{f}' = [f_1 \cdots f_{n-1}]^\dagger$.

The *spectral moment, spectral cumulant,* and *cyclic polyspectrum* are defined as follows. Consider the n complex-demodulate time-series $X_T(t, f_j)$ for $j = 1, \cdots, n$, associated with narrow bandpass filtered versions of $x(t)$, where

$$X_T(t, f) = \int_{t-T/2}^{t+T/2} x(v) e^{-i2\pi f v} \, dv. \tag{14}$$

The limit as $T \to \infty$ of the limiting time-average of the product of these spectral components is called the *spectral moment function* (SMF) of order n

$$S_x(\boldsymbol{f})_n \triangleq \lim_{T \to \infty} \left\langle \prod_{j=1}^{n} X_T(t, f_j) \right\rangle, \tag{15}$$

and it can be shown that Dirac deltas can be factored out as follows:

$$S_x(\boldsymbol{f})_n = \sum_{\alpha} \bar{S}_x^{\alpha}(\boldsymbol{f}')_n \delta(\boldsymbol{f}^\dagger \mathbf{1} - \alpha), \tag{16}$$

where $\delta(\cdot)$ is the Dirac delta function. However, the factor $\bar{S}_x^{\alpha}(\boldsymbol{f}')_n$ contains additional Dirac deltas for many signals and $n > 2$ (e.g., BPSK and $n = 4$).

The *spectral cumulant function* (SCF) of order n is given by

$$P_x(\boldsymbol{f})_n = \sum_{P = \{\nu_k\}_{k=1}^{p}} \left[k(p) \prod_{j=1}^{n} S_x(\boldsymbol{f}_{\nu_j})_{n_j} \right], \tag{17}$$

where $\boldsymbol{f}_{\nu_j}$ is the vector of n_j frequencies with subscripts in the set ν_j, and it follows from (16) that Dirac deltas can again be factored out:

$$P_x(\boldsymbol{f})_n = \sum_{\beta} \bar{P}_x^{\beta}(\boldsymbol{f}')_n \delta(\boldsymbol{f}^{\dagger}\mathbf{1} - \beta). \tag{18}$$

Analogous to the definition of the cyclic spectrum (and power spectrum) in [14], the factor $\bar{P}_x^{\beta}(\boldsymbol{f}')_n$ is defined to be the *cyclic polyspectrum* (CP) and is given explicitly by

$$\bar{P}_x^{\beta}(\boldsymbol{f}')_n = \sum_{P=\{\nu_k\}_{k=1}^{p}} \left[k(p) \sum_{\boldsymbol{\alpha}^{\dagger}\mathbf{1}=\beta} \bar{S}_x^{\alpha_p}(\boldsymbol{f}'_{\nu_p})_{n_p} \prod_{j=1}^{p-1} \left\{ \bar{S}_x^{\alpha_j}(\boldsymbol{f}'_{\nu_j})_{n_j} \delta(\boldsymbol{f}_{\nu_j}^{\dagger}\mathbf{1} - \alpha_j) \right\} \right]. \tag{19}$$

As first shown in [2], the CP is the $(n-1)$-dimensional Fourier transform of the RD-CTCF $\bar{C}_x^{\beta}(\boldsymbol{u})_n$ (cf. (13)). This is a generalization of the Wiener relation between the power spectrum and autocorrelation from second-order stationary time-series (cf. [14]) to nth-order cyclostationary time-series. Within the stochastic-process framework of generally nonstationary processes, it should be called the *cyclic Shiryaev-Kolmogorov* relation [16], which is the generalization of the Wiener-Khinchin relation (cf. [14]). Because the RD-CTCF can be absolutely integrable, the CP—unlike the SMF—contains no Dirac deltas. That is, all Dirac deltas present in the individual terms in (19) cancel.

Let us now see how the cumulant arises as the solution to the problem of generating pure nth-order sine waves. For low orders n, it is easy to mathematically characterize a pure nth-order sine wave in a way that matches our intuition. For notational simplicity, we choose the case of no conjugated factors in (4). For $n = 1$, the moment sine waves (the sine-wave components of the polyperiodic TMF) are, by definition, pure 1st-order sine waves. For $n = 2$, all products of 1st-order moment sine waves can be subtracted from the 2nd-order moment sine waves to obtain the pure 2nd-order sine waves, which are denoted by $\sigma_x(t, \tau_1, \tau_2)_2$,

$$\begin{aligned} \sigma_x(t, \tau_1, \tau_2)_2 &\triangleq \hat{E}^{\{\alpha\}}\{x(t+\tau_1)x(t+\tau_2)\} - \hat{E}^{\{\alpha\}}\{x(t+\tau_1)\}\,\hat{E}^{\{\alpha\}}\{x(t+\tau_2)\} \\ &= R_x(t, \boldsymbol{\tau})_2 - R_x(t, \tau_1)_1\, R_x(t, \tau_2)_1. \end{aligned}$$

There are several interesting points to be made concerning pure 2nd-order sine waves: (*i*) since $R_x(t, \tau_i)_1, i = 1, 2$, and $R_x(t, \boldsymbol{\tau})_2$ are 1st- and 2nd-order moments respectively, then $\sigma_x(t, \tau_1, \tau_2)_2$ is a temporal covariance function; (*ii*) if $R_x(t, \tau)_1 \equiv 0$, then there are no lower-order sine waves, and the 2nd-order moment sine waves are equal to the pure 2nd-order sine waves; (*iii*) if the variables $x(t+\tau_1)$ and $x(t+\tau_2)$ are statistically independent (in the temporal sense [14, 15]), then $\hat{E}^{\{\alpha\}}\{x(t+\tau_1)x(t+\tau_2)\} = \hat{E}^{\{\alpha\}}\{x(t+\tau_1)\}\,\hat{E}^{\{\alpha\}}\{x(t+\tau_2)\}$ and therefore $\sigma_x(t, \tau_1, \tau_2)_2 = 0$, that is, there is no pure 2nd-order sine wave for this particular pair of delays τ_1 and τ_2. This latter point shows that the set of pure cycle frequencies $\{\beta\}$ can be considerably different from the set of impure (moment) cycle frequencies $\{\alpha\}$.

The pure 3rd-order sine waves are obtained next. From the 3rd-order moment sine waves, we want to subtract each possible product of lower-order sine waves, but only once each. Thus, we subtract products of *pure* 2nd-order and *pure* 1st-order sine waves from the 3rd-order moment sine waves, rather than subtracting products of 1st- and 2nd-order moment

sine waves:

$$\sigma_x(t,\boldsymbol{\tau})_3 = \hat{E}^{\{\alpha\}}\left\{\prod_{j=1}^{3} x(t+\tau_j)\right\} - \sigma_x(t,\tau_1,\tau_2)_2\ \sigma_x(t,\tau_3)_1 - \sigma_x(t,\tau_1,\tau_3)_2\ \sigma_x(t,\tau_2)_1$$
$$-\sigma_x(t,\tau_2,\tau_3)_2\ \sigma_x(t,\tau_1)_1 - \sigma_x(t,\tau_1)_1\ \sigma_x(t,\tau_2)_1\ \sigma_x(t,\tau_3)_1\ .$$

Observe that there are no other possible products of *pure* lower-order sine waves. The terms in the sum of products that are subtracted can be enumerated by considering the distinct partitions of the index set $\{1,2,3\}$. A partition of a set G is a collection of p subsets of G, $\{\nu_j\}_{j=1}^{p}$, with the following properties: $G = \bigcup_{j=1}^{p} \nu_j$ and $\nu_j \bigcap \nu_k = \emptyset$ for $j \neq k$. The set P_3 of distinct partitions of $\{1,2,3\}$ is given by

$$\begin{array}{ll} p=1: & \{1,2,3\} \\ p=2: & \{1,2\},\{3\} \quad \{1,3\},\{2\} \quad \{2,3\},\{1\} \\ p=3: & \{1\},\{2\},\{3\}\ . \end{array}$$

Thus, we can express the pure 3rd-order sine wave $\sigma_x(t,\boldsymbol{\tau})_3$ as a sum over the elements of P_3:

$$\sigma_x(t,\boldsymbol{\tau})_3 = R_x(t,\boldsymbol{\tau})_3 - \sum_{\substack{P_3 \\ p\neq 1}} \left[\prod_{j=1}^{p} \sigma_x(t,\boldsymbol{\tau}_{\nu_j})_{n_j}\right], \tag{20}$$

where $\boldsymbol{\tau}_{\nu_j}$ is a subset of $\{\tau_j\}_{j=1}^{3}$ with elements having indices in ν_j, and n_j is the number of elements in ν_j. Notice that, as in the case of $n=2$, if the 1st-order moment sine waves are zero, then the 3rd-order moment sine waves are equal to the pure 3rd-order sine waves. In this case, there are no *products* of lower-order sine waves to subtract from the moment sine waves.

The formula for the pure nth-order sine waves is

$$\sigma_x(t,\boldsymbol{\tau})_n = R_x(t,\boldsymbol{\tau})_n - \sum_{\substack{P_n \\ p\neq 1}} \left[\prod_{j=1}^{p} \sigma_x(t,\boldsymbol{\tau}_{\nu_j})_{n_j}\right], \tag{21}$$

where P_n is the set of distinct partitions of the index set $\{1,2,\cdots,n\}$. The pure-sine-waves formula (21) gives all the pure nth-order sine waves associated with the delay set $\boldsymbol{\tau}$. A single pure nth-order sine wave with frequency β can be selected by computing the Fourier coefficient:

$$\sigma_x^{\beta}(\boldsymbol{\tau})_n\, e^{i2\pi\beta t} = \left\langle \sigma_x(u,\boldsymbol{\tau})_n\ e^{-i2\pi\beta(u-t)} \right\rangle, \tag{22}$$

and can be expressed in terms of pure lower-order sine waves by using the Fourier series for each $\sigma_x(t,\boldsymbol{\tau}_{\nu_j})_{n_j}$ in (21):

$$\sigma_x(t,\boldsymbol{w})_k = \sum_{\beta_k} \sigma_x^{\beta_k}(\boldsymbol{w})_k\, e^{i2\pi\beta_k t}, \qquad \boldsymbol{w} = [w_1 \cdots w_k]^{\dagger}, \tag{23}$$

where the sum is over all cycle frequencies β_k of order k. Thus, the strength of a single pure nth-order sine wave is given by

$$\sigma_x^{\beta}(\boldsymbol{\tau})_n = R_x^{\beta}(\boldsymbol{\tau})_n - \sum_{\substack{P_n \\ p\neq 1}} \left[\sum_{\mathbf{1}^{\dagger}\boldsymbol{\beta}=\beta} \prod_{j=1}^{p} \sigma_x^{\beta_j}(\boldsymbol{\tau}_{\nu_j})_{n_j}\right], \tag{24}$$

where $\boldsymbol{\beta}$ is the p-dimensional vector of pure cycle frequencies $[\beta_1 \ \cdots \ \beta_p]^\dagger$ and $\mathbf{1}$ is the p-dimensional vector of ones. Hence, the pure-sine-wave strength $\sigma_x^\beta(\boldsymbol{\tau})_n$ is given by the CTMF $R_x^\beta(\boldsymbol{\tau})_n$ with all products of pure lower-order sine-wave strengths, for sine waves whose frequencies sum to β, subtracted out. From (11), it is clear that the pure-sine-wave strength $\sigma_x^\beta(\boldsymbol{\tau})_n$ is identical to the CTCF $C_x^\beta(\boldsymbol{\tau})_n$.

Finally, let us see how the CTCF (and the CP) is signal selective. Let the signal $x(t)$ consist of the sum of M mutually independent signals $\{y_m(t)\}_{m=1}^M$,

$$x(t) = \sum_{m=1}^{M} y_m(t). \tag{25}$$

Then the addition rule for cumulants [4, 17] can be used to show that the nth-order TCF for $x(t)$ is the sum of TCFs for $\{y_m(t)\}$,

$$C_x(t, \boldsymbol{\tau})_n = \sum_{m=1}^{M} C_{y_m}(t, \boldsymbol{\tau})_n. \tag{26}$$

Thus, the pure nth-order sine waves in the delay products of each $y_m(t)$ add to form the pure nth-order sine wave in the delay product of $x(t)$:

$$C_x^\beta(\boldsymbol{\tau})_n = \sum_{m=1}^{M} C_{y_m}^\beta(\boldsymbol{\tau})_n. \tag{27}$$

The TMF does not in general obey this useful cumulative relation (27). That is, the nth-order TMF for $x(t)$ is not the sum of nth-order TMFs for each $y_m(t)$: $R_x(t, \boldsymbol{\tau})_n \neq \sum_{m=1}^M R_{y_m}(t, \boldsymbol{\tau})_n$. An exception is the case of zero-mean signals and $n \leq 3$, for which moments and cumulants are equal, which is a commonly encountered case in HOS.

To illustrate how (27) can be applied in practice, consider the situation in which $\{y_m(t)\}$ represent M interfering signals that overlap in time and frequency, but each $y_m(t)$ possesses some distinct nth-order cycle frequency, say β_m. Then it follows from (27) that

$$C_x^{\beta_m}(\boldsymbol{\tau})_n = C_{y_m}^{\beta_m}(\boldsymbol{\tau})_n, \quad m = 1, 2, \cdots, M. \tag{28}$$

This indicates that the presence or absence of each of the signals $y_m(t)$ can be detected by measuring (estimating) the CTCFs of $x(t)$ for the cycle frequencies $\{\beta_m\}$, and that parameters of each of the signals, on which these CTCFs depend, can be estimated. As illustrated in [14, 12, 13] for second order and in [4] for higher order, this signal-selectivity property can be exploited in numerous ways to accomplish noise-and-interference-tolerant signal detection and estimation.

As another application, let $M = 2$, $y_1(t)$ be non-Gaussian, and $y_2(t)$ be Gaussian. Then $C_{y_2}(t, \boldsymbol{\tau})_n \equiv 0$ for $n \geq 3$ and, from (26), we have $C_x(t, \boldsymbol{\tau})_n = C_{y_1}(t, \boldsymbol{\tau})_n, \quad n \geq 3$, which indicates the detectability of $y_1(t)$ with no knowledge about $y_2(t)$ except that it is Gaussian.

As an example of the cyclic polyspectrum, we consider the class of digital QAM signals described by their complex envelopes, which can be expressed as $x(t) = \sum_{m=-\infty}^{\infty} a_m p(t - mT_0 - t_0)$, where $p(t)$ is the complex pulse and $\{a_m\}$ is the complex digital data. Assuming that $\{a_m\}$ is an independent sequence, we have shown [10, 5, 11] that the CP for the set of

variables $\{x^{(*)_j}(t+\tau_j)\}_{j=1}^{n}$ (with $\tau_n = 0$), where $(*)_j$ denotes an optional conjugation of the jth variable, is given by

$$\bar{P}_x^{\beta}(\boldsymbol{f}')_n = \frac{C_{a,n}}{T_0} P((-)_n[\beta - \mathbf{1}^{\dagger}\boldsymbol{f}'])^{(*)_n} \prod_{j=1}^{n-1} P((-)_j f_j)^{(*)_j} e^{i2\pi\beta t_0}, \quad \beta = k/T_0, \tag{29}$$

where $(-)_j$ is the optional minus sign corresponding to the optional conjugation $(*)_j$, $C_{a,n}$ is the cumulant of a_m, and

$$P(f) = \int_{-\infty}^{\infty} p(t) e^{-i2\pi f t}\, dt. \tag{30}$$

Thus, the CP is simply a scaled product of n pulse transforms.

B Cumulants of Rectangular-Pulse PAM Signals

The maxima of the absolute value of the nth-order cyclic cumulants for PAM signals with full-duty-cycle rectangular pulses are derived in this appendix.

For the signal model

$$x(t) = \sum_{j=-\infty}^{\infty} a_j p(t + jT_0 + t_0), \tag{31}$$

where

$$p(t) = \begin{cases} 1, & |t| \le T_0/2 \\ 0, & |t| > T_0/2, \end{cases} \tag{32}$$

and $\{a_j\}$ is an independent, identically distributed symbol sequence, the nth-order cyclic temporal cumulant function (CTCF) is given by

$$C_x^{\alpha}(\boldsymbol{\tau})_n = \frac{C_{a,n}^m}{T_0} \int_{-\infty}^{\infty} \prod_{k=1}^{n} p(t+\tau_k) e^{-i2\pi\alpha t}\, dt\, e^{i2\pi\alpha t_0}. \tag{33}$$

Let t_1 equal the difference between the largest and smallest of the delay variables

$$t_1 \triangleq \max_{i \neq j} |\tau_i - \tau_j|$$

if this number is less than T_0 and equal to T_0 otherwise. Then the product of the shifted rectangle functions in the integrand of (33) is itself equal to a rectangle with width $T_0 - t_1$. It is easy to evaluate the integral (33), differentiate the result with respect to t_1, set this derivative equal to zero and solve for t_1. The result is

$$\max_{\boldsymbol{\tau}} |C_x^{\alpha}(\boldsymbol{\tau})_n| = \frac{|C_{a,n}^m|}{\pi|k|} \quad \text{for } t_1 = \frac{(2|k| - 2m - 1)T_0}{2|k|}, \quad m = 0, 1, \cdots |k-1|.$$